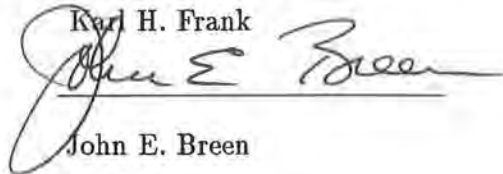


STAY CABLE ANCHORAGE SYSTEM TESTS

APPROVED:

A handwritten signature in cursive script, appearing to read "Karl H. Frank", written over a horizontal line.

Karl H. Frank

A handwritten signature in cursive script, appearing to read "John E. Breen", written over a horizontal line.

John E. Breen

STAY CABLE ANCHORAGE SYSTEM TESTS

by

JEFFREY ALLEN MOORE, B.S.C.E

THESIS

**Presented to the Faculty of the Graduate School of
The University of Texas at Austin
in Partial Fulfillment
of the Requirements
for the Degree of**

MASTER OF SCIENCE IN ENGINEERING

THE UNIVERSITY OF TEXAS AT AUSTIN

May 1989

To Mom, Dad, Vicki and Mark

ACKNOWLEDGEMENTS

I wish to express my great thanks at this time to those individuals who have been most instrumental in helping me to retain my sanity and complete this thesis:

Dr. Karl H. Frank of the Department of Civil Engineering, The University of Texas at Austin, for his suggestions and ability to impress upon me the importance of simple common sense throughout all phases of the project.

Jon Vought, Peter Buergi, and company at VSL Corporation, who sponsored the research leading to this thesis.

Blake Stasney, Wayne Fontenot, Dick Marshall, Wayne Little, and Alec Tahmassebi for their technical support in the maintenance and repair of the test equipment.

Patrick Ball, for his ace welding jobs in high places, and for his constant source of caustic humor.

Miss Irene Moore, for her daily lunchtime companionship, and who will be sorely missed for her insight into "Days of Our Lives."

Miss Sharon Cunningham, for the terrific assistance she gave in the preparation of this thesis and many other "small" items along the way.

Mrs. Jean Gehrke, for the assistance she provided as a graphics artist.

Kenneth Mark Merryman, a good friend, who I will miss every time I go sailing or watch an old movie.

Lyle Payne, for so many years of true friendship, who taught me how to be more of a "people" person and who never stopped telling me how proud he was of me.

My family, for their constant support and desire to see me succeed throughout my twenty-three years of existence thus far.

Jeffrey A. Moore

April, 1989
Austin, Texas

TABLE OF CONTENTS

	<u>Page</u>
CHAPTER 1 INTRODUCTION	1
CHAPTER 2 BACKGROUND	6
2.1 Stay Arrangements	6
2.1.1 Longitudinal stay arrangements	6
2.1.1.1 Harp arrangement	7
2.1.1.2 Radiating arrangement	7
2.1.1.3 Fan arrangement	7
2.1.1.4 Star arrangement	7
2.1.2 Transverse stay arrangements	9
2.1.2.1 Single plane system	9
2.1.2.2 Double plane system	10
2.1.2.3 Triple plane system	10
2.2 Types of Stay Cables	10
2.2.1 Wire rope stays	10
2.2.2 Locked coil strand stays	12
2.2.3 Parallel wire stays	12
2.2.4 Parallel strand stays	13
2.2.5 Threaded bar stays	13
2.3 Anchorage Systems	15
2.3.1 Threaded bar anchorages	15
2.3.2 Hot-poured socket	15

2.3.3	HI-AM anchorage	17
2.3.4	Strand anchorages	18
2.3.4.1	Wedge-trumpet anchorage	19
2.3.4.2	Wedge anchorage	20
2.3.4.3	Wedge-stiffening tube anchorage with coated strands	20
2.4	Corrosion Protection	22
2.4.1	Tube protection systems	23
2.4.1.1	Polyethylene pipe	23
2.4.1.2	Stainless steel tubing	24
2.4.2	Filler materials	24
2.4.3	Individual wire/strand protection	25
2.4.4	Remedial protection systems	26
2.4.5	New techniques	26
2.5	New Developments in Cable Stay Systems	27
2.6	Summary	27
CHAPTER 3 TYPES OF FATIGUE AND FATIGUE TESTING		29
3.1	Wire Fatigue	29
3.2	Fatigue in Parallel Wire Stays	31
3.3	Fatigue in Parallel Strand Stays	32
3.4	Fatigue Testing of Cables	34

CHAPTER 4	PREVIOUS TESTS	36
4.1	Strand Tests	36
4.1.1	Testing apparatus	36
4.1.2	Paulson, Frank, and Breen	37
4.1.2.1	Test method	38
4.1.2.2	Results	38
4.1.2.3	Applications to cable stays	42
4.1.3	Lamb and Frank	43
4.1.3.1	Test method	44
4.1.3.2	Results	45
4.1.3.3	Applications to stay cable anchorages	48
4.2	Parallel Wire Stay Tests	50
4.2.1	Testing apparatus	50
4.2.1.1	Pasco-Kennewick stay tests	50
4.2.1.2	Luling stay tests	51
4.2.2	Pasco-Kennewick intercity bridge stay tests	52
4.2.2.1	Test method	52
4.2.2.2	Results	53
4.2.3	Luling bridge stay tests	54
4.2.3.1	Test method	54
4.2.3.2	Results for 103 wire specimen	55
4.2.3.3	Results for 271 wire specimen	55
4.2.3.4	Results for 211 wire specimen	55
4.2.3.5	Results for 307 wire specimen	56
4.2.4	Summary	56

4.3	Parallel Strand Stay Tests	59
4.3.1	Stallings	59
4.3.1.1	Description of test specimen	59
4.3.1.2	Testing apparatus	59
4.3.1.3	Test method	61
4.3.1.4	Results	61
4.3.2	Houston ship channel crossing stay tests	62 .
CHAPTER 5 BAYTOWN BRIDGE STAY TESTS		63
5.1	Test Instrumentation	63
5.2	Test Specimen Preparation and Installation	68
5.3	Test Procedure	78
5.4	Test Results	88
5.5	Summary of Test Results	100
5.5.1	Load behavior	100
5.5.2	Wire breakages	100
5.5.3	Longitudinal cracking	100
5.5.4	Stiffness and wedge seating	100
CHAPTER 6 SUMMARY AND RECOMMENDATIONS FOR FURTHER STUDY		103
APPENDIX A : LOAD CELL CALIBRATION INFORMATION		106
APPENDIX B : STRAIN GAGE DATA		111
REFERENCES		114

LIST OF TABLES

<u>Table</u>		<u>Page</u>
2.1	Typical ultimate strength and effective modulus values for stay cables	11
2.2	Survey of various stay systems in use	28
3.1	PTI recommended testing guidelines	35
4.1	Contact Ratios [22]	47
4.1	Summary of LDR values established in static load distribution tests [22]	48
5.1	Load events versus time	79
5.2	19 strand specimen center wire and wedge seating data	81
5.3	19 strand specimen elongation data	83
B.1	Strain gage data for 19 strand specimen	111

LIST OF FIGURES

<u>Figure</u>	<u>Page</u>
1.1 Studies by Thul [1]	3
1.2 Studies by Taylor [1]	4
2.1 Typical longitudinal arrangements for bridge stays [7]	8
2.2 Typical transverse arrangements for bridge stays [7]	9
2.3 Wire rope [4]	11
2.4 Locked coil strand [4]	12
2.5 Parallel wire stay with hexagonal arrangement [3]	13
2.6 Typical seven wire prestressing strand [3]	14
2.7 Mechanical connectors for threaded bar stays [8]	14
2.8 Typical threaded bar anchorage [8]	15
2.9 Hot-poured socket [3]	16
2.10 Effects of casting temperature on wire ultimate strength [3]	17
2.11 Hi-Am anchorage [3]	18
2.12 Wedge-trumpet anchorage details [3]	19
2.13 Wedge anchorage details [9]	21
2.14 Two-piece wedge system for wedge anchorage	21
2.15 Wedge-stiffening tube anchorage with coated strands [11]	22
3.1 Fatigue crack initiation in wire [7]	30
3.2 Pouring temperature vs. wire fatigue life [1]	32

3.3	Friction-type anchorage system for strand	33
4.1	Strand fatigue setup [21]	37
4.2	Protective gripping measure employed [21]	39
4.3	Double chuck system for anchoring strand [21]	40
4.4	Design model and its test data, recommended by Paulson, Frank and Breen [21]	41
4.5	Developed S-N curve versus AASHTO Category A and B curves [21]	42
4.6	Effect of wedge type on fatigue strength for tests, 33.8 ksi stress range [22]	46
4.7	Log(N)/Log(Nmax) versus LDR for 47.2 and 33.8 ksi stress ranges [22]	49
4.8	Center buttonhead and end plate seating during quasi-static loading	57
4.8	Center buttonhead and end plate seating during fatigue test	58
4.9	Center buttonhead and end plate seating during creep tests	58
4.10	FSEL large scale fatigue and tensile test machine [29]	60
5.1	Test set-up and strain gage locations	64
5.2	Four-inch steel plate slid into position	65
5.3	Strand/wedge references for anchorhead	67
5.4	Measurement of center wire and wedge seating with a depth gage and stationary fixture	68
5.5	Linear potentiometer to measure specimen elongation	69

5.6	Load-maintainer plate holding grout load	70
5.7	Rotation restraint device	70
5.8	Velocity transducer attached to bottom anchorage	71
5.9	Specimen assembly station	71
5.10	Strand supplied for testing, with steel cage	73
5.11	Hollow steel "bullet" to aid strand in passing through pipe assembly untangled	73
5.12	Steel helical spacer inserted in polyethylene stay length	74
5.13	All 19 strands installed	74
5.14	Spring plate mounted on bottom anchorhead	75
5.15	Gap in polyethylene stay pipes to allow bending during installation	75
5.16	Lifting of specimen	76
5.17	Preseating of wedges with monostrand jack	77
5.18	Primary grouting from bottom anchorage	85
5.19	Siphoning of bleed water from top anchorage	85
5.20	Secondary grouting procedure	86
5.21	Grout cap removed; break occurred at top of strand extensions	86
5.22	Load-elongation curve for 19 strand cable stay specimen	89
5.23	Center wire slip in strand 4 at bottom anchorhead	92
5.24	Circumferential crack distribution in grout	92
5.25	Longitudinal cracking of grout	93

5.26	Strand contact points on polyethylene pipe	94
5.27	Wire break locations	95
5.28	Outer wire failure in wedges of top anchorhead, strand 4	96
5.29	Ductile wire break in strand 4	96
5.30	Wire breaks near top anchorhead in strand 10	97
5.31	Outer wire failure 3 to 6 inches from bearing face of top anchorhead, strand 10	97
5.32	Outer wire failure in wedges of top anchorhead, strand 10	98
5.33	Wire break in strand 18 in stay length	98
5.34	Outer wire failure in stay length, strand 18	99
5.35	Outer wire failure in wedges of top anchorhead, strand 18	99
5.36	Grout cube strength over time	102
A.1	Calibration of load cell SN 850326C UT 397640	107
A.2	Calibration of load cell SN 850326A UT 397642	107
A.3	Calibration of load cell SN 850326D UT 397641	108
A.4	Calibration of load cell SN 850326B UT 397639	108
A.5	Load cell group calibration	109
A.6	Group calibration with strain indicator	110
A.7	Group calibration with closed loop test control unit	110

ABBREVIATIONS

kip	1000 pounds force
ksi	kips per square inch
psi	pounds per square inch
f_{pu}	wire/strand ultimate tensile strength
f_{su}	specified minimum ultimate load, based on nominal cross-sectional area and f_{pu}
E	Young's Modulus
LDR	load distribution ratio
GUTS	guaranteed ultimate tensile strength
S-N	stress range vs. specimen life, cycles
PTI	Post-Tensioning Institute
TLP	tension leg platform

CHAPTER 1 INTRODUCTION

The use of cable stays in bridge structures is not new to the field of structural engineering. Documented use of such structures dates back over 350 years. Given the relatively high rate of failure of many of these earlier structures, though, cable-stayed bridges apparently fell from favor with bridge builders [1]. In the last 50 years, however, the cable-stayed bridge has been resurrected as a viable design alternative.

Several factors exist for the resurgence of this type of structure. In recent years the costs associated with designing and constructing a bridge structure of large span have increased appreciably, and it has been shown that the cable-stayed alternative is an economical choice for many span lengths. More efficient use of high-strength steels in cable-stayed bridge structures has also made this type of bridge favorable. Increased knowledge of the behavior of steel and better quality control in the fabrication process have helped to eliminate many of the modes of failures that previously occurred with bridge structures of this type. In addition, the high degree of indeterminacy associated with cable-stayed bridges no longer poses a monumental task of analysis as more powerful tools of analysis are now available. Finally, the aesthetic qualities afforded by a cable-stayed bridge structure are virtually unparalleled. These factors, among others, have helped to bring the cable-stayed bridge a respectable status as an economical and safe design alternative.

During its 350 year history, the cable-stayed bridge was a factor in both major engineering feats and failures. As early as 1617, the Venetian engineer Verantius built a bridge with a number of inclined chain stays assisting in supporting the road deck [1,2]. In early 19th century England, Redpath and Brown built the first iron cable-stayed bridge, the King's Meadow footbridge. This bridge, which spanned approximately 34 meters, used wire cable stays that attached to a cast iron tower [1]. Additionally, the eminent american engineer John Roebling made a partial use of cable stays in the construction of the Brooklyn Bridge. Completed in 1883, the bridge spanned the East River in New York and is still in use today [3].

On the other hand, relatively few bridge structures built during this wide time period utilized cable stay systems in any form. This is undoubtedly because of

the fact that cable-stayed bridge collapses gained great notoriety at the time. For instance, a bridge erected across the Saale River in Nienburg, Germany, collapsed in 1825, only one year after completion; the failure was blamed on the chain stays. In England during the early 19th century, a number of suspension bridges with inclined stays failed, due to insufficient resistance to wind loading. This led to partial abandonment of cable stays in England. After reporting on some of these failures, the french engineer Navier suggested the use of pure suspension bridges rather than cable-stayed bridges. Thus the cable stayed bridge concept fell from grace with most bridge designers. The main causes for these early failures, though, were construction defects and a general misunderstanding of the mechanics involved. For instance, cables in the earlier stayed bridges generally offered only passive resistance to deck load as they were not pretensioned. Thus significant deformation of the bridge deck would first occur before the stays would perform their proper function [4].

Advancement in the art of analyzing and designing cable-stayed structures was not possible until only recently, as the generally high degree of indeterminacy associated with such structures called for more powerful tools of analysis such as the modern computer. Additionally, the advantages of a cable-stayed system were not fully appreciated until after World War II, when steel was in short supply in war-ravaged Europe, and an estimated 15,000 bridges that were destroyed in the war had to be rebuilt [1]. The cable-stayed configuration was particularly attractive at that time, not from an aesthetic standpoint, but because of its economical use of high-strength steel as a tension member. Accordingly it was the European community who established the art of designing today's modern cable-stayed bridges. In 1952 Leonhardt designed a cable-stayed bridge across the Rhine River in Dusseldorf, which was completed in 1958 [4]. Generally considered by bridge designers and historians alike to be the first modern cable-stayed bridge, the Stromsund Bridge in Sweden was designed and constructed by German firms and completed in 1955 [4].

The understanding and use of cable stays on bridge structures has advanced to the point that they are an economical design alternative for long spans. This is a region where suspension or truss bridges have traditionally dominated. Thul compared center span length requirements to total length for existing three-span continuous girder bridges, cable-stayed bridges and suspension bridges in West Germany [1]. Although his study did not explicitly consider bridge costs, the data

compiled by Thul does implicitly reflect on the economics involved in choosing a particular bridge type to meet span requirements. The results of Thul's study would indicate that continuous girder bridges are the most economical alternative in the shorter span range up to about 700 feet. Suspension bridges become the more economical choice with required center spans a minimum of 1000 feet. However, Thul found that cable-stayed bridges provide the most economical alternative in the intermediate range of center spans, from 700 to 1000 feet. This corresponded to a center-to-span-total-length range of 50 to 60%. The results of Thul's study, completed in 1966, are depicted in Figure 1.1.

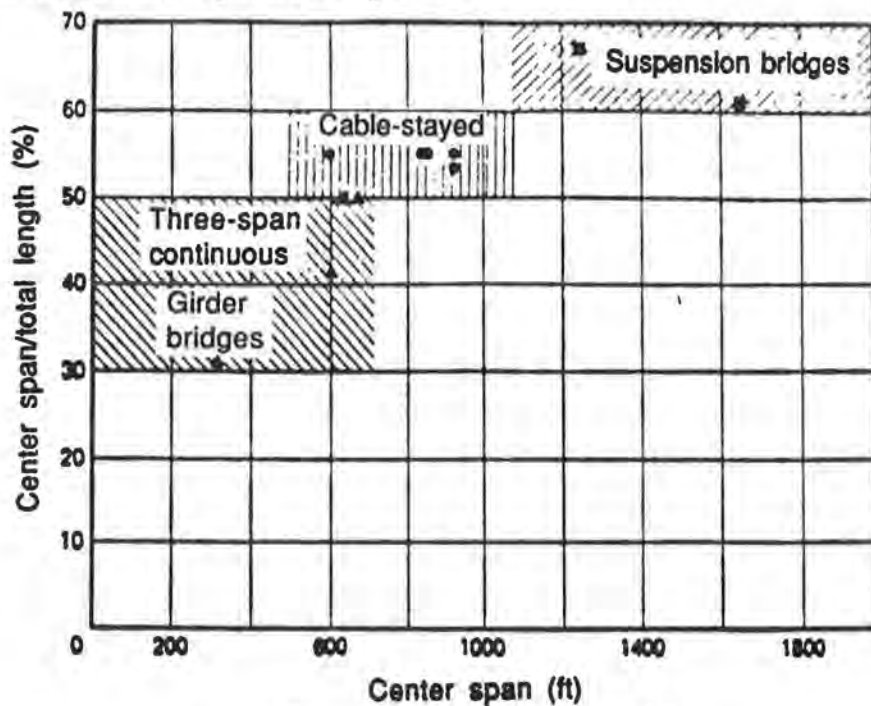


Figure 1.1 Studies by Thul [1]

A study by Taylor in 1969 correlated center span lengths to required weight of steel per square foot of deck space for the same alternative designs as Thul. Taylor determined that, once again, cable-stayed bridges prove to be the most economical

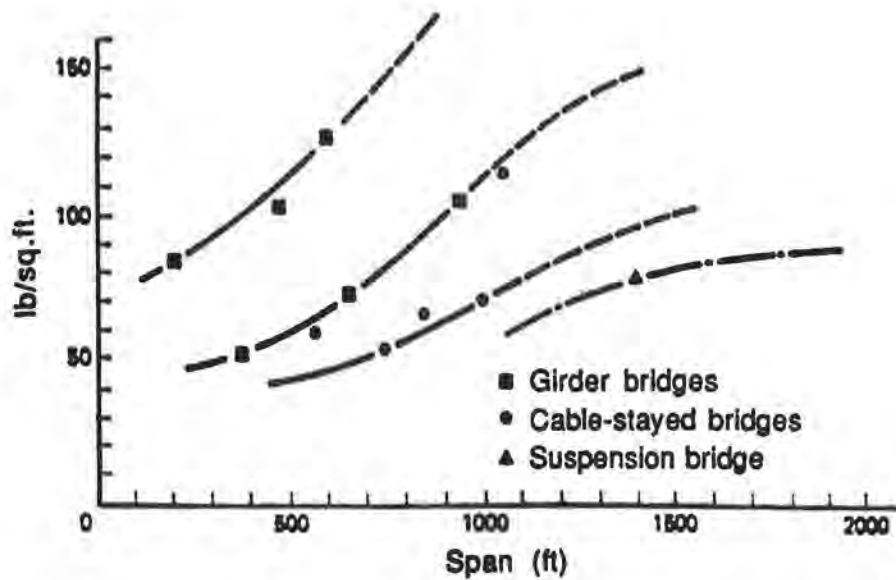


Figure 1.2 Studies by Taylor [1]

for intermediate spans in the range of 700 to 800 feet [1]. Figure 1.2 depicts the results of Taylor's findings.

Continued advancement in related technologies and improved construction methods since the studies by Thul and Taylor were completed have shown that the cable-stayed alternative is economical for increasingly longer spans. The cable-stayed bridge is proving to be competitive in the realm in which suspension bridges have historically dominated. A final design submitted in 1978 for the proposed Great Belt Bridge in Denmark utilized the cable-stayed configuration with a main span of 780 meters [3]. Additionally, the Normandie Bridge in France, which is slated for completion in late 1993, will be the world's longest cable-stayed bridge with a main span of 2808 feet [5]. After studying design practices and bidding results, Zellner and Saul believe that for spans up to 6000 feet the cable-stayed bridge with steel deck structure is the most economical solution [6].

Cable-stayed bridges in use today have shown not only to be aesthetically pleasing and economical, but also aerodynamically sound. The use of cable stays

in certain configurations has allowed the use of shallower girders because the cable anchorages on the bridge deck provide adequate torsional stiffness.

Since the modern cable-stayed bridge was developed in Europe, most of the commonly used anchorage systems in use today have also been developed by the European community. Some of the major anchorage systems in use today are Freysinnet, VSL, and Dywidag, all European developments. Accordingly, a significant amount of associated research on stay cable anchorage system behavior has been conducted by the European research community. Testing facilities like EMPA, in Switzerland, and the Technical University in Munich, West Germany, have long conducted testing of cable stay systems.

Only recently, due in part to the escalating costs associated with building medium- to long-span structures, has particular attention been paid in the United States to this type of bridge structure. The first vehicular cable-stayed bridge constructed in the U.S. was the Sitka Harbor Bridge, completed in 1972 [1]. More recent examples of the cable-stayed configuration in use in the U.S. include the Luling Bridge in Louisiana, the Pasco-Kennewick Intercity Bridge in Washington State, the Dames Point Bridge in Florida, and the Sunshine Skyway Bridge in Tampa, Florida. Cable-stayed bridges have also been proposed for many new bridge projects, such as the Baytown Bridge in Baytown, Texas.

The increase in the construction of cable-stayed bridges in the U.S. has led to studies in the field by American research organizations as well. Research in the area of stay cable anchorage systems, as well as the prestressing strand used in many of the modern anchorage systems, has been and continues to be conducted at the Phil M. Ferguson Structural Engineering Laboratory (FSEL) at The University of Texas, Austin.

The purpose of this thesis is to discuss typical cable stay arrangements and anchorage systems and summarize previous testing at FSEL related to the field of cable stays. In addition, current research in the field of stay cable anchorage systems at the University of Texas is discussed.

CHAPTER 2 BACKGROUND

This chapter presents an overview of the various design options for cable stay systems, including stay arrangements, stay cable and anchorage alternatives, corrosion protection methods, and new developments in stay cable research.

2.1 Stay Arrangements

The principle means of transmitting load from the bridge deck to the tower(s) in a cable-stayed bridge is through the stays. The stay arrangement chosen for a bridge is dependent on a number of factors. Among these factors are aesthetic value, cost, the tower height-to-center span, the number of traffic lanes, and the types of loads to be resisted by the bridge.

2.1.1 Longitudinal stay arrangements. The longitudinal arrangement of cable stays is generally a function of the desired span to height ratio of the bridge under consideration. In general, fewer stays are required for shorter spans and tower heights for a given set of loading conditions. Conversely, longer spans and tower heights require more stays. Additionally, bridges have been constructed using only a few large stays, the result being a structure with a lower degree of indeterminacy. They have also been constructed using many smaller stays, which simplifies any necessary replacement of individual stays on the completed structure. Of course, cost is also a factor in determining the chosen arrangement. For example, fewer but larger stays will impose large concentrated loads on the tower and bridge deck at the point of anchorage. Thus various appurtenances such as bearing and web stiffeners may be required to transfer stay forces to the deck. A final consideration to be made involving the longitudinal cable arrangement concerns the proposed method of bridge deck and tower construction. For example, balanced cantilever construction utilizing the stays as temporary supports would require continuous support in the form of numerous stays. Many different stay arrangements exist, and their functions are

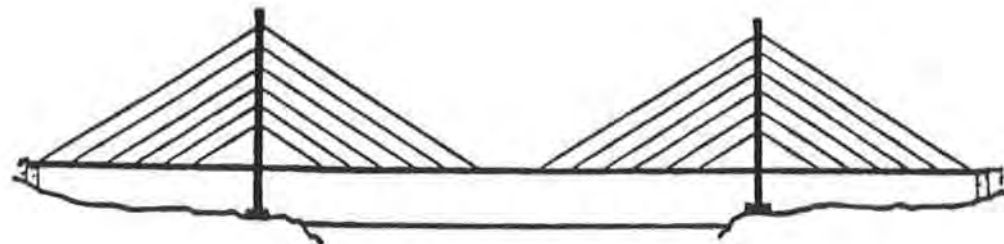
described below. Figure 2.1 shows the typical longitudinal arrangements of bridge stays.

2.1.1.1 Harp arrangement. In the harp form, the cable stays are parallel and spaced equally from one another; the result has striking aesthetic advantages, as the name might imply. This stay arrangement produces bending moments in the tower due to the distributed stay forces. The harp arrangement is often used in bridges with main spans of up to about 200 meters, particularly where the aesthetic appearance is important [2].

2.1.1.2 Radiating arrangement. In the radiating form, all the cables run from the bridge deck to a single point on the tower. One advantage of the radiating cable arrangement is that the stays are as close to vertical as possible. This maximizes their vertical load-carrying capacity and reduces the level of axial compression in the bridge deck imposed by the stays. Because of the steeper stay angle afforded in this arrangement, the flexural loading on the tower is small; it must, however, be resistant to buckling. In large structures with numerous cable stays, it can become difficult to accommodate all the anchorages at the top of the tower.

2.1.1.3 Fan arrangement. The fan arrangement is essentially a combination of the radiating and fan arrangements. The stay cable anchorages in the fan arrangement are uniformly distributed over the upper part of the tower, which makes them easier to accommodate than in the radiating layout. Compared with the harp form, the necessary cable cross-section is smaller due to the steeper angle that the stays make with the bridge deck.

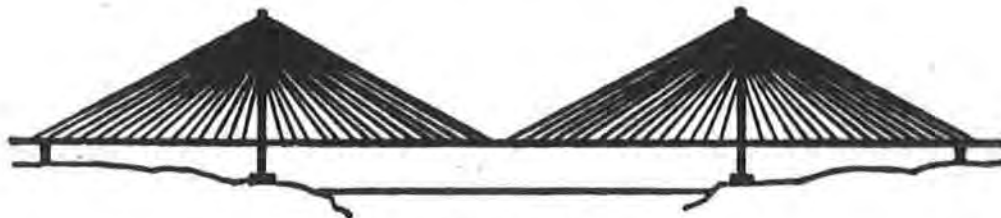
2.1.1.4 Star arrangement. In the star arrangement the cable stays anchor to the tower at different points but anchor to the bridge deck at a common point, which is usually an abutment or end pier of the bridge. The efficiency of the star arrangement is low due to the shallow angle that the stays make with the bridge deck. With this arrangement, bearing and web stiffeners may be required to adequately transfer the large concentrated deck load to the abutment or pier. Additionally, the few stays used in this arrangement make their replacement a very expensive process.



HARP ARRANGEMENT



RADIATING ARRANGEMENT



FAN ARRANGEMENT



STAR ARRANGEMENT

Figure 2.1 Typical longitudinal arrangements for bridge stays [7]

2.1.2 Transverse cable arrangements. Bridge cable stays may lie in either a single, double, or triple plane configuration in the transverse direction. They may also lie in oblique or vertical planes. The choice of transverse configuration depends to a great extent on aesthetics, the types of loads to be encountered (their magnitudes and direction), and the torsional stiffness of the bridge deck utilized. Figure 2.2 shows the typical transverse arrangements of cable stays.

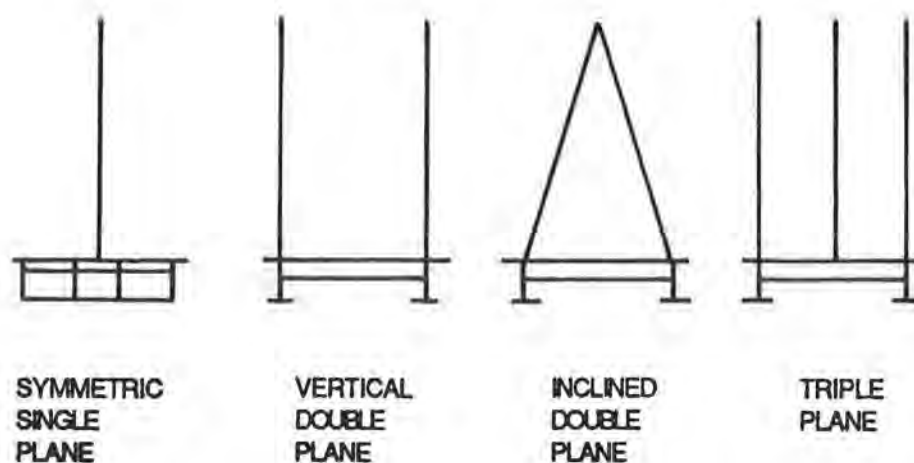


Figure 2.2 Typical transverse arrangements for bridge stays [7]

2.1.2.1 Single plane system. The single plane arrangement of cable stays generally runs along a median strip which divides the bridge deck into two lanes of traffic. This arrangement is generally favorable from an aesthetic standpoint as it allows the motorist an unobstructed view over the bridge. Placement of the stays in the median strip also reduces the amount of deck space taken up by the stays and allows smaller deck widths.

The single plane of stays can only resist symmetrical deck loads. They provide no torsional stiffness. Torsional loads created by uneven deck traffic or wind loads must be resisted by the deck itself.

2.1.2.2 Double plane system. The double plane system may employ stays either in parallel vertical planes or at some oblique angle. In the vertical arrangement, the stays anchor to the edge of the bridge deck, and attach to the edge of the bridge tower structure. In the oblique arrangement, the stays also anchor at the edge of the bridge deck, but attach to the tower structure at a common point along its transverse centerline. Either arrangement provides torsional stiffness to withstand uneven deck gravity loadings. If the stays are arranged at an oblique angle, the stays carry transverse loads such as wind loading through truss action.

2.1.2.3 Triple plane system. A triple plane system using vertical stays has also been suggested for use in urban areas where load requirements are great. The stays would be arranged in vertical planes in the median strip and along the edges of the bridge deck. The use of this system would allow for three or four lanes of traffic in each direction, as well as lanes for bus or rail travel [1].

2.2 Types of Stay Cables

The choice of cable type for a proposed bridge project is an extremely important one. A cable system utilizing higher strength steels will result in smaller volumes of steel required for the bridge stays; thus the weight of the stays will be less. Self-weight of the stays can become an important consideration when considering an arrangement using stays of very long length. The reason for this concern is that the effective modulus of the stay is inversely proportional to the length of the stay and its catenary curve due to self-weight. In addition, the magnitude of drag forces on the stays imposed by wind forces will be minimized by a reduced cross-sectional area.

Many different cable systems have been used as bridge stays. Typical ultimate strength and effective modulus values associated with many of the cable systems in use today are listed in Table 2.1. The evolution of these cables and their relative merits are discussed in this section.

2.2.1 Wire rope stays. Wire rope systems, as shown in Figure 2.3, were used in early cable-stayed bridges. Due to their relatively low strength, low elastic modulus, and poor performance in fatigue, they are no longer proposed in present-day construction [2].

Table 2.1
Typical ultimate strength and effective modulus
values for stay cables

stay cable	f_u , ksi	E, ksi
A603 wire rope	220	20,000
locked coil	–	25,400
A722 threaded bar	150	about 28,000
A421 parallel wire	240	about 29,000
A416 parallel strand	270	27,000 to 28,000



Figure 2.3 Wire rope [4]

2.2.2 Locked coil strand stays. Locked coil strands consist of an inner core made up of round wires, surrounded in turn by several layers of wedge- or keystone-shaped wires, which are in turn surrounded by several layers of Z- or S-shaped wires. This arrangement is shown in Figure 2.4. The main advantage of this cable arrangement is the inherent corrosion protection provided by the tightly interlocked wire layers [4]. These cables have been used in conventional suspension bridge construction. They have also been used extensively in many early european cable-stayed bridges, but have not been utilized in this country to date.

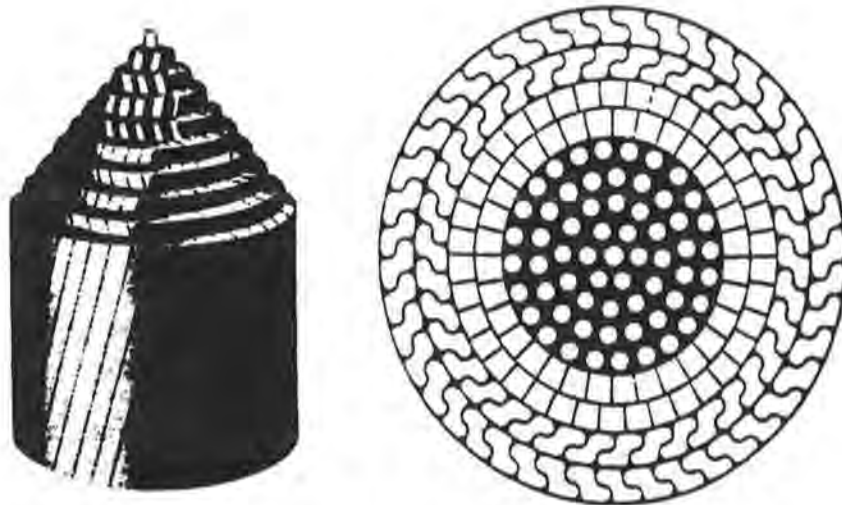


Figure 2.4 Locked coil strand [4]

2.2.3 Parallel wire stays. The cables for these stays consist of parallel wires. The wires are the same as those used in prestressed concrete construction. The wire diameter is usually on the order of 1/4 inch. Due to the anchoring system employed with parallel wire stays, the complete cable must be accurately prefabricated to the predetermined length and be transported to the site. Site fabrication is therefore not possible.

The hexagonal arrangement of the parallel wires in the completed stay has generally been shown by experience to yield a simple geometrical pattern which

allows for equal wire lengths. This in turn allows for a more uniform stressing of the wires in the stay [1]. Figure 2.5 shows a parallel wire stay with the hexagonal arrangement.

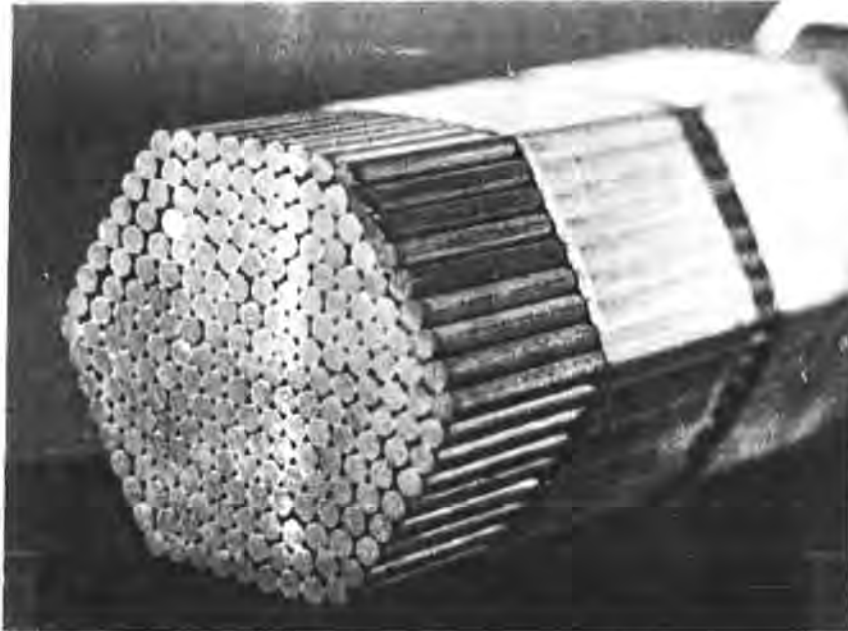


Figure 2.5 Parallel wire stay with hexagonal arrangement [3]

2.2.4 Parallel strand stays. Seven wire prestressing strand is well suited to cable stay applications. The strand consists of six wires helically wrapped around a center wire. Figure 2.6 shows a typical seven wire strand. Normally strands with a GUTS of 270 ksi are used, however strands with 300 ksi GUTS are also available [8]. Cable stays comprised of parallel strands can be assembled on the job site, utilizing local facilities. The anchorage connections do not require controlled shop conditions [2].

2.2.5 Threaded bar stays. High-strength threaded bars are also used in cable stay applications. The bars comprising these stays are available from the manufacturer in lengths of up to 60 feet. Since most stay lengths are greater than the manufactured lengths of the threaded bars, mechanical connectors are available to mate the ends of the bars, as shown in Figure 2.7. On site fabrication is possible, since the bars can be cut to length using equipment that is available at the jobsite.



Figure 2.6 Typical seven wire prestressing strand [3]

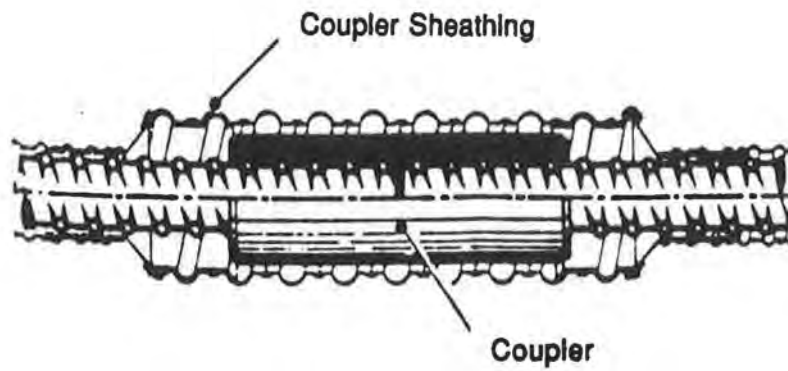


Figure 2.7 Mechanical connectors for threaded bar stays [8]

2.3 Anchorage systems

The stay cable anchorage systems that have been developed depend to a great extent on the type of cable they are used to anchor. Many of the anchorage systems commonly specified are described below.

2.3.1 Threaded bar anchorages. This anchorage is exclusive to stay systems using threaded bars. Threaded bars may be anchored individually or as a group in a common anchorhead. A typical anchorage for a single threaded bar is shown in Figure 2.8. Load transmittal with this type of anchorage system is mechanical, i.e. through the threads, and not dependant on wedging action, as with most strand anchorages.

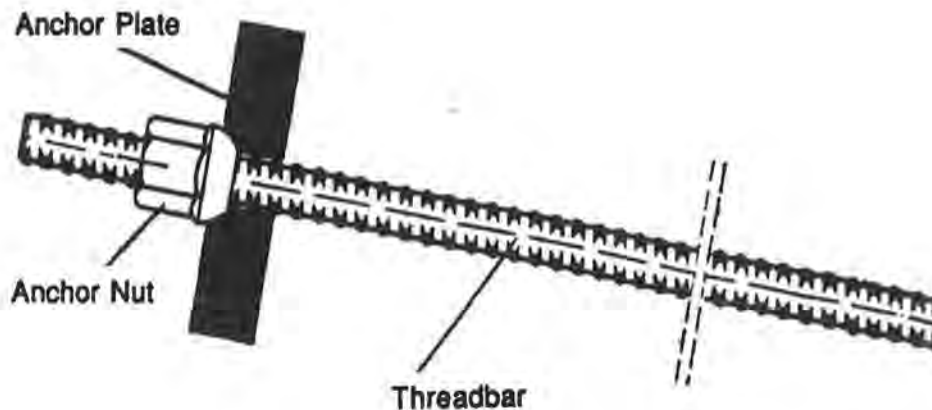


Figure 2.8 Typical threaded bar anchorage [8]

2.3.2 Hot-poured socket. The poured socket is an anchorage system commonly associated with locked coil and parallel wire stays. This type of system is shown in Figure 2.9. In this technique, the stay cable extends through a steel cylinder, or socket, with a conical cavity. The cable ends are splayed apart and a hot

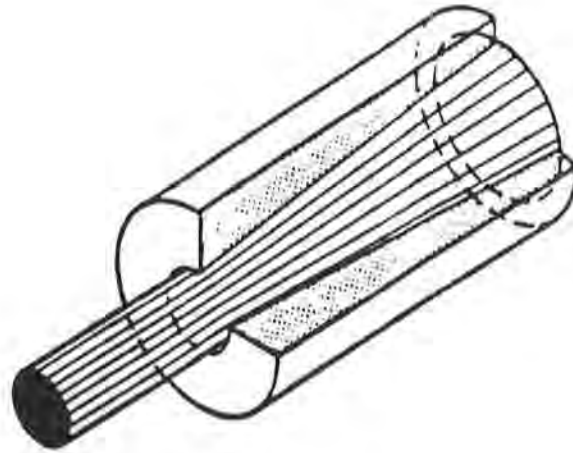


Figure 2.9 Hot-poured socket [3]

metal, typically comprised of a zinc alloy, is then poured into the socket. The metallic compound, when cured, transmits the wire tensile forces into the socket through shear and compression due to wedging action that develops.

One of the major shortcomings of this type of anchorage is the hot casting temperature of the socket. Studies have shown that high casting temperatures reduce both the ultimate strength of the wires in the vicinity of the socket and the fatigue life of the wires [3]. Figure 2.10 shows the effects of casting temperature on the wire ultimate strength. A reason for the reduction in the ultimate strength of the wires has been suggested by Gimsing [3]; the wires derive their high strengths from the cold drawing process, and the increase in wire temperature during casting relieves some of the stresses built in from the cold working process. The effects of pouring temperature on the fatigue resistance of wires are discussed in Chapter 3. Using lead alloys as the base metallic compound, cooler pouring temperatures of around 350°C are possible. The unfavorable creep properties associated with lead, however, have resulted in its lack of use. Instead, alloys with a zinc base are used. Zinc alloy

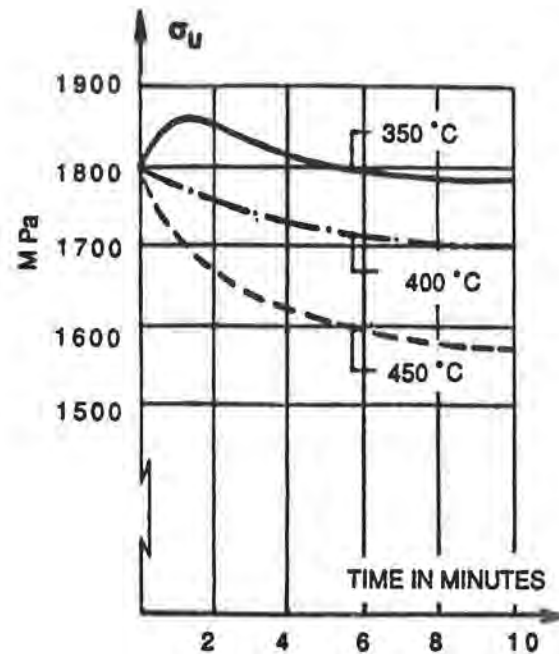


Figure 2.10 Effects of casting temperature on wire ultimate strength [3]

sockets are poured at a temperature of 400- 420°C, and if a zinc-copper alloy is used (2% copper), good resistance to creep is afforded.

2.3.3 Hi-Am anchorage. The Hi-Am, or “high- amplitude” anchorage system, was developed by Fritz Leonhardt in 1968 as an answer to many of the problems of heat encountered in the hot poured socket [1]. The system, shown in Figure 2.11, consists of a steel cylinder with conical cavity similar that of the hot-poured socket. The wire ends in the Hi-Am system are provided with buttonheads which anchor to a locking end plate. The plate holds the individual wires in place at a sufficient distance from each other during casting of the socket to ensure an even pour around the wires. The pouring compound is composed of an epoxy resin, zinc dust, and small steel balls. The compound is poured into the socket at ambient temperatures and cured at a temperature of around 100 to 200°F, depending on the epoxy used. The wire tension force is transmitted to the socket through arching action that develops in the socket. The hardened material has negligible creep properties in comparison with the hot poured socket. Additionally, the Hi-Am composite socket material has a coefficient of friction greater than that of the hot poured socket; therefore smaller socket tapers are required to transfer the tension force in the wires. This results in a

required socket diameter that is smaller in comparison to the hot poured socket. By virtue of ambient pouring temperature and relatively low curing temperature, wires in the Hi-Am anchorage have higher fatigue resistance and no reduction in ultimate strength.

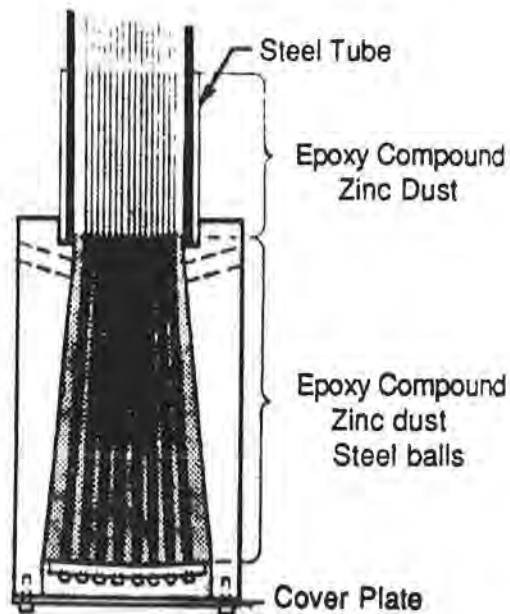


Figure 2.11 Hi-Am anchorage [3]

In the United States, because of the relative abundance and higher strength of seven wire prestressing strand, designers have increasingly specified cable stays and anchorage systems employing strand. This trend has resulted in less demand for the Hi-Am anchorage. Recently, though, a limited use of button-headed strand has been made in West Germany. However the success of Hi-Am systems using this hybrid strand has not been assessed at this time [1]. If this test program proves to be successful, the Hi-Am anchorage may see a resurgence.

2.3.4 Strand anchorages. Various strand anchorages have been used in recent cable stay designs utilizing seven wire prestressing strand. All of the systems currently used employ a friction-type wedge device to anchor the strands. Many variations on this theme have been proposed and are discussed below.

2.3.4.1 Wedge-trumpet anchorage. A manufacturer has developed a stay using seven wire parallel prestressing strands which are individually anchored in a common anchorhead using a wedge system. The anchorage system shown in Figure 2.12 consists of the following main components: a trumpet, which accommodates the flare of the strands within the anchorage, heavy steel pipe, trumpet extension, base plate, anchorhead with wedges, spanner nut, and epoxy resin, cement, or similar grout filler material. The strands are anchored in the anchorhead using a typical three-piece wedge system. The steel pipe is filled with the filler material under full dead load stress. Fluctuations in the total stay force due to live loads are transmitted from the strand through the hardened filler material to the steel pipe and into the bearing plate. This removes the fatigue-prone strand anchorages from cyclic load ranges. The ring nut is provided to adjust the tension in the stay. This anchorage system may be either preassembled under controlled conditions, or it may be assembled on site [1, 3].

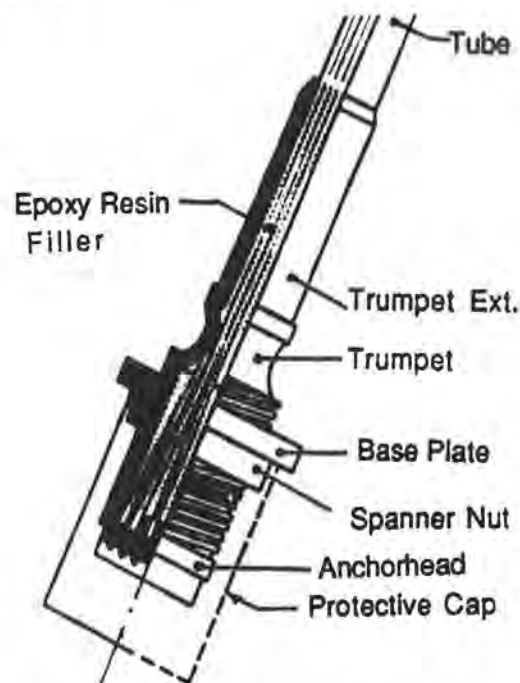


Figure 2.12 Wedge-trumpet anchorage details [3]

2.3.4.2 Wedge anchorage. Another manufacturer has developed a stay anchorage that is an adaptation of their anchorage system used in post-tensioning construction [9]. The system, shown in Figure 2.13, uses 0.6 inch diameter prestressing strand and consists of a bearing plate, anchorhead and two-piece wedges, polyethylene transition pipe and stay pipe, threaded coupler, reducer, steel tension ring reinforcement, and filler material. The threaded coupler connects the steel anchorhead to the polyethylene pipe. Each piece in the wedge is split, as shown in Figure 2.14, in an attempt to ensure a more uniform friction force around the strand. A reducer is provided at the junction of the transition and stay pipes to accommodate the flare in the strands as they exit the anchorhead. The steel tension ring reinforcement surrounds the reducer. The tension ring reacts against hoop stresses that are generated when the strand is tensioned. Adjustment of the stay tension is provided for at the stressing anchorage of the stay with a threaded anchorhead and ring nut. In this system relatively little transfer of cyclic load away from the wedge gripping region is possible, as the polyethylene pipe possesses relatively little tensile strength (typically 3500 psi at yield [10]) and forms a poor bond with the filler material. Tests conducted by the author on this stay system are described in detail in Chapter 5.

2.3.4.3 Wedge-stiffening tube anchorage with coated strands. A third strand anchorage technique has been proposed recently for use. Shown in Figure 2.15, it consists of the following main components: epoxy coated strands, steel tube extension, steel stiffening tube, anchor plate, anchorhead with wedges, steel shims, and filler material. The strands are anchored individually in the anchorhead using a special three-piece wedge system to grip the epoxy-coated strands. The steel stiffening tube is positioned with respect to the steel tube extension with machine screws. Under full dead load stress the steel pipe is filled with the filler material through the injection cap, and any fluctuations in total stay force due to live loads are transmitted from the strand to the hardened filler material and into the bearing plate through shear studs in the stiffening tube. With this alternative the shear transfer is mechanical rather than being dependant on the bond formed between the filler material and pipe. This transfers any superimposed cyclic load away from the fatigue-prone strand anchorages and into the steel pipes. The steel shims are provided to properly tension the stay. This anchorage system may be either preassembled under controlled conditions, or it may be assembled on site.

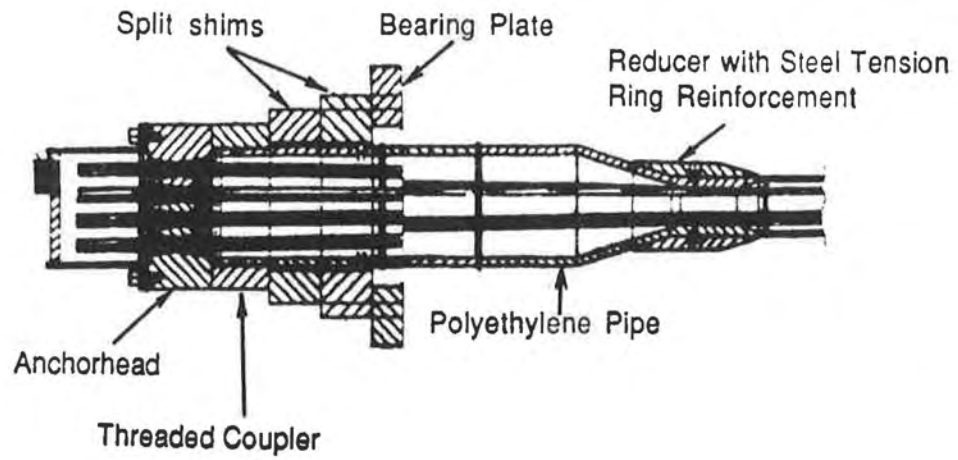


Figure 2.13 Wedge anchorage details [9]

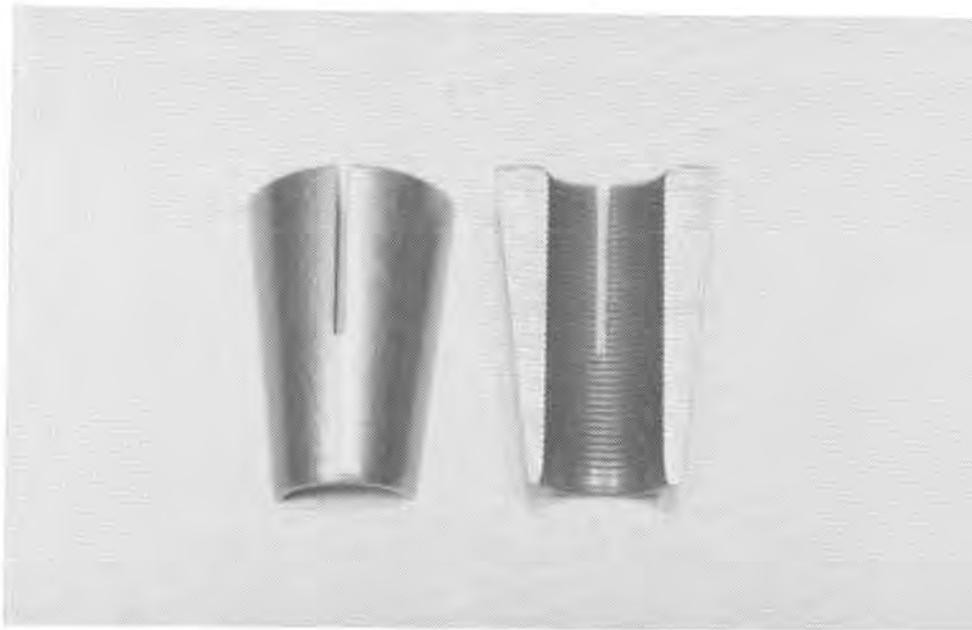


Figure 2.14 Two-piece wedge system for wedge anchorage

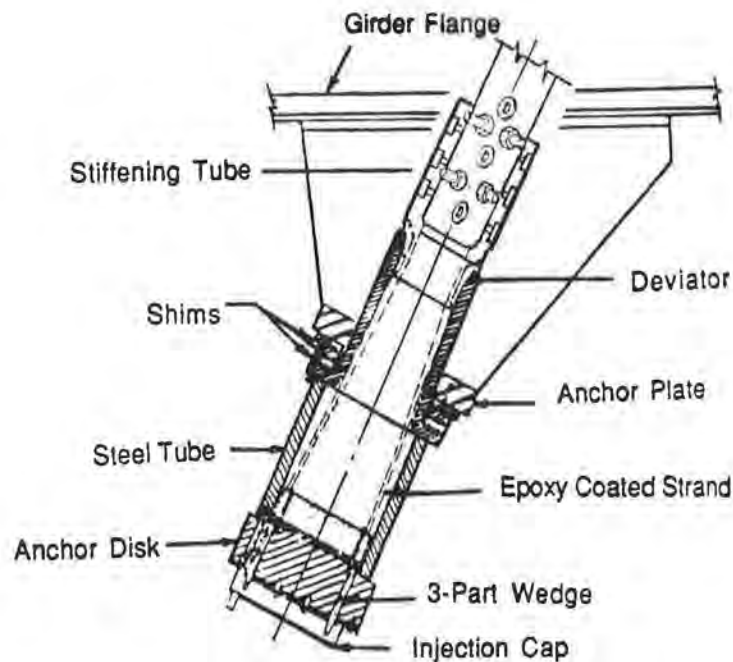


Figure 2.15 Wedge-stiffening tube anchorage with coated strands [11]

2.4 Corrosion Protection

Corrosion protection for stay cables is considered to be of paramount importance in the design of cable stay systems. Corrosion has significant adverse effects on the fatigue life of steel stay cables. These effects are discussed in more detail in Chapter 3. Many of the cable stayed bridges are built in coastal environments and subject to corrosion from salt-air. Others exist near centers of industry where airborne sulphur, phosphorous, and carbon monoxide are present. Even cable-stayed bridges situated in less taxing environments may be susceptible to corrosion problems due to the threat of what is generally referred to as "acid rain."

Recent worldwide interest has been paid to the problem of cable corrosion. This interest is due to the fact that many of the early and even recent cable-stayed bridges built are beginning to experience fatigue and corrosion problems, requiring in many instances complete replacement of the stays. In fact, the problem of corrosion appears to be serious enough that the Federal Highway Administration now requires the allowance for complete replacement of individual stays on new bridges [12, 13]. Because of the costs associated with replacement of an entire stay, designers are

turning to systems which allow for inspection and replacement of individual wires or strands. The end result of this requirement is that bridge designers are now specifying stays utilizing site-fabricated strand or threaded bar systems.

Selection of a corrosion protection system is generally a function of cost of the protection, weight of the protection (as this will increase the self-weight of the stay itself), the ease of individual wire or strand inspection and replacement, and operating environment. This section summarizes many of the commonly employed methods used for protecting stay cables in corrosive environments.

2.4.1 Tube protection systems. Most stay systems incorporate the use of tubing members as a portion of their corrosion protection scheme. The wire or strand bundle comprising the stay is inserted in a tube, which serves as an outer protective layer against corrosion. As an additional benefit, the drag forces on the stays produced by wind loading are minimized if the stay cables are encased in a smooth circular surface. The tubing also provides containment for corrosion-inhibiting filler materials, such as epoxy, wax, or cement grout, which encase the strand. The use of these corrosion inhibitors is discussed further in Section 2.4.2. The actual tubing members in a stay are normally comprised of either stainless steel or polyethylene.

2.4.1.1 Polyethylene pipe. Polyethylene pipe containing carbon black for protection against ultraviolet radiation is the most common cover for stays. Polyethylene provides excellent resistance to the diffusion of water vapor. Entire pre-fabricated stays encased by polyethylene pipe can be coiled and shipped to the jobsite for installation. Due to the bending stiffness of the completed stay, the coil must be of large radius, typically on the order of 15 to 20 feet for stay diameters of 4 to 5 inches [14]. The pipes can also be shipped in straight sections for site fabrication, where the pipes in the completed stay are connected with a butt fusion weld. Unfortunately, polyethylene also exhibits undesirable temperature-dependant properties; polyethylene has a high coefficient of thermal expansion, equal to 8×10^{-5} in/in/°F, as compared to 6.5×10^{-6} in/in/°F for mild steel and 5.5×10^{-6} in/in/°F for concrete. This difference in coefficients of expansion results in movement of the various stay components relative to each other. When this relative movement occurs, pathways at the interface of the pipe and filler material are opened which allow the intrusion of water and air. Additionally, the relatively low strength and temperature effects

on polyethylene leads to other problems. Louis Garrido, formerly with the Louisiana Department of Transportation, has reported on many splits in the polyethylene pipe protecting the Luling bridge stays. He states that grouting during hot weather which is sustained for some time, combined with brief periods of low temperatures, can result in longitudinal pipe splitting. Additionally, care of the polyethylene pipe must be taken during the stay stressing operation. Garrido goes on to say that cracking in the pipe near the back stays can also be attributed to overstressing of the stays during grouting [13].

2.4.1.2 Stainless Steel Tubing. Stainless steel tubes have an advantage in that their coefficient of thermal expansion equal to $9.9 \times 10^{-6} \text{in/in/}^\circ\text{F}$, similar to that of the rest of the stay. One disadvantage to the use of stainless steel ducts is that their large diameter-to-thickness (D/t) ratio allows the tube walls to inelastically deform, or kink, when bent to sharp angles. Thus the steel tubes must be transported to the jobsite in straight sections, where they are later joined together.

2.4.2 Filler materials. Generally the remaining voids inside the tube encasing the completed cable stay are filled with a filler material. The material completely encases the individual cables in the stay to prevent corrosion of the cables. At the present, this material consists of either cement grout, an epoxy resin, or petroleum wax. The material is injected into the tube at high pressure through vents in the anchorages or ports at various locations along the length of the stay. The material protects the strands by filling voids through which corrosive agents could otherwise attack the strand.

Cement grout has been used for a number of years as a filler material for bridge stays. Use of this protection system dates back to 1926, when the Spanish engineer Torroja constructed a guyed aquaduct of reinforced concrete, the stay cables of which were sheathed in concrete for corrosion protection [2]. With its alkaline properties, cement grout provides additional corrosion protection.

The grouting and curing procedure generally takes place with the completed stay in tension under the full dead load of the bridge deck. However, the generally poor tensile characteristics of cement grout lead to cracking when the tensile load of the stay is increased much beyond the prestressed grout load. These

cracks can provide pathways for various corrosive agents to attack the stay cables. An additional problem has been experienced with cement grout. Full scale static and fatigue tests of a stay using epoxy-coated strand were conducted in Germany for the Quincy Bayview Bridge [1]. The stay was pressure-grouted from the lower anchorhead with a cement grout for corrosion protection. Dissection of the specimen upon completion of the tests revealed significant fatigue damage at corroded areas in the wires. This is believed to be due to water from the grout penetrating the interstices in the strand at the cut end of the strand in the anchorhead. To eliminate this problem of intrusion in the field, additional protection measures were required. Epoxy painting of all cut strand ends was required, and plastic caps were attached to the ends with an epoxy sealing material [11].

Epoxy resins and petroleum waxes have also been proposed for use in stays. A lack of published data regarding their performance in bridge stays prevents further discussion, but both have been employed in various stay systems.

Only the wax protection system, when used with a wedge anchorage system, appears to allow for removal and inspection of individual strands in the stay. The cement grout and epoxy fillers develop significant bonding forces to the strand which prevent easy removal of the strands for inspection or replacement.

2.4.3 Individual wire/strand protection. Possibly the best way of ensuring the integrity of the stay cable is to galvanize its components. The galvanizing process coats the cable with a zinc layer which is resistant to corrosion. Galvanizing of individual wires in the locked coil strands or parallel wire stays has been employed with some degree of success. However, inspections of older bridges with galvanized stay cables [13] seem to indicate that galvanizing alone does not alleviate the problem of corrosion. Galvanizing of seven wire prestressing strand also shows promise. The anchorage regions must be well protected, though, as the strand will be exposed due to the biting action of the wedge teeth.

Yet another promising method for protection of individual strands is the use of epoxy-coated strand or the sheathing of each strand in an a polyethylene jacket. Epoxy-coated strands were used on the Quincy Bayview Bridge in Illinois [11]. These methods of protection have not been used extensively as the concepts are still relatively new. However, the methods prove promising for use where inspection

and removal are mandated. If the strands are sheathed in a polyethylene jacket, then the greasing of the strands prior to insertion in the jacket provides for easy inspection and removal, even in a cement or epoxy grout. Care must be taken to strip away the coating or jacket from the wedge gripping region, as the teeth must make sufficient contact with the strand; otherwise, slippage of the strand may occur. Special wedges were designed for the Quincy Bayview Bridge to ensure that the wedge teeth cut through the epoxy cleanly and came to bear on the strand [11].

2.4.4 Remedial protection systems. Plastic or polyurethane tape can be used to wrap the strands in a protective layer or to protect the stay tubes themselves. The concrete Post-Tensioning Institute, or PTI, recommends the wrapping of polyethylene pipe with PVF (Tedlar) tape to reduce temperature variations on the stay [26]. Tape alone is not recommended as a permanent measure of protection, however. Painting of the stay tubes or cable bundle may also offer nominal protection. It is also recommended by PTI that steel stay tubes are painted to help prevent corrosion and reduce temperature variations [26].

2.4.5 New techniques. A new technique for corrosion prevention of cables has been developed recently in Europe. The method, which is applicable to stays employing any type of cable system, uses a self-propelled machine which hermetically seals the cable group by winding and folding tinned copper around them. Acrylic foam is introduced into the fold to make an airtight connection. The machine first wraps the cable with a butyl tape and follows with the copper at a force of about 1000 pounds. The machine propels itself by using the folds of copper to push itself up the cable. The process also shows promise for rehabilitation purposes; test runs have been made at the Kurt Schumacher Bridge in Mannheim, West Germany [13]. However, the relative success of this test program has not yet been evaluated.

Another promising development involves the use of newly developed high-strength materials in place of steel as bridge stay cables. Composite spiral strands of Kevlar or glass fibers have also been developed which exhibit high strength, on the order of 210 ksi for Kevlar and 240 ksi for glass [15]. However they also have low elastic modulus values, on the order of 8400 ksi for Kevlar and 4800 ksi for glass. These values are based on strands composed of material rods with a 63%

unidirectional fiber content in a polyester resin matrix. Additionally, the costs associated with these materials are great. Data regarding the fatigue performance and corrosion resistance of these composites is not yet available.

2.5 New Developments in Cable Stay Systems

A new bundle type has recently been proposed which is essentially a variation of the parallel wire arrangement. Schlaich and Bergermann [16] have studied an improved version of the parallel wire bundle, utilizing either wires or strands, with no restriction on the overall bundle size or capacity. The stay is comprised of many of these bundles. The parallel wire bundle is twisted to a long lay length of 30 times the diameter of the individual wire or strand in the bundle to minimize any reduction in longitudinal stiffness of the completed stay. The twisting of these wires "ties" the bundle together, resulting in a compact surface which may then be coated with a polyurethane material for corrosion protection. This twist is held at the ends of the bundles by temporary anchorages. As an added benefit, the twisting of the wire bundle forces the wires to spread out uniformly and conically in the socket at the anchored end of the stay. This ensures a voidless cast down to the cone base. This type of anchorage is discussed previously in Section 2.3.1. The researchers state that an elastic modulus of the completed stay can be assumed to reach about 95% of the modulus of an individual wire.

2.6 Summary

To summarize the various cable systems, anchorages, and corrosion protection systems available for cable-stayed bridges, a brief literature survey was conducted by the author to chronologically list the various systems employed to date. The results of this survey, shown in Table 2.2, show a general movement away from systems specifying locked coil strands or parallel wires. Correspondingly, the movement also tends away from anchorage systems using hot-poured or Hi-Am anchorages. In general, more systems are being designed using seven wire prestressing strands with wedge-type anchorages. The growing trend appears to involve the utilization of cement grout in polyethylene tubes for corrosion protection. The driving force behind this trend is lower cost. However, as was shown previously in this chapter, the durability and difficult inspection of these systems is in question.

Table 2.2 Survey of Various Stay Systems in Use

Bridge	Stay cable	Anchorage	Corrosion protection
Main Bridge (West Germany) 1971	threaded bar	mechanical	encasement of stay in polyethylene pipe
New Galecopper Twin Bridge (Holland) 1971	locked coil	hot-poured	galvanized outer wires
North Bridge (West Germany) 1972	parallel wire	Ni-Am	wires embedded in polyurethane zinc-chromate, then wound by polyester film
St. Nazaire Bridge (France) 1974	locked coil	hot-poured	galvanized outer wires
Brotonne Bridge (France) 1977	parallel strand	wedge-type	encasement of stay in cement grout and steel pipe
Kawasaki-Bashi Footbridge (Japan) 1978	locked coil	hot-poured	painted coil
Pasco-Kennewick Bridge (USA) 1978	parallel wire	Ni-Am	encasement of stay in cement grout and polyethylene pipe, taping of pipe
Kohlbrand Bridge (West Germany) 1981	locked coil	hot-poured	galvanized outer wires, red lead filling inner wires, painted pipe
Tiber Bridge (Italy) 1981	parallel strand	wedge-type	encasement of stay in polyethylene pipe, sheathing of individual strands in polyethylene jacket
Tjorn Bridge (Sweden) 1982	locked coil	hot-poured	galvanized outer wires
Airport Hotel Footbridge (Hong Kong) 1982	parallel strand	wedge-type	encasement of stay in cement grout and polyethylene pipe
Morikoshi Bridge (Japan) 1984	parallel strand	wedge-type	encasement of stay in cement grout and polyethylene pipe
Sunshine Skyway Bridge (USA) 1986	parallel strand	wedge-type	encasement of stay in cement grout and steel pipe
Quincy Bridge (USA) 1987	parallel strand	wedge-type	encasement of stay in cement grout and polyethylene pipe, epoxy coated strand
Tampico Bridge (Mexico) 1988	parallel strand	wedge-type	galvanized strand, encasement of stay in petroleum wax and polyethylene pipe
Skytrain Crossing (British Columbia) 1988	parallel wire	Ni-Am	galvanized wires and encasement of stay in grease blocking compound
Dame Point Bridge (USA) 1988	threaded bar	mechanical	encasement of stay in cement grout and steel pipe
Charleroi Bridge (Belgium) (under construction)	parallel strand	wedge-type	encasement of stay in epoxy resin and polyethylene pipe, sheathing of individual strands in polyethylene jacket
Wandre Bridge (Belgium) (under construction)	parallel strand	wedge-type	sheathing of individual strands in polyethylene jacket and encasement of stay in stainless steel pipe

CHAPTER 3

TYPES OF FATIGUE AND FATIGUE TESTING

Failure of the bridge stay cables have principally come from three main sources: tensile failure of the cable due to overloading of the stays, corrosion of the cables, and fatigue failure of the cables due to cyclic loading during service. Tensile failures in cables are well understood; this type of failure was found to occur mainly in the early cable-stayed bridges, as discussed in Chapter 1. Under normal operating conditions this mode of failure is prevented from occurring. Corrosion-related failures have proven to be an on-going problem. The Maracaibo Bridge in Venezuela and the Kohlbrand Estuary Bridge in Germany required replacement of cables after only a few years of service because of severe corrosion [13]. The corrosion protection methods currently used are outlined in Chapter 2. Fatigue failures can occur under the normal design service conditions. Hence it becomes important also to prevent the fatigue failure mode. Prevention of this mode will help to ensure the integrity of the stay under normal working conditions and provide an adequate factor of safety against tensile failure under conditions of maximum loading.

Fatigue is a phenomenon common to all types of bridge stay cable systems. The intent of this chapter is to discuss the effects of fatigue on the two most commonly employed systems, the parallel wire stay and the parallel strand stay. The fatigue mechanisms common to both are discussed below. Finally, a discussion of the typical testing to assess cable fatigue resistance is also presented.

3.1 Wire Fatigue

Fatigue failure in a wire occurs when a fatigue crack initiates and propagates through the cross-section to such a point that the stress in the wire exceeds its ultimate tensile strength. The result is a sudden type of failure, which occurs in shear. The wire fatigue crack and subsequent failure generally occurs as the result of a stress concentration at that point. These stress concentrations are due to

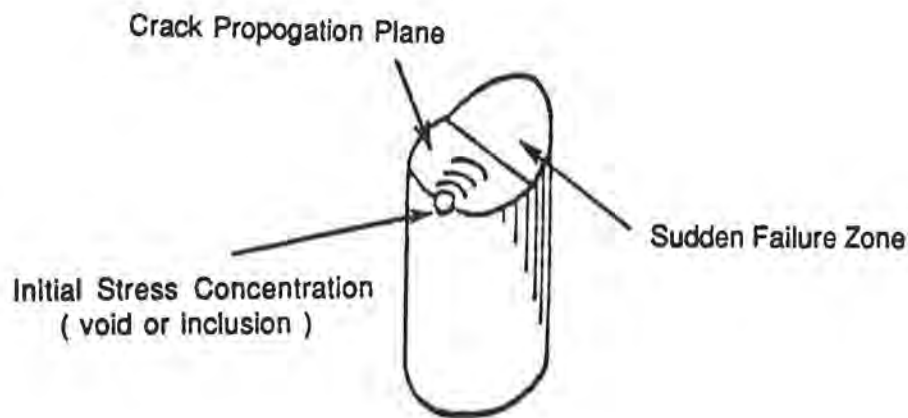


Figure 3.1 Fatigue crack initiation in wire [7]

the presence of surface defects. The initiation and propagation of a fatigue crack through the wire is shown in Figure 3.1.

The most significant factor resulting in a decrease of wire fatigue life is the surface defect [7]. The types of surface flaws most common in a wire are:

1. textural and metallurgical flaws
2. shape defects or flaws due to the manufacturing process
3. mechanical damage incurred after manufacturing
4. corrosion damage

Textural and metallurgical flaws are due either to chemical anomalies in the wire structure or the wire drawing process. Textural flaws are those that appear as the result of decarburization of the wire. In addition, the use of dirty drawing dies can result in the undesired inclusion of carbide inclusions, ferritic stringers, or inorganics.

Manufacturing defects, the most common of the types of surface defects [7], are the result of poor wire handling during the manufacturing process. Cracks may occur either at kinks in the wire or may occur directly as a result of the drawing process.

Post-manufacturing defects are characterized by nicks or notches which occur after the wire has left the die. Inspection of the wire before it is placed in the stay group should provide a measure of safety against inclusion of post-manufacturing defects.

Corrosion or rusting causes surface roughening and pitting in the wire. Corrosion is a serious problem as it occurs as a result of environment, and so all of the wires in similar storage or use are susceptible as well. Corrosion, besides attacking the wire surface, also penetrates the crack as well and forces the crack to open. The volume of the corroded particles in the crack expands with continued oxidation, forming a wedge which forces the crack to deepen.

3.2 Fatigue in Parallel Wire Stays

With regard to parallel wire stays, fatigue studies of completed stays with Hi-Am anchorages have generally demonstrated the random nature of wire fatigue failures along the entire stay length [17, 18, 19, 20]. However, parallel wire stays with hot-poured anchorages exhibit poor fatigue behavior near the anchorage zone.

The degrading effects of hot-pouring on the ultimate strength of wires near the anchorage zone have already been discussed in section 2.3.2. Furthermore, these studies have shown that the consequences of hot pouring extend to the fatigue resistance of the wires as well [1]. Studies conducted on parallel wire stays with zinc-copper alloy anchorages for the Toyosata-Ohashi Bridge in Japan have demonstrated the effects of hot pouring temperature on wire fatigue life. The study results, which shows a marked decrease in fatigue life for an increase of pouring temperature from 450°F to 480°F, are shown in Figure 3.2.

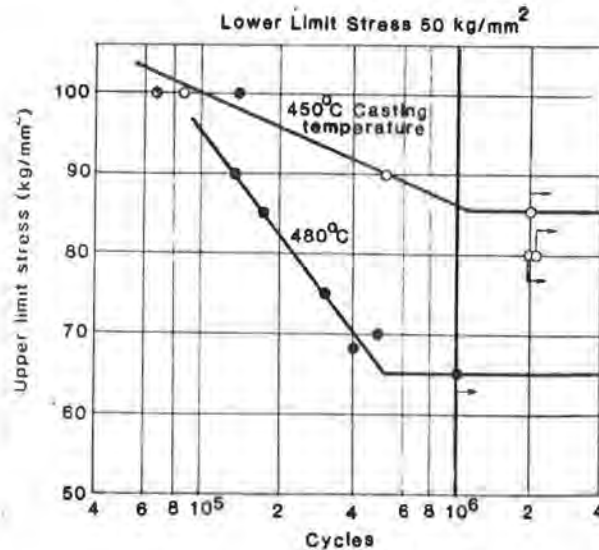


Figure 3.2 Pouring temperature vs. wire fatigue life [1]

3.3 Fatigue in Parallel Strand Stays

The problem of fatigue also exists in stays comprised of seven wire prestressing strands. The mechanisms acting to produce fatigue failures in strands are similar in many respects to those acting on the single wire. Surface defects are the prominent cause of failure in strand as well and are present for the same reasons. With strands, the more complex distribution of stresses in the helically wound wires must also be taken into account. In addition the interaction of the individual wires in the strand must also be examined. A discussion of these stresses and interactions is presented by Dykers [7].

Both single prestressing strand and parallel strand stays have been shown through testing to be fatigue-prone in the anchorages [1, 21, 22, 23]. These stays employ friction-type anchorages to anchor each strand individually, as shown in Figure 3.3. The anchorages rely on wedging action and generally consist of three main elements: the strand, wedge (typically two, three, or four pieces), and the strand group anchorhead. Tensile load in the strand is transferred to the wedges and then into the anchorhead. Transfer of the strand tensile force takes place mechanically in

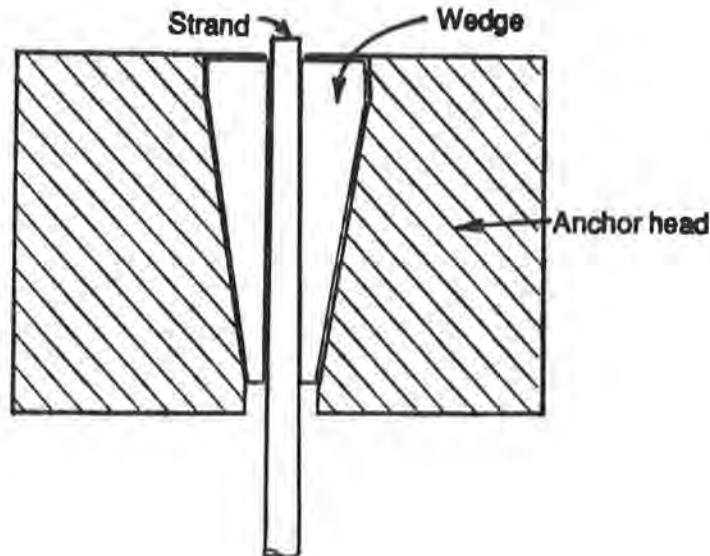


Figure 3.3 Friction-type anchorage system for strand

the wedge teeth through serrations in the strand. The strand serrations are caused by the wedging action which takes place between the wedges and the strand. Thus a weak link develops in the strand in the form of a stress concentration due to the presence of a notch in the strand. The weak link is further agitated by relative movement of the separate components under conditions of cyclic loading.

The relative movement of these components produces a type of fatigue referred to as "fretting." Fretting is considered to be an extension of the adhesive and abrasive wear theories, and may take place through a variety of mechanisms. A discussion of these mechanisms is beyond the scope of this thesis but studies by Yates [24], Wollmann [25], and Lamb and Frank [22] provide a treatment of the subject.

In general, though, a fatigue crack in a strand wire will initiate and propagate at the point of abrasion caused by the wedge teeth. The crack will continue to propagate until such a time that the shear failure mode occurs.

3.4 Fatigue Testing of Wires, Strands, and Stays

Many types of tests have been proposed and used to study the effects of loading on wires and strands or complete stays for cable-stayed bridges. However, the most influential parameter on fatigue life has been found to be the stress range. The constant amplitude fatigue test is the accepted test for studying the effects of stress range on fatigue life. It is conducted by imposing a mean level of stress and then superimposing a stress range of constant amplitude. The stress range chosen for use in testing is dependent to a large extent on the ranges that will be experienced by the actual stay in service on the bridge. For instance, if the bridge deck is made of reinforced concrete, then the dead load may be quite high and the magnitude of the live load due to traffic may be only a small fraction of the dead load. In this case the mean stress will be relatively high, but the stress range may be quite low and the fatigue life great. Conversely, in a bridge with a steel deck, the dead load-to-live load ratio may be smaller. Thus the mean stress will be comparatively lower, and the stress range will increase, resulting in a shorter fatigue life.

PTI has recommended guidelines for the fatigue testing of stays and stay cable material, which are outlined in Table 3.1 [26]. Their recommended guidelines for testing are based on the constant amplitude fatigue test. PTI recommends various minimum stress ranges and cycles to be used in testing the cable material, depending on both the type of stay material and whether or not the structural application follows a redundant load path. With respect to fatigue testing of stays, an acceptance criteria is established by PTI of less than two percent failure of the individual wires in the stay. Following the fatigue test, the stay should be loaded statically to a value not less than 95% of the actual tensile strength of the cable material. In addition to axial stresses, certain flexural stresses exist in bridge stay cables due primarily to wind loading, bending at saddle connections in the tower (if they are used), and eccentricities due to uneven tensioning. Therefore, it is also recommended by PTI that any flexural stress range in excess of 3 ksi shall be added to the axial fatigue stress range due to live load plus impact.

In the following chapter the results of many tests are presented, all of which use the constant amplitude fatigue test as their basis for comparison.

Table 3.1 PTI Recommended Testing Guidelines

SUMMARY OF FATIGUE STRESS RANGE VALUES, F_r (ksi)^(a)

Type of Stay	No. of Cycles (b)	Allowable Design Fatigue Stress Range		Stay Test Fatigue Stress Range (c)*	Component Fatigue Test Stress Range (d)*
		Redundant Load Path	Nonredundant Load Path		
Strand (e) or uncoupled bars (f) AASHTO Category B	$2 \times 10^6 +$	16	16	23	26
	2×10^6	18	16		28
	5×10^5	27.5	18		37.5
	1×10^5	45	27.5		55
Wire (g) AASHTO Category B plus 5 ksi	$2 \times 10^6 +$	21	21	28	41
	2×10^6	23	21		43
	5×10^5	32.5	23		52.5
	1×10^5	50	32.5		70
Bars (f) with (epoxy filled) couplers AASHTO Category D	$2 \times 10^6 +$	7	5	15	17
	2×10^6	10	7		17.5
	5×10^5	16	10		23.5

(a) Any flexural stress range in excess of 3 ksi shall be added to the axial fatigue stress range due to live load plus impact.

(b) See Table 10.3.2A

(c) To ensure fatigue quality of stays, it is recommended that the stay specimens be tested at 2×10^6 cycles.

(d) Individual strand, bar, wire; or glued, coupled bar, respectively.

(e) See Section 3.2.2.

(f) See Section 3.2.3.

(g) See Section 3.2.1.

* Upper bound stress level shall be $0.45 F_u$.

CHAPTER 4 PREVIOUS TESTS

As was mentioned previously in Chapter 1, research in the field of stay cable anchorage systems has long been conducted by organizations such as EMPA and the Technical University in Munich. The Japanese have also conducted tests on anchorage systems, as was discussed in Chapter 3. In the U.S. much of this research has been conducted by Ferguson Laboratory (FSEL) at The University of Texas at Austin. Because an abundance of data from the tests conducted at FSEL was readily available the author chose to concentrate on those tests. Numerous tests on seven wire prestressing strand have also been conducted at FSEL. Many of the studies were performed with prestressing and post-tensioning applications in mind; however the results of these studies have also led to a better understanding of the fatigue mechanisms and projected service life of cable stay systems using seven wire prestressing strand.

It is the intent of this chapter to discuss some of these strand and stay tests. Particular attention is paid to the testing apparatus, results, and applications to stay cable anchorage systems.

4.1 Strand Tests

Tests conducted by Paulson, Frank, and Breen, and Lamb and Frank are discussed in this section. In both studies, the same testing apparatus was used and is described in this section.

4.1.1 Testing apparatus. A test system concept developed previously for a cable stay fatigue study [17, 18] was used for the single strand static and fatigue tests in this chapter. The test system consisted of a centerhole ram and extension chair with a hollow load cell to allow passage of the strand through the system. The strand was anchored with grips at both ends. This arrangement (shown in Figure 4.1), when centered with interface discs, ensured that all elements of the load system were either in tension or compression; essentially no moment was introduced into the

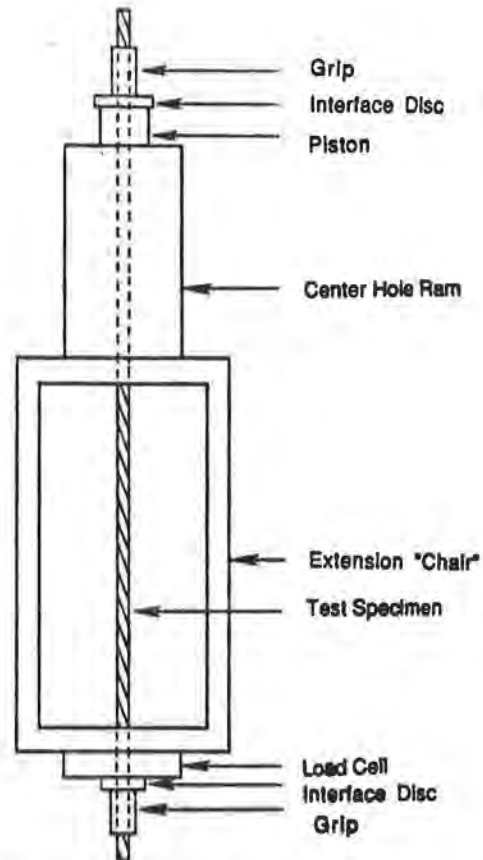


Figure 4.1 Strand fatigue setup [21]

system. The load control system used was a closed-loop hydraulic servo-controlled system.

4.1.2 Paulson, Frank, and Breen. Paulson, Frank, and Breen developed a data base which contained results of published fatigue studies of prestressing strand, in addition to their own series of fatigue tests [21]. Using regression analysis techniques, a stress range vs. fatigue life, or S-N, curve for prestressing strand was developed, which was used as the basis for a strand fatigue design equation. The design equation developed was compared with then-current AASHTO specifications for structural steel and was found to lie midway between Category A and Category B curves for redundant structures (a redundant structure is defined by AASHTO

as one with multiple load paths where a single fracture in a member cannot lead to collapse of the structure [27]).

4.1.2.1 Test method. Premature failure of the strand in the grip region due to indentation of the strand by the jaws of the grip was undesirable. The purpose of these tests was to determine the fatigue strength of the strand in air rather than in the wedge gripping region. Hence, proper gripping of the strand was of great importance. To alleviate the problem of premature grip failures, the strand was first prepared by placing at each end of the strand soft iron wire inlays (0.1 inch diameter), which were predeformed to match the grooves between the outer wires of the strand. The strand ends were then wrapped with aluminum foil to prevent the jaw serrations from biting into the strand. As the protective measures employed increased the diameter of the strand in the gripping region, the strand was gripped with an oversized chuck. This protective method of gripping, shown in Figure 4.2, performed satisfactorily. Strand slippage still tended to occur at high load levels and some strand failures still occurred in the grip if the proper number of aluminum foil layers were not used. As an improvement upon the protective measure employed, the strand was gripped with a double chuck system, as shown in Figure 4.3. The strand in the primary chuck was prepared with the aluminum foil and wire inlays and the strand in the secondary chuck was left unprotected. Using this system of gripping, any slippage that occurred in the primary chuck would force the secondary chuck to bear down on the wedges protruding from the lower chuck. This would force the wedges in the primary chuck to seat even further. This new preventative measure performed well throughout the remainder of the tests, eliminating the slippage problem.

The strands were cut to a length of about 72 inches for installation in the test setup. Their test lengths varied between 48 and 55 inches.

Cyclic loading of the specimens was conducted until a wire fatigue failure in the strand occurred. The fatigue tests were conducted at a frequency of 3 to 12 Hz, depending on the amplitude of the desired stress range, specimen response, and centerhole ram being used.

4.1.2.2 Results. The results of this study indicated that the fatigue of strand varies according to the manufacturer and also among the strand from a single

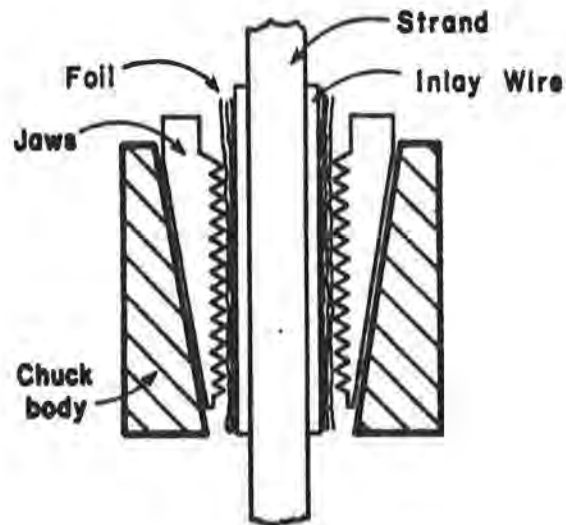


Figure 4.2 Protective gripping measure employed [21]

manufacturer. In current prestressed girder construction, no fatigue requirements are imposed on the strand. Therefore, the fatigue performance of the strand used in girders is unknown. In order to provide a conservative fatigue design stress for the strand, a lower bound approach was taken to account for the variability of fatigue performance due to manufacturing variables and length effect in the sample. Paulson, Frank, and Breen proposed the following relationship between stress range and strand fatigue life:

$$\text{Log } N = 11.0 - 3.5 \text{ Log } S$$

where

$S =$ fatigue stress range in ksi

$N =$ number of fatigue cycles

Their suggested model is shown, along with all the failure points upon which it is based, in Figure 4.4.

This relation is also plotted in Figure 4.5, along with the AASHTO specifications for Category A and B structures.

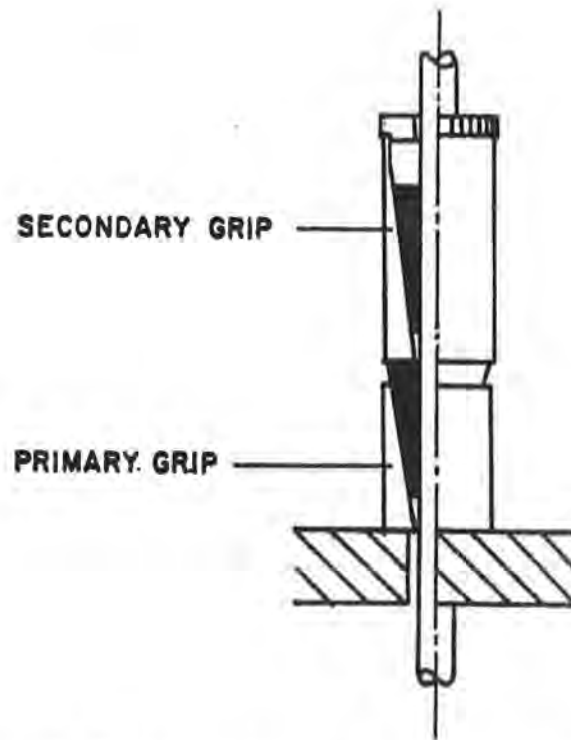


Figure 4.3 Double chuck system for anchoring strand [21]

Then-current ACI Committee 215 recommendations for cracked girders were that the strand stresses be kept below 10% of f_{pu} , or 27 ksi for Grade 270 strand for all girders, regardless of the expected number of cycles likely to be seen throughout its life. Although Committee 215 does not make this distinction between the number of cycles in their design recommendation, Paulson, Frank, and Breen assumed this to be a fatigue limit recommendation; that is, this is an allowable stress range which precludes strand damage due to wire fatigue. Their recommendation that uncracked girder fatigue be treated by AASHTO Category B fatigue design steel stresses for redundant load path structures was intended to provide a conservative design recommendation which meshes with overall highway structure design practices. Category B values allow higher stress ranges for lightly traveled bridges and progressively lower stress ranges for more heavily traveled bridges.

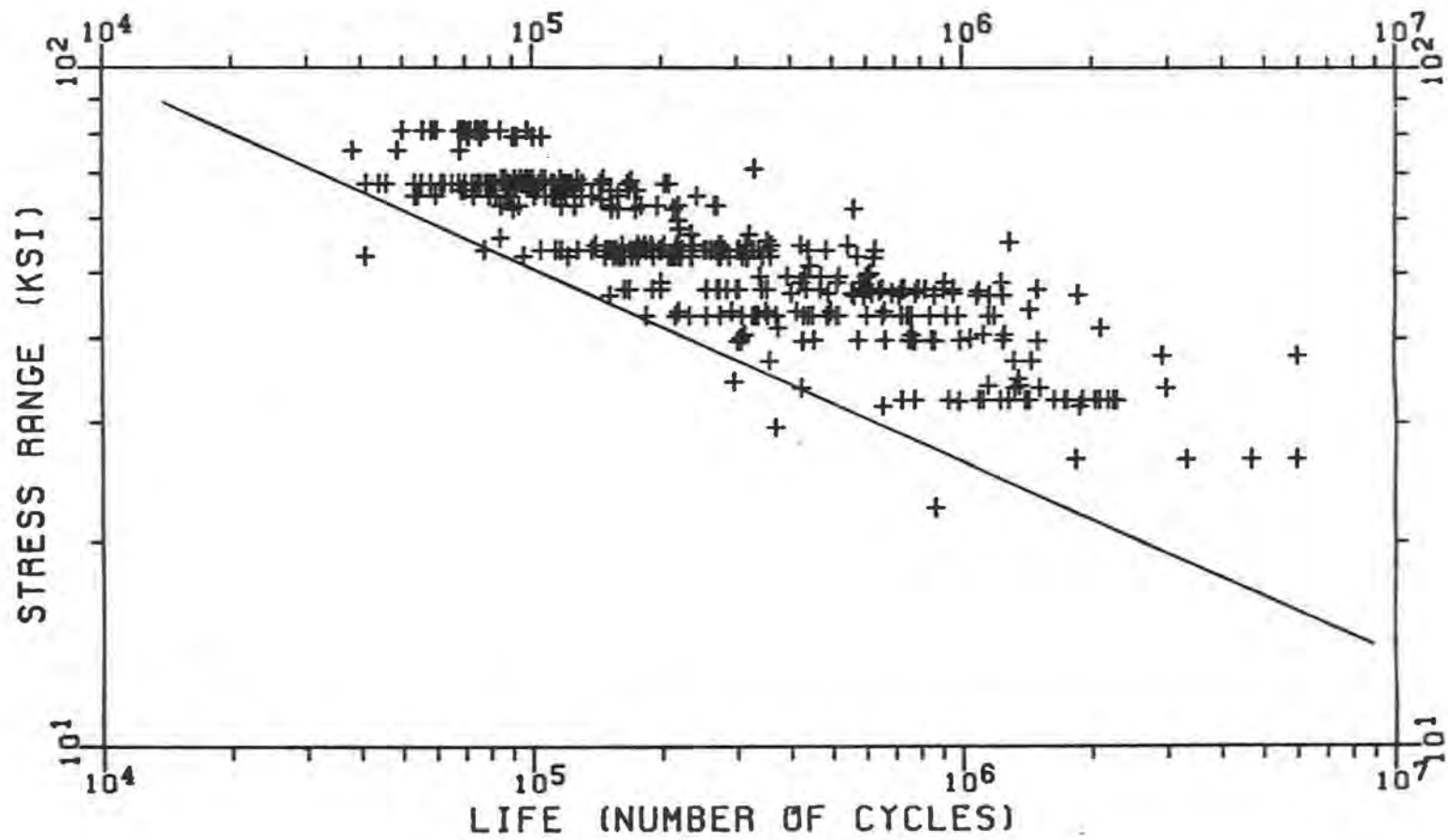


Figure 4.4 Design model and its test data, recommended by Paulson, Frank and Breen [21]

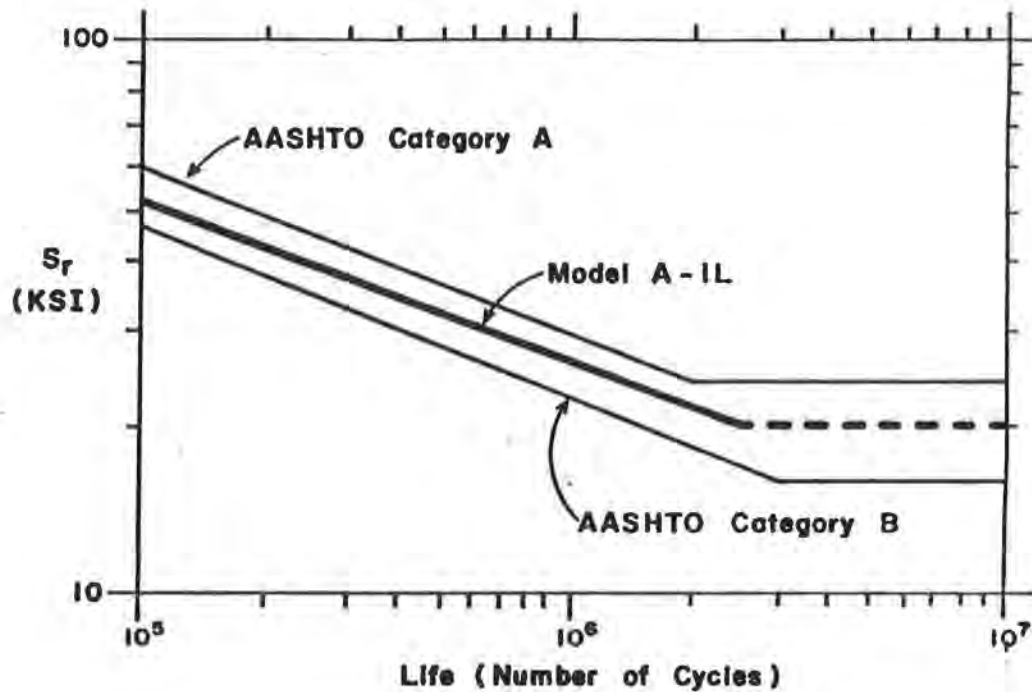


Figure 4.5 Developed S-N curve versus AASHTO Category A and B curves [21]

Category B was recommended for checking the allowable fatigue stresses in cracked girders. Designing to this category would provide an extreme lower bound to all the strand data collected and would preclude the possibility of fatigue problems regardless of the strand size, strength, and relaxation characteristics. Their results also indicated that Category B was satisfactory as a basis for designing other strand tension systems, such as cable stays, when considering the design service life of the strand. It was noted, however, that for cable stays the fatigue performance of the socketing or grip system must be evaluated separately.

4.1.2.3 Applications to cable stays. Again Paulson, Frank, and Breen concluded that a direct application of the study's results to cable stays is

appropriate, as the type of loading seen by the stays is identical to the type of loading applied to the specimens in their analysis.

The problem arises, however, in establishing the credible fatigue load to consider. Their solution was to base design of redundant cable stays on the values given for AASHTO Category B. If the stay is nonredundant, then the higher Category B values for nonredundant load path structures should be used. This approach ties the design of such members to the general AASHTO approach and allows some flexibility in design according to expected traffic frequency and loading type, as mentioned earlier.

The authors pointed out that the recommended model put forth in this paper is based on tests of strand from many different sources, and represents lower bound fatigue behavior of the samples tested. Strand used in bridge stays is often supplied by a single manufacturer, but may be from many coils and different manufactured lengths of strand. It is most likely that the proposed design model will be a lower bound representation of the strand used, but if the strand has unusually poor fatigue characteristics due to manufacturing processes, the design model suggested may not be sufficiently conservative and the stays may fail unexpectedly. In other cases, the designer may wish to base design on higher stress ranges than given by the lower bound model. A solution to these situations recommended by Paulson, Frank, and Breen was to require testing of samples of the strand to be used in the stays. At least one sample should be obtained from each manufactured length of strand actually used to construct the stays. The tests should investigate both the fatigue life at the maximum expected stress range and also fatigue life at the assumed threshold stress range. The tests should be conducted at the highest expected minimum stress and the tests should not be considered run out until ten million cycles have been reached. Because the fatigue strength of a test specimen decreases with a corresponding increase in specimen length [28], they should be of the longest practical length, but not less than 4 feet. From each sample obtained, at least three specimens should be tested at both the high and low stress ranges. The results of these tests would indicate whether or not the strand was of a consistently poor quality, and fell below the lower bound curve for Category B structures.

4.1.3 Lamb and Frank. Conducting fatigue tests on prestressing strand is difficult because of the frequent occurrence of premature failures in the anchorage

zone rather than the free length of cable. A fatigue-resistant anchorage for seven wire prestressing strand was developed and studied by Lamb and Frank [22]. Their results of strand fatigue tests indicate that a dual anchorage system—using copper or aluminum wedges in the primary grip, which have been formed to match the strand, and a secondary grip composed of standard prestressing wedges—produce an anchorage which can attain the fatigue strength of the strand.

The fatigue test results were correlated with load distribution measurements, finite element analysis, electron microscopy of the fractures, and various wear models. The studies and correlations of Lamb and Frank have resulted in a better understanding of the factors relating to the fatigue performance of the wedges studied.

A further optimization of the anchorage was possible based on the results of the theoretical studies; however, the dual anchorage as developed using copper wedges in the primary grip proved to be adequate.

Additionally, Lamb and Frank considered the developed anchorage to be equally applicable to stay cable anchorages. Their developed anchorage can improve the fatigue resistance of strands in stay anchorages as well. Their developed anchorage also allows for individual insertion and removal of the strands making up a cable stay.

4.1.3.1 Test method. The test setup and procedure for the fatigue of single strands using these anchorages was identical to that used by Paulson, Frank, and Breen and is shown in Figure 4.1. Similarly, the strand was anchored with the double grip system as shown previously in Figure 4.3. One-half inch and 0.6 inch diameter Grade 270 strand were chosen for the study.

To examine grip behavior, wedges of identical dimensions but different material types were fabricated for this research. Three-part wedges made of 2024 alloy aluminum, copper, and 4340 alloy steel were chosen for the primary grips in tests on the 0.5 inch strand. The general configuration for the wedges was modeled after Supreme Products Jaw Number 638. The wedge materials used in testing the 0.6 inch strand were mild steel, hardened (heat-treated) steel, and tungsten carbide-coated steel. The strands were anchored using a two-piece wedge system.

The design of the aluminum, copper and steel wedges was based on the principle that plastic deformation of the wedge material should be allowed to occur in order to provide a larger contact area between the strand and wedge. For this reason, the wedges were designed with serrations on the interior surface so that large contact stresses would form at the wedge tips upon application of the tensile stress in the strand. The large tip contact stress would lead to plastic flow of the wedge material along and around the exterior wires of the prestressing strand resulting in a better distribution of stress along the strand. In addition, the use of "undeformed" and "pre-deformed" wedges was investigated. Pre-deformed wedges are defined as wedges whose serration pattern has already been plastically deformed from previous tests; undeformed wedges are wedges which have not previously been tested.

The fatigue tests were conducted for the strand using different wedge materials at various stress ranges and frequencies. Static and cyclic load distribution tests were also conducted to determine the extent of load sharing between the primary and secondary grips for each of the different wedge materials tested. A centerhole load cell, placed between the primary and secondary grips, measured the amount of load carried by the secondary grip. The difference between the total applied tensile load and that sensed by the load cell was the load carried in the primary grip.

4.1.3.2 Results. The results of the fatigue and load distribution tests indicate that both pre-deformed copper and aluminum wedges are capable of providing an anchorage which allows the strand to reach its specified fatigue strength. These results are summarized in Figure 4.6. Additionally, the difference in strand fatigue strength obtained with the undeformed and pre-deformed wedges is shown in Figure 4.6.

The contact area between the pre-deformed wedges and strand was assessed during the static load distribution tests through the use of a "Contact Ratio" (CR). The contact ratio was defined as the ratio of the actual area of wedge/strand contact to the total outer surface area of the strand in the grip region. The contact ratios and the inferred tensile strengths (based on hardness tests) of the wedges for the aluminum, copper, and steel wedges are shown in Table 4.1. The values for mild and heat-treated steel wedges were not determined, although some plastic deformation of the wedges did occur. It is noted that the contact ratio increases with decreasing inferred tensile strength (hardness).

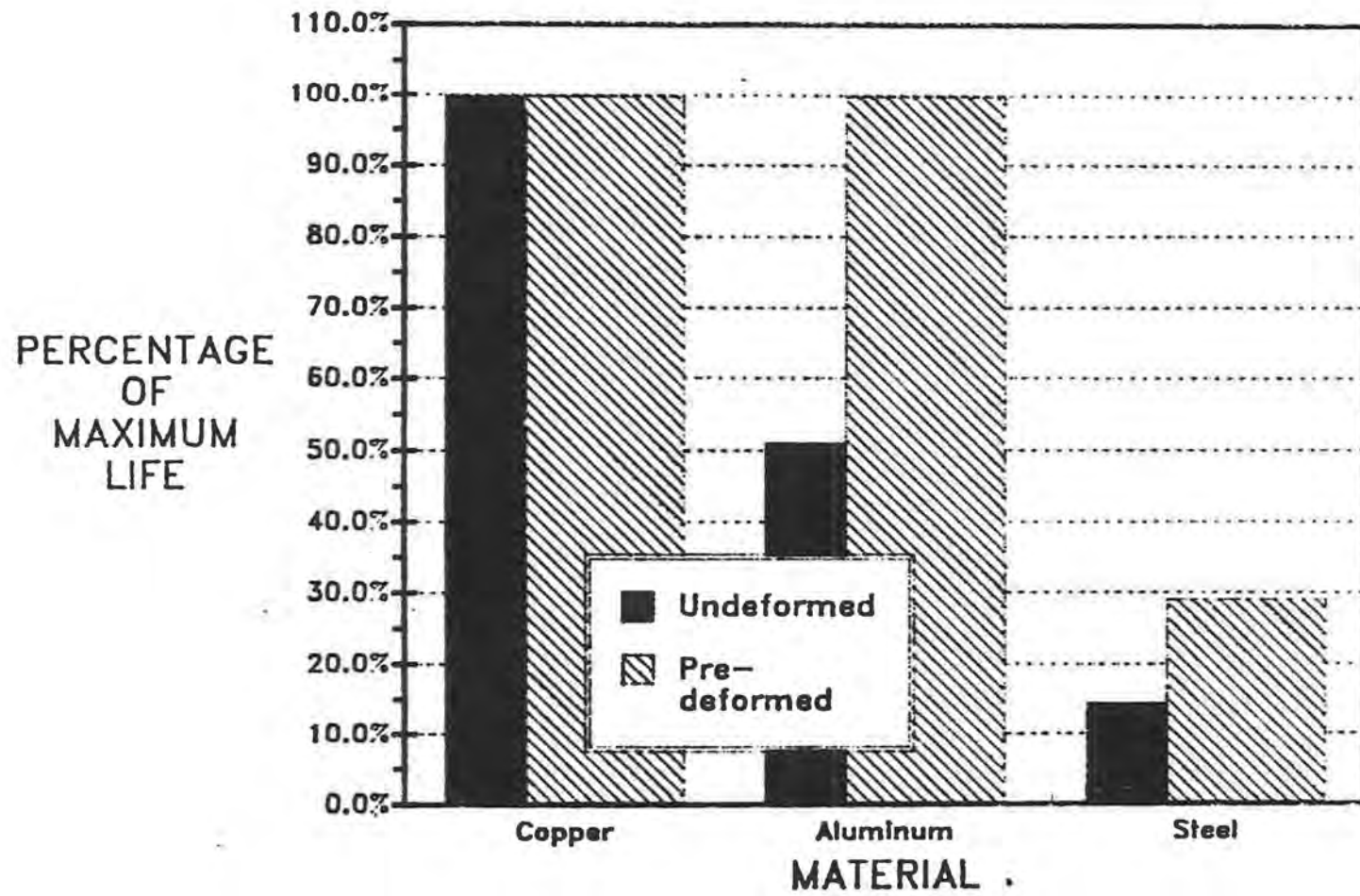


Figure 4.6 Effect of wedge type on fatigue strength for tests, 33.8 ksi stress range [22]

Table 4.1
Contact Ratios [22]

Material	Inferred F_u , ksi	CR
Copper	40.4	0.60
Aluminum (2024)	77.0	0.41
Steel (4340)	230.0	0.30

In general, the wedges made of materials with the greater hardness produced the lower strand fatigue lives. The reason for this is fairly straightforward; harder materials tend to deform less and, as a consequence, their serration patterns are more effective in providing frictional resistance. As a result, primary grips composed of harder materials carry more of the total strand tension than primary grips of “softer” materials. This is evidenced through the use of a “load distribution ratio,” or LDR. The LDR is defined as follows:

$$\text{LDR} = T_{p_{\max}} / T_{\max},$$

where $T_{p_{\max}}$ is the maximum load transferred by the primary grip to the secondary grip, and T_{\max} is the maximum load applied to the strand. Table 4.2 summarizes LDR values for each material used in the static load distribution tests.

As is shown in Table 4.2, pre-deformed copper wedges offer the lowest LDR of all the wedges used in testing. Results of the fatigue load distribution tests, shown in Figure 4.7, demonstrate the influence of the grip LDR on strand fatigue resistance. Load distribution tests were not performed using pre-deformed heat-treated or mild steel wedges since fatigue tests were not performed on the 0.6-inch diameter strand with these wedges. Load distribution data is not available for the tungsten carbide-coated wedges either. They did not deform plastically and produced early strand tensile failures before any fatigue load was applied.

In summary, the fatigue performance of strands anchored with wedges of soft primary grip material was far better mainly because of the lower frictional and

Table 4.2

Summary of LDR values established in static load distribution tests

Material	Wedge	LDR
Copper	undeformed	0.53
	pre-deformed	0.27
Aluminum (2024)	undeformed	–
	pre-deformed	0.43
Steel (4340)	undeformed	0.63
	pre-deformed	0.57
Mild Steel	undeformed	0.51
	pre-deformed	–
Heat-Treated Steel	undeformed	0.67
	pre-deformed	–

normal contact stresses resulting from the greater distribution of load in the primary grip. This conclusion was verified in the finite element study. A parametric study using finite element analysis demonstrated that any increase in the stiffness of the primary grip, due to either a change in modulus or geometric dimension, increased the contact stresses on the strand.

4.1.3.3 Applications to stay cable anchorages. Since each strand in a cable stay is individually anchored, Lamb and Frank believed that the results of this research should apply as well to cable stay applications using seven wire prestressing strand. However, certain factors must be taken into account which stray from the conditions under which the research was conducted.

A reduced strand fatigue strength should still be expected with the stays due to the length effects, mentioned previously in Section 4.1.2.3. Because the length effect applies only to the free length of strand, the beneficial effects of any changes made to the anchorage are correspondingly negated.

Another factor pointed out by Lamb and Frank for consideration is corrosion of the anchorage region. Cable stays are often used on bridges in salt-air

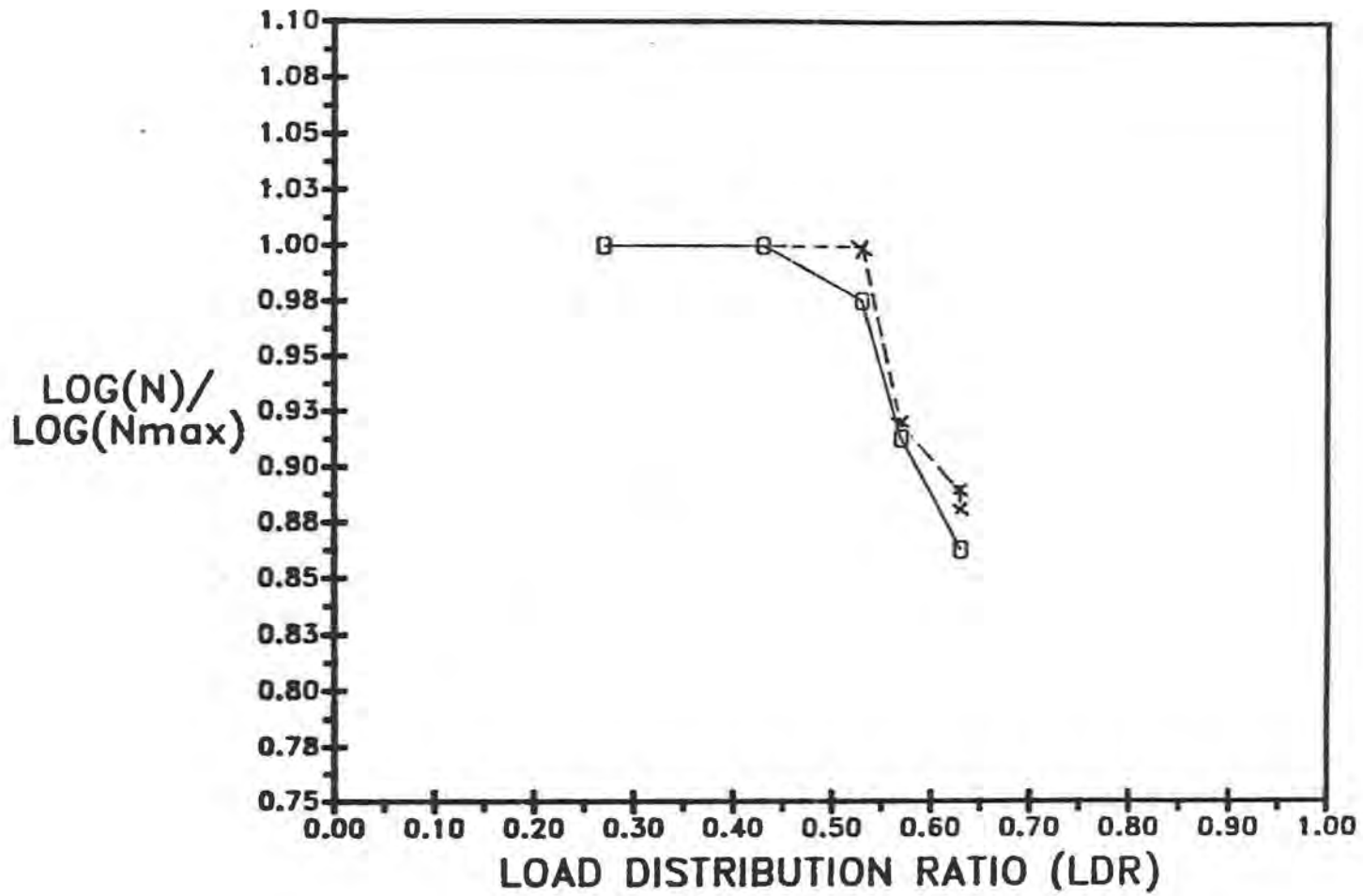


Figure 4.7 $\text{Log}(N)/\text{Log}(N_{\text{max}})$ versus LDR for 47.2 and 33.8 ksi stress ranges [22]

environments. Therefore the use of copper or aluminum wedges in the anchorage could lead to serious corrosion problems unless the anchorage and/or wedges are properly treated.

The beneficial effects of initially overtensioning the strand will also improve the fatigue resistance of the anchorage gripping region. Overtensioning forces the secondary grip to carry more of the load in relation to the primary grip when the load in the strand is reduced to the in-service maximum.

A final benefit to the use of single strand anchorages in cable-stayed bridges is the ease of maintenance and replacement of individual strands. This, of course, would only be possible in stays encased in a grease or similar non-binding anti-corrosive agent, rather than cement grout.

4.2 Parallel Wire Stay Tests

The nature of the tests outlined in this section were essentially verification tests of parallel wire stays with Hi-Am anchorages proposed for use on actual cable-stayed bridge projects.

4.2.1 Testing apparatus. The testing apparatus used in the Pasco-Kennewick and Luling stay tests are essentially the same, however certain differences exist which are described below.

4.2.1.1 Pasco-Kennewick stay tests. Force during the creep and ultimate strength test was applied with a centerhole ram. The fatigue portion of the test was conducted using a 50 in³ Riehle Los pulsator. A 1.5 million pound center-hole load cell was mounted in series with the ram to measure the applied force during each test. An extension was placed at the bottom of the ram to increase the length of the loading system to 100 inches. Split washers were placed between the sockets, load cell, ram, and extension to connect and center the various components. The entire setup was supported on a braced tripod frame. The specimen was installed by lowering it through the centerhole ram, load cell, and extension.

Test instrumentation for the static tests consisted of a digital strain indicator for measuring load cell output and strain gage readings, dial gages to measure end

plate and buttonhead movement, and direct current variable differential transformers to measure specimen elongation. Output of biaxial strain gage rosettes mounted on the socket castings of the second specimen was recorded on an analog-digital recording system and reduced with a personal computer. Loads during the fatigue test of the second specimen were monitored with an amplitude measuring module and oscilloscope. The programmed load input and load cell output were displayed on the oscilloscope, and the programmed load was adjusted as necessary.

Wire breaks in the second specimen during the fatigue test were monitored with a velocity transducer and strip chart recorder. The transducer amplified noise in the system caused by a wire break to produce a pulse on the recorder. The speed of the strip recorder was constant; therefore the cycle at which a pulse was recorded could be determined from the recorder travel speed and the testing frequency.

Both specimen tests were conducted in the order shown above. During all phases of testing the load, end plate and buttonhead movement, and socket strains were monitored as described previously.

4.2.1.2 Luling stay tests. The testing apparatus used in the Luling stay tests was identical to that used in the Pasco-Kennewick tests, with the following exceptions, which are discussed below.

All specimens, with the exception of the 311 wire specimen, were fabricated with 1.5 million pound centerhole load cell between the sockets. Loads were applied using centerhole rams with varying capacities, depending on the magnitude of the test load. The loads in all tests but the 103 wire specimen were measured using pressure transducers as the loads in those tests exceeded the capacity of the centerhole load cell. Loads during the fatigue portion of the tests were controlled with a servo controlled closed-loop system. These loads were monitored throughout the tests with an amplitude measurement module with digital readout of the maximum and minimum loads. Specimen elongation was monitored throughout the tests with dial gages. Strain gage rosettes were attached to the sockets of the 271 and 307 wire specimens. The strain gage output was recorded with a high-speed data acquisition system and analyzed on a high-speed computer.

4.2.2 *Pasco-Kennewick Intercity Bridge stay tests.* Frank, Breen, and Campbell conducted a series of fatigue, creep, and ultimate strength tests on two parallel wire cable stays with hybrid epoxy-steel sockets for the project sponsor [20].

4.2.2.1 **Test method.** The first specimen tested was an 83 parallel wire button head stay with hybrid epoxy-steel sockets. The wires had a nominal diameter of 1/4 inch and a minimum specified ultimate strength of 240 ksi. Three tests were performed on this specimen in the following sequence:

- (1) Creep test of socket with casting No. 1 at $0.45f_{su}$ (440 kips) for five hours at $80 \pm 3^{\circ}\text{C}$.
- (2) Room temperature creep test at $0.75f_{su}$ (735 kips) for ten hours.
- (3) Ultimate strength test.

The specimen test length between the bearing ends of the sockets was 100 inches. A seven wire, 3/8 inch diameter prestressing strand was spirally wrapped around the cable to provide confinement for the wires. The ends of the strand were embedded in the epoxy in the socket at either end. Also embedded in the epoxy of one socket was a 4 inch diameter plastic pipe which encased the wire bundle.

The second specimen tested was identical to the first specimen with two exceptions. First, the prestressing strand was wrapped loosely to prevent it from carrying any of the applied load. Secondly, 4-1/2 inch diameter steel pipe sections were screwed into the socket at either end and confined the plastic pipe. Two tests were performed on this specimen in the following sequence:

- (1) Constant amplitude fatigue tests to 2 million cycles, at a lower stress level of $0.35f_{su}$ (342 kips) and an upper stress level of $0.45f_{su}$ (440 kips).
- (2) Ultimate strength test.

Elevated temperature creep tests on the first specimen were conducted by enclosing the lower socket casting in an electric heater. The specimen was loaded to the proper level, at which time the heater was turned on. The temperature inside the socket was monitored with thermocouples. No discernable socket deformation occurred during the elevated temperature creep test. Upon completion of the creep test, the specimen was allowed to cool, and the room temperature test was

conducted. During loading of the specimen to the desired level, significant seating in the socket occurred at approximately $0.66f_{su}$ (645 kips). Strain gage data and socket diameter measurements confirmed that the socket had inelastically deformed. Loading of the specimen continued to the desired level of $0.75f_{su}$ (735 kips), and no further significant seating occurred. The maximum seating that occurred during the room temperature creep test was 0.002 inches. The ultimate strength test was then conducted. The load in the specimen reached a maximum of $1.09f_{su}$ (1062 kips), at which time eight wires failed. The test was concluded at this point.

The fatigue test of the second specimen was conducted at a frequency of 3.5 Hz. No wire breaks occurred during the 2 million load cycles. The specimen was then loaded statically to failure. One wire break occurred during the ultimate strength test at a level of 572 kips. The maximum load attained by the specimen was 1022 kips ($1.04f_{su}$).

4.2.2.2 Results. Examination of the first specimen revealed that seven wires had failed, and that the confining prestressing strand (the eighth wire break detected) also failed. Distribution of the wire failures along the specimen length appeared to be random. The fact that the prestressing strand failed is an indication that it carried a portion of the applied load during testing. Inspection of the socket that had deformed inelastically revealed two large longitudinal cracks in the socket casting. Information gathered on the measurement of the center buttonhead and end plate seating revealed that the majority of seating took place during the initial loading to $0.45f_{su}$. Very little occurred during the creep test and room test, and a substantial portion of the total seating occurred during the ultimate strength test. These facts are summarized in Section 4.2.4.

Examination of the second specimen after the conclusion of the ultimate test revealed that the premature wire break was due to a fatigue crack which had propagated across one half of the failure surface. The remaining wire failure surfaces were all noted to be ductile. The majority of the seating which occurred is evenly split between the initial quasi-static loading to $0.45f_{su}$ and the ultimate strength test. Center buttonhead and end plate seating data during the tests on the second specimen is also found in Section 4.2.4. Very little seating occurred as a result of the cyclic loading.

4.2.3 *Luling Bridge stay tests.* Dykers and Frank conducted a series of creep, fatigue, and ultimate strength tests on four Hi-Am anchored cable stays supplied by the project sponsor [15]. The four specimens consisted of 103, 211, 271, and 307 1/4-inch diameter parallel wires with an ultimate tensile strength of 240 ksi. A summary of the test procedure follows for each specimen:

103 wire specimen

- (1) Constant amplitude fatigue test to 2 million cycles at a lower stress level of $0.35f_{su}$ (424.8 kips, based on the nominal wire strength) and an upper stress level of $0.45f_{su}$ (546.2 kips).
- (2) Ultimate strength test.

211 wire specimen

- (1) High temperature socket creep test at $0.45f_{su}$ (1118.9 kips) for 5 hours with an internal socket temperature equal to or greater than 176°F.
- (2) Room temperature creep test at $0.75f_{su}$ (1864.8 kips) for 10 hours.
- (3) Ultimate strength test.

271 wire specimen

- (1) Constant amplitude fatigue test to 2 million cycles at a lower stress level of $0.35f_{su}$ (1117.7 kips) and an upper stress level of $0.45f_{su}$ (1437.1 kips).

307 wire specimen

- (1) High temperature socket creep test at $0.45f_{su}$ (1628 kips) for 5 hours with an internal socket temperature equal to or greater than 176°F.
- (2) Room temperature creep test at $0.75f_{su}$ (2713.3 kips) for 10 hours.
- (3) Ultimate strength test.

4.2.3.1 **Test method.** The test assemblies for all four specimens consisted of two hybrid epoxy steel sockets connected to the ends of a cable consisting of parallel 1/4 inch diameter wires. The lengths of the completed stays varied from 101 inches to 107 inches between the bearing ends of the sockets. These variations in length were necessary to accommodate different size hydraulic rams and loading

system configurations used throughout the series of tests. In order to maintain wire compactness, the stays were wrapped helically with a 3/8 inch diameter prestressing strand, the ends of which were embedded in the epoxy sockets. However, this wire was cut after assembly and before testing to prevent its contribution to the actual strength of the specimen, as was found to occur in the tests by Campbell, Frank, and Breen.

4.2.3.2 Results for 103 wire specimen. The fatigue portion of the test was conducted at a frequency of 3Hz. Four wire breaks were detected by the velocity transducer during the fatigue test. Following the fatigue test the specimen was loaded to failure, which occurred at 1283.4 kips ($1.06f_{su}$). Total specimen elongation during the ultimate strength test amounted to 5.1 percent.

All of the fatigue breaks were found to occur inside the anchorage socket within 1 inch of the socket bearing face. No problem with the socket was discovered that would cause the failures that occurred.

The buttonhead and end plate seating that occurred at various stages of the test are summarized in Section 4.2.4. A majority of the seating occurred during the initial loading to $0.45f_{su}$, and during the fatigue test only little seating occurred.

4.2.3.3 Results for 271 wire specimen. The fatigue portion of the test was conducted at a frequency of 1.1Hz. Eighty three wire breaks were detected by the velocity transducer during the fatigue test, and the test was concluded at that point (1,366,000 cycles). The distribution of the wire breaks along the specimen length during the test appeared to be random.

The buttonhead and end plate seating that occurred during the fatigue test is summarized in Section 4.2.4. A majority of the seating occurred during the initial loading to $0.45f_{su}$, and that during the fatigue test relatively little seating occurred.

4.2.3.4 Results for 211 wire specimen. The elevated temperature tests and room temperature tests were conducted in a manner similar to that discussed in Section 4.2.1.1. Buttonhead and end plate seating is summarized in Section 4.2.4. During the high temperature creep test, a buttonhead seating of 0.007 inches took place in the top socket, compared to no net seating in the bottom socket. The buttonhead and end plate seating showed again to be almost identical as the load

was increased to $0.75f_{su}$ for the room temperature creep test. Further seating took place during the ultimate strength test. A load of 2822.75 kips ($1.14f_{su}$) was reached in the ultimate strength test, and the test was concluded. Total specimen elongation amounted to 4.64 percent. Wire break distribution was again shown to be random in location.

4.2.3.5 Results for 307 wire specimen. The elevated temperature and room temperature creep tests were performed as discussed previously in 4.2.2.3. Thermal equilibrium of the encased socket was finally achieved at 188°F. Buttonhead and end plate seating is shown in 4.2.4. During loading of the specimen to $0.75f_{su}$ to perform the room temperature creep test, a buttonhead seating of 0.009 inches took place in the top socket. The buttonhead and end plate seating showed again to be almost identical as the load was increased to $0.75f_{su}$ for the room temperature creep test. Further seating took place during the ultimate strength test. A load of 3795.4 kips ($1.05f_{su}$) was reached in the ultimate strength test, and the test was concluded. Total specimen elongation amounted to 4.8 percent at ultimate load and 5.44 percent at rupture. Wire break distribution was again shown to be random in location.

4.2.4 Summary. To summarize the section on parallel wire stay tests, end plate and buttonhead seating data for all of the tests have been combined to demonstrate the relative insignificance of the end plate with respect to load capacity. Figures 4.8a through d show the relationship between seating and increasing quasi-static load. Figure 4.9 shows the seating that occurred as a result of cycling between $0.35f_{su}$ and $0.45f_{su}$. Figures 4.10a and b show the relationship between creep at a constant load and seating. It is informative to note that for most cases the seating of the center buttonhead and endplate are essentially identical within the accuracy of the measuring technique. This would indicate that no beneficial "anchoring" effects are garnered using an end plate; its effectiveness lies only in maintaining the wire pattern in the socket during casting. From these figures it is evident that no matter what the loading situation may be, the buttonheads and end plates will seat by the same amount. The end plate will not restrain the wires from pulling through the socket.

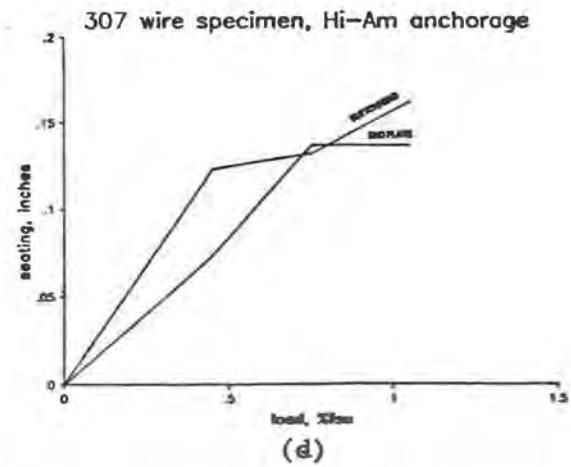
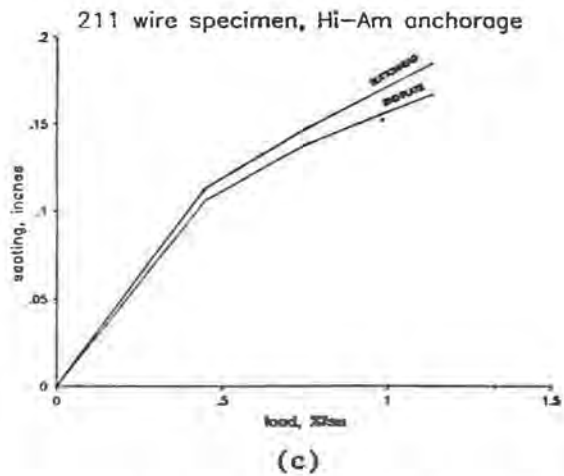
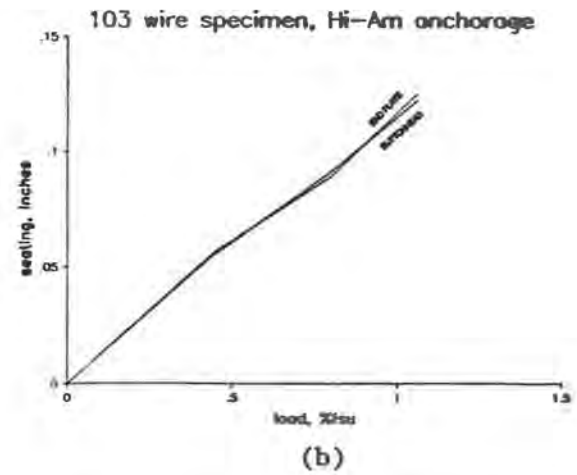
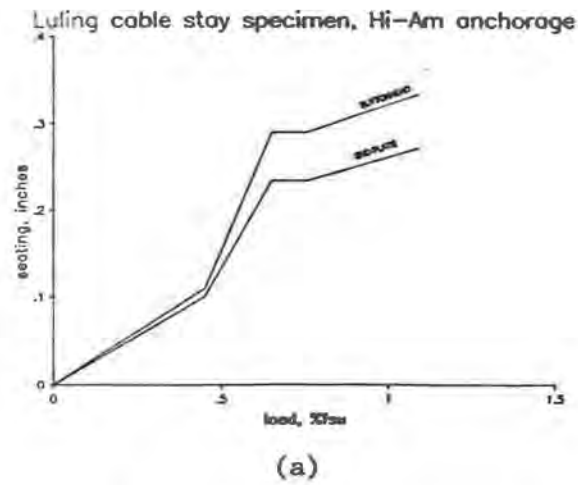


Figure 4.8 Center buttonhead and end plate seating during quasi-static loading

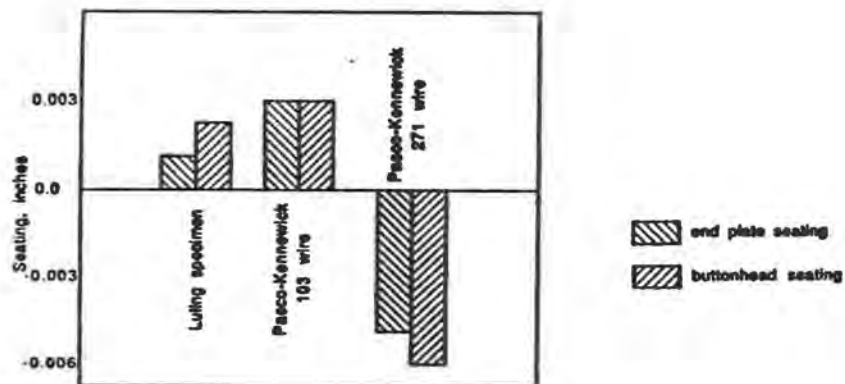


Figure 4.9 Center buttonhead and end plate seating during fatigue test

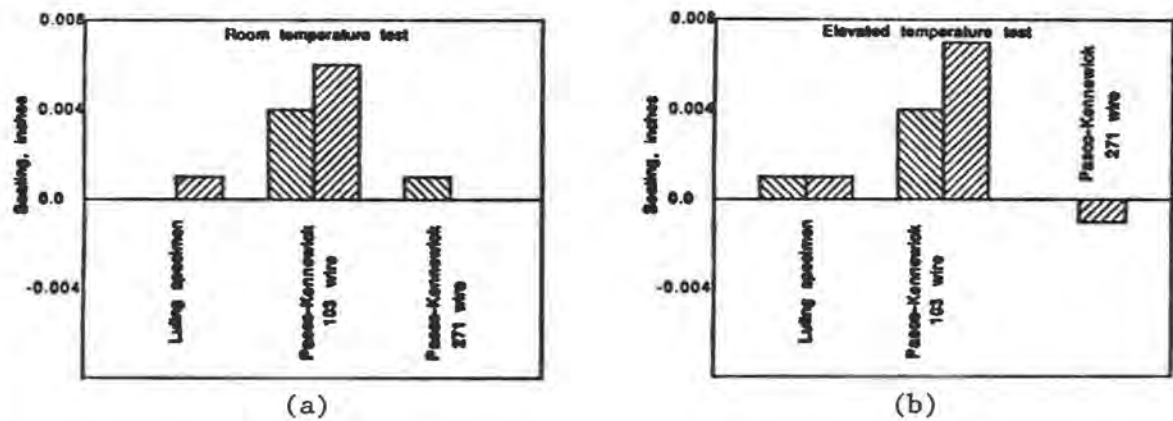


Figure 4.10 Center buttonhead and end plate seating during creep tests

4.3 Parallel Strand Stay Tests

The tests outlined in this section were conducted on parallel strand systems with wedge-type anchorages. The tests conducted for the Houston Ship Channel Crossing were verification tests.

4.3.1 Stallings. Research by Stallings was oriented toward identifying and answering some of the fundamental questions regarding fatigue behavior and stay cable fatigue life prediction [29]. Analysis for fatigue life prediction was conducted on a probabilistic basis. Three different statistical distribution functions were examined. From these functions, estimates of cable life were obtained which accounted for length and bundle effects. The experimental phase of Stallings' work involved the testing of both individual strand tests and a cable stay consisting of 61 parallel strands. The results of the experimental phase were used to provide an accuracy check for the cable fatigue life prediction methods.

A discussion of Stallings' analytical work is beyond the scope of this paper, however a discussion in this chapter is presented on the testing of the 61 strand cable stay.

4.3.1.1 Description of test specimen. The cable stay specimen consisted of 61 0.6 inch diameter low relaxation seven wire prestressing strand with an ultimate tensile strength of 270ksi. The anchorage system consisted of a common anchorhead; all strands were anchored to the common anchorhead individually with a three-piece wedge system. The overall specimen length was 184 inches \pm 1 inch.

4.3.1.2 Testing apparatus. The test frame, shown in Figure 4.10, consists of a concrete spacer block and two steel spacers. The load cells used to monitor the loads were located between the concrete spacer and upper steel spacer. Loads were applied with a 4.5 million pound capacity centerhole ram situated atop the upper steel spacer. The load controlling system and data acquisition system are described in detail in Chapter 5. No measurements of center wire or wedge seating were recorded during the testing. The specimen was assembled in the test frame by threading each strand through the top and bottom anchorheads. The strands were uniformly tensioned with a prestressing monostrand jack to a load of approximately 6 kips. The top wedges were power seated. Under a load of 1608 kips (121.5 ksi, or

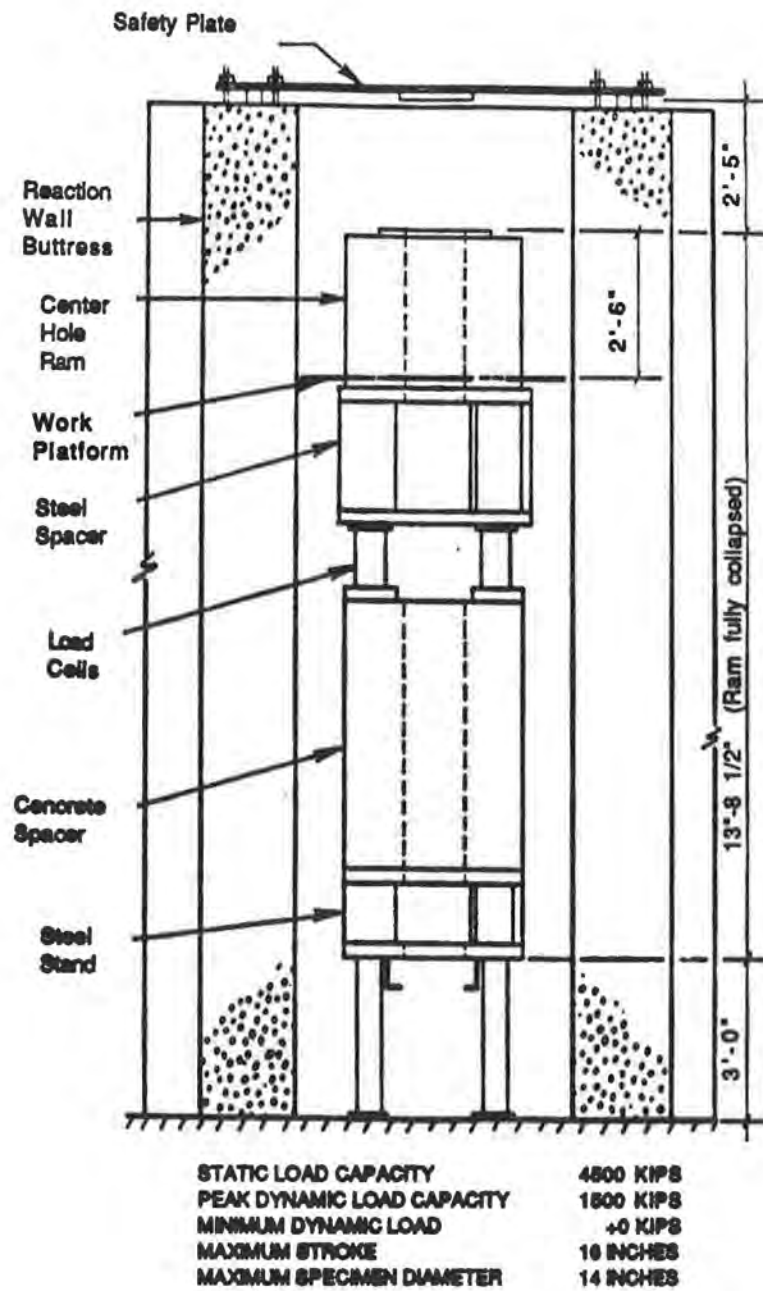


Figure 4.11 FSEL large scale fatigue and tensile test machine [29]

0.44 fpu), epoxy was poured over the ends of the strands and the wedges at the top anchorage and allowed to dry under load.

4.3.1.3 Test method. A 2 million cycle constant amplitude fatigue test was conducted on the specimen. The test was run at a lower fatigue load of 0.36 fpu (1304 kips) and an upper fatigue load of 0.44 fpu (1608 kips). The cycling was conducted at a frequency that varied between 0.62 and 0.72Hz. However, due to the large number of wire breaks that occurred during the fatigue portion (112 of the 427 individual strand wires, or 26% of the wires) the fatigue test was concluded at 1,247,660 cycles.

An ultimate strength test followed the cable fatigue test. The maximum load attained was 1820 kips (0.50 fpu) and occurred at a strain of 0.008in/in.

4.3.1.4 Results. Inspection of the specimen revealed a total of 121 wire breaks occurred during the fatigue and ultimate strength tests. Of the 121 wire breaks, 119 were discovered in an outside wire at a fatigue crack at the leading tip of the anchorage wedges. These break locations occurred within the wedges at an average distance of 1/4 inch from the tip. In the other two cases, One break occurred in a fatigue crack located in the free length. The remaining break occurred in a center wire inside the wedges.

Of the 115 fatigue breaks, it was found that 92 of them had occurred in the bottom anchorage and 23 in the top anchorage with epoxy coating. This indicated that the epoxy coating may have helped to improve the fatigue life of the strand.

Further inspection revealed that two forms of slip had occurred. 23 of the strands exhibited outside wire slip, in which the outside wires slipped relative to the wedges. A total of 13 of these strands slipped through without having any wire breaks. 12 of them slipped through wedges covered in epoxy at the top anchorhead. Stallings has explained the reason for the correlation between outer wire slip and epoxy. The epoxy, which was very fluid when first poured on the anchorage, filled the spaces between the wedge pieces and between the wedges and strand. During the ultimate strength test the epoxy, by now hardened, did not allow the wedges to close and develop the required clamping force to hold the strand in place. Thus the use of epoxy had detrimental effects on the ultimate strength of the strand.

Center wire slip was found to occur in at least 53 of the 61 strands in the stay. Stallings believes that the slip occurred for the same reasons as the outer wire slip.

Finally, it can be noted that the ultimate capacity of the cable stay was severely limited by the presence of so many fatigue cracks and slippage. Outer wire slip was shown to be detrimental to the load-carrying capacity of the stay. Stallings makes certain recommendations for the use of an epoxy injection on future anchorages. The stress at which the epoxy is applied is important in that the epoxy will not keep the wedges from closing until that stress level is once again reached. Thus it would be important that on bridges the epoxy procedure take place at a stress level above what might be expected during service. Since PTI recommends static verification testing of stays to 95% of GUTS, it would be necessary to inject the epoxy at a stress above this level. This recommendation by Stallings is seen by the author as somewhat unrealistic.

4.3.2 Houston Ship Channel Crossing stay tests. The author has completed static and fatigue tests on a 19 strand cable stay specimen using essentially the same test frame as described in Section 4.3.1.2. The tests, performed for the Houston Ship Channel Crossing in Baytown, Texas, are discussed in detail in the following chapter.

CHAPTER 5 BAYTOWN BRIDGE STAY TESTS

This chapter contains results of fatigue and static tests of a 19-strand cable stay specimen using 0.60 inch diameter, seven wire, low relaxation prestressing strand. The stays are currently proposed for use on the Houston Ship Channel Crossing in Baytown, Texas. The strand and components for fabrication of the specimen were provided by the project sponsor for testing.

Two tests were performed on the specimen. They were as follows:

- (1) Static tests on the specimen before grouting to determine the stiffness of the strand group alone, static tests on the grouted specimen before and after every 500,000 cycles during the fatigue testing to determine the stiffness of the composite specimen, and
- (2) Fatigue tests to 2×10^6 cycles, followed by a static test to 95% of the ultimate tensile strength of the specimen as determined by individual strand tensile tests.

A description of the major components in the stay and their function is noted previously in Section 2.3.4b.

5.1 Test Instrumentation

A schematic of the FSEL large force tension test facility and the assembled specimen is shown in Figure 5.1. With the exception of certain modifications which are discussed in this section, the test frame used in these experiments is identical to that used in the test by Stallings. The reader is referred to Chapter 4 for a detailed description of the test frame.

Fatigue distress of the existing lower steel spacer was observed during previous stay tests conducted by Stallings. In an effort to improve the facility's fatigue resistance during cyclic loading of the specimen, a 4-inch thick steel plate was bolted to the lower steel spacer. In order to install the plate, the machine was jacked up from its stand using four hydraulic rams and a common lifting frame. The

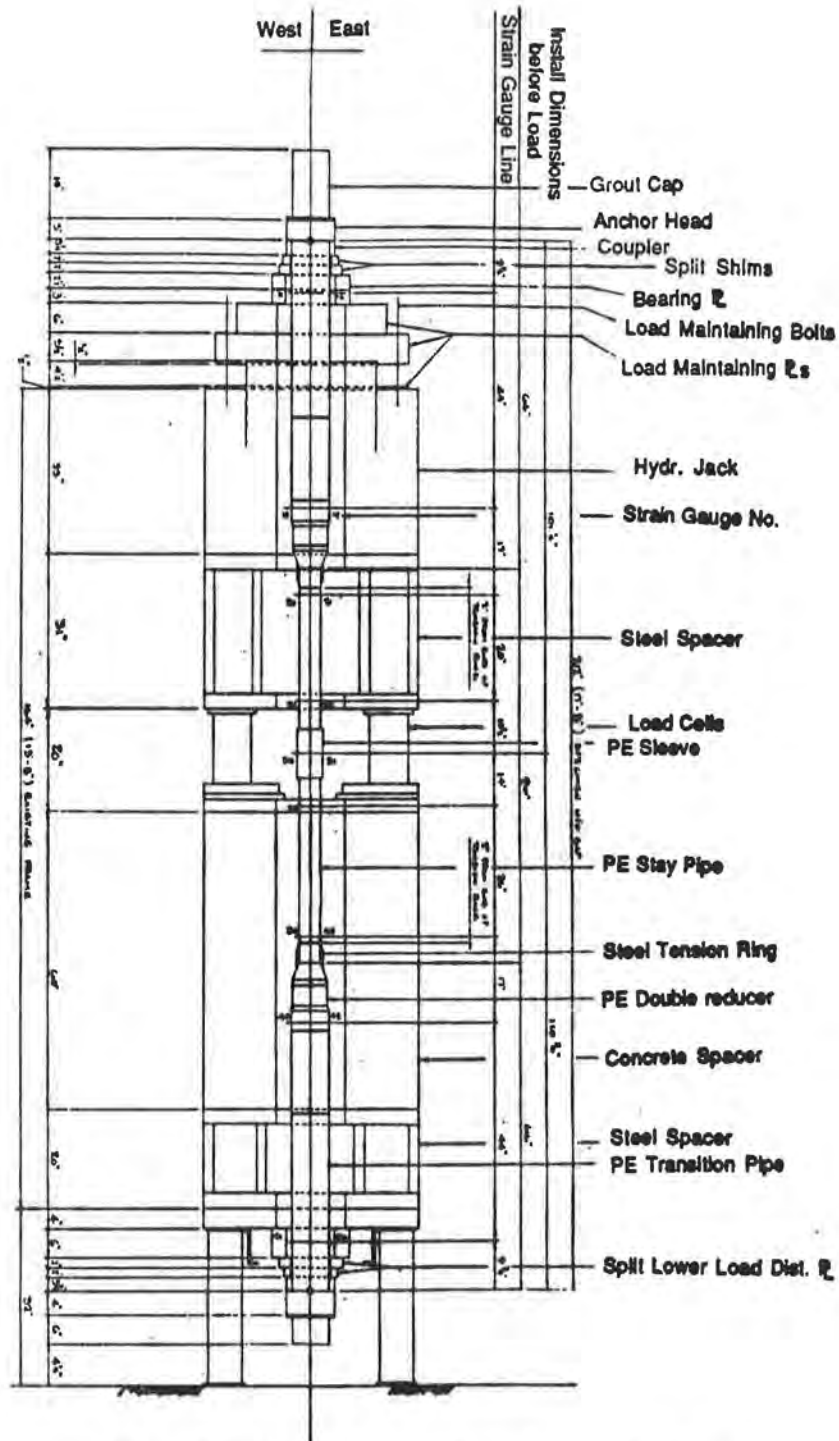


Figure 5.1 Test set-up and strain gage locations



Figure 5.2 Four-inch steel plate slid into position

fatigue plate was then slid into position, as shown in Figure 5.2 and the test frame was reattached to its stand.

Loads were applied to the specimen with the 2250 ton capacity centerhole ram. The ram was powered hydraulically by a 70 gpm pump.

Prior to testing, the load cells were calibrated both individually and as a group using a National Bureau of Standards-calibrated load cell. The calibration procedure and collected data are included in Appendix A.

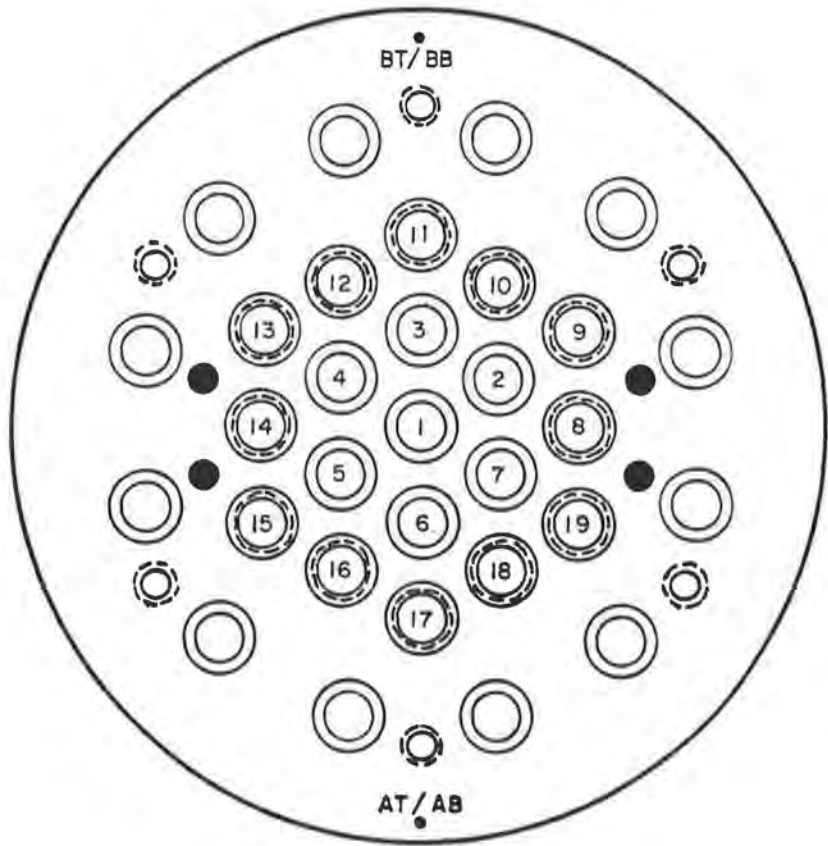
The fatigue loads of the test program were controlled by a closed loop system, consisting of a servo-valve controller, function generator, and cycle counter. The static portion of the test was conducted using the same system; however the load program was applied manually, without the aid of the function generator. A peak detector was used to monitor the loads applied to the specimen during both the fatigue and static portions of the test program. The peak detector continually updated and displayed the current value of the maximum and minimum fatigue loads.

Axial strain gage data, load levels, and specimen displacements were recorded with a data acquisition system utilizing a personal computer. The computer controls an external scanner and converts the measured voltage into engineering units. The gages were quarter-bridge gages with a gage factor of 2.12 and a gage length of 6 mm. A two volt excitation was used for the strain gages.

Center wire and wedge seating were measured for three strands on both the top and bottom anchorheads. Strands 1, 6, and 17, shown in Figure 5.3, were chosen for the measurements. The measurements were made with a depth gage and a stationary measurement fixture, as shown in Figure 5.4, to an accuracy of within ± 0.001 inch. The measurements from the surface of the fixture to the center wires and wedges were recorded. The movement of each point was determined by taking the difference between consecutive measurements. Measurement of reference points on both the top and bottom anchorhead faces were also taken to establish the repeatability of the readings. Specimen elongation was monitored with a linear potentiometer shown in Figure 5.5.

The pretension in the strands was held during the grouting and curing of the grout with a mechanical load maintaining system. The load maintainer consisted of a 5-1/2 inch thick steel plate with 33 1-1/4 inch diameter high-strength bolts. Nuts were welded to the bottom of holes drilled through the plate. To achieve the desired pretension, the ram was extended until that pretension was reached. The bolts were then extended beyond the plate and through the nuts to bear on a 1/2 inch thick steel bearing ring bolted to the outside of the ram. The bolt extension was adjusted to take into account the elastic compression of the bolts and steel plate so that the desired pretension was achieved. Additional locking nuts were used to secure the bolts during the fatigue test. This arrangement is shown in Figure 5.6. Only half the bolts were used to maintain the load in this test due to the small load levels specified.

Twisting of the specimen during testing was prevented with a device consisting of a stationary roller bearing and travel surface, as shown in Figure 6. Two rotation restraint devices were attached to the load maintainer plate on opposite sides of the specimen to reduce the lateral force applied to the centerhole ram.



Note:
Anchorhead Reference
Points AT/AB and BT/BB

Figure 5.3. Strand/Wedge references for anchorhead



Figure 5.4. Measurement of center wire and wedge seating with a depth gage and stationary fixture

Wire breaks occurring during cycling were monitored with a velocity transducer that was attached to the bottom anchorage as shown in Figure 5.8. The velocity transducer was connected to a “one-shot” circuit with an adjustable threshold which amplifies any incoming voltage that is above the normal operating noise level of the system. The output from the circuit was connected to the Y-axis of an X-Y recorder. A calibrated time base was used for the X-axis. Any voltage signal above the normal operating noise received by the “one-shot” results in a short pulse to the X-Y recorder, and appears as a “spike” on the plot.

5.2 Test Specimen Preparation and Installation

The ungrouted specimen was assembled and installed by technicians provided by the sponsor with the assistance of University personnel in accordance with the sponsor’s test provisions. Assembly of the specimen was conducted under the



Figure 5.5 Linear potentiometer to measure specimen elongation

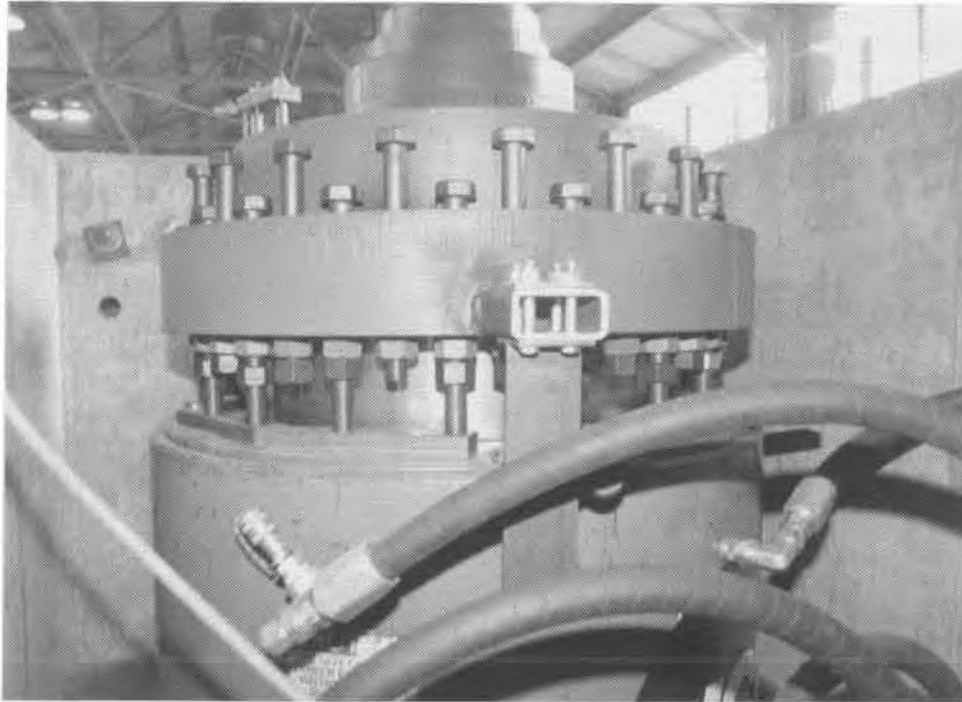


Figure 5.6 Load-maintainer plate holding grout load



Figure 5.7 Rotation restraint device

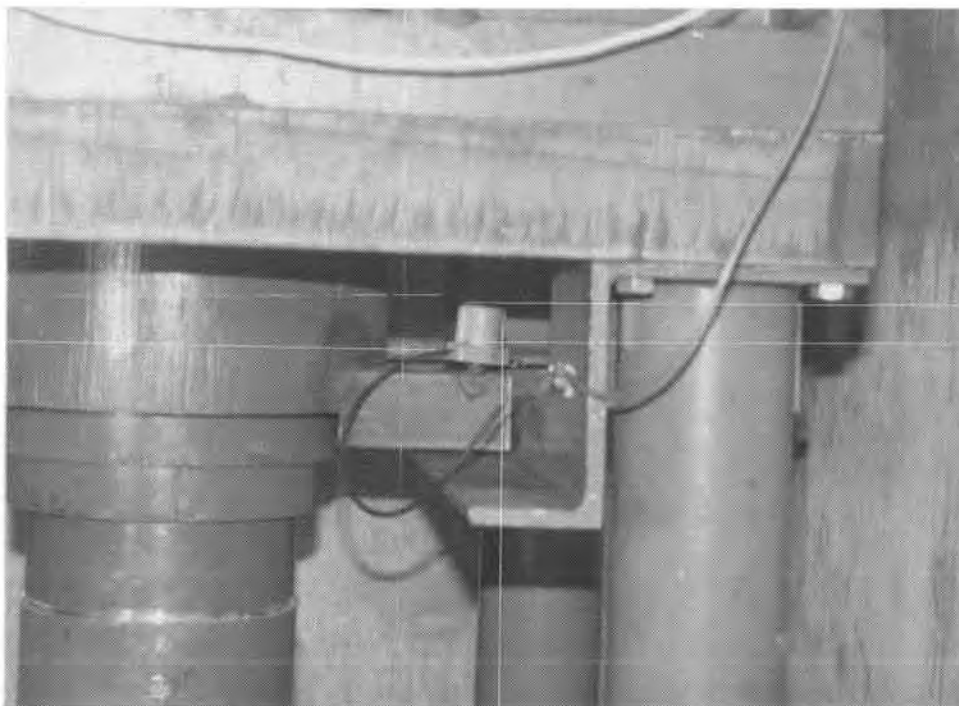


Figure 5.8 Velocity transducer attached to lower anchorage

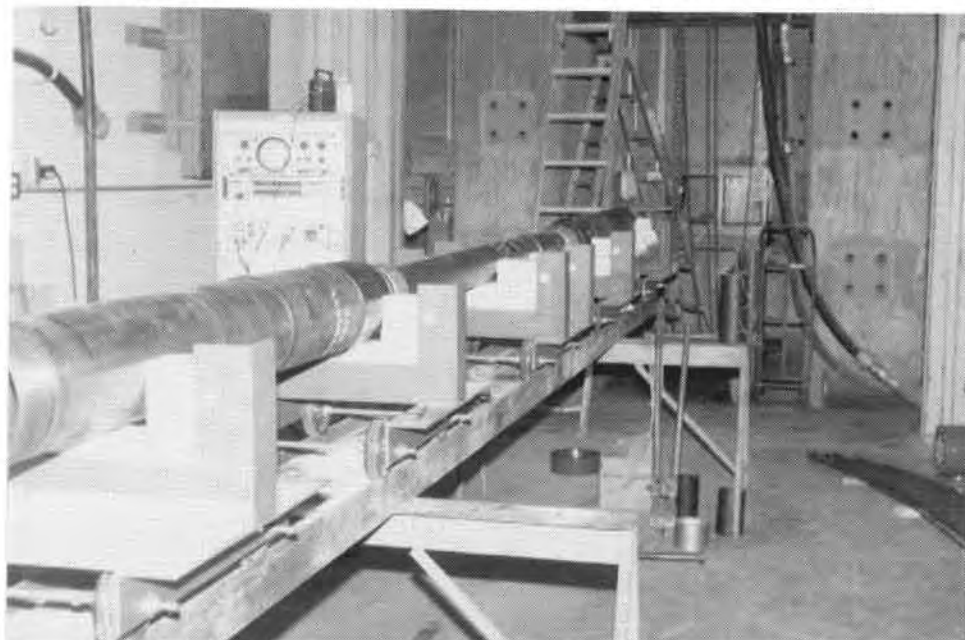


Figure 5.9 Specimen assembly station

direction of the sponsor and witnessed by Texas Department of Highways and Public Transportation personnel.

A work station was constructed for the assembly of the specimen and is shown in Figure 5.9. It consists of a number of "trolley carts" mounted to a wide flange beam. The cart wheels were grooved for travel along the flange tips of the beam, which was supported on saw horses. The trolley carts supported the pipe sections and anchorheads during the assembly process. They also allowed longitudinal positioning of the various components during the construction of the specimen.

The strand provided for use in the test was stored in a metal cage at Ferguson Laboratory, as shown in Figure 5.10. The 19 strands used were cut to a length of 23 feet, longer than the necessary tested length of 17 feet-06 inches, in order to facilitate ease of specimen fabrication and preseating of wedges. The strands used in the testing were inspected by the sponsor to ensure that no surface anomalies were present. The strands were passed individually through the anchorheads and pipe components. Hollow steel "bullets" were taped to the ends of the strands that were passed through the components. Figure 5.11 shows these "bullets." The bullets kept the strands from becoming entangled in the tension ring area or with the helical steel spacer in the stay length shown in Figure 5.12. Figure 5.13 shows all 19 strands initially installed before the components were pushed into position with the carts. Each strand was anchored with a two-piece wedge system, shown previously on Figure 2.14. The wedges were then held in place before preseating and during the installation procedure with a device shown in Figure 5.14. It consisted of springs which fit over the ends of each strand. These springs were larger than the strand but smaller than the outside diameter of the wedges. A plate was bolted to the anchorhead which then compressed the springs and forced the wedges to seat.

Axial strain gages were applied to the polyethylene pipe at locations shown in Figure 5.1.

Reference lines were marked at the mating region of the two stay lengths to ensure that the specimen did not twist during installation. A gap of 2 inches remained at the mating region of the stay pipes, as shown in Figure 5.15. This gap enabled the specimen to bend at that point during installation in the test machine. With the aid of both newly installed overhead crane and existing laboratory traveling

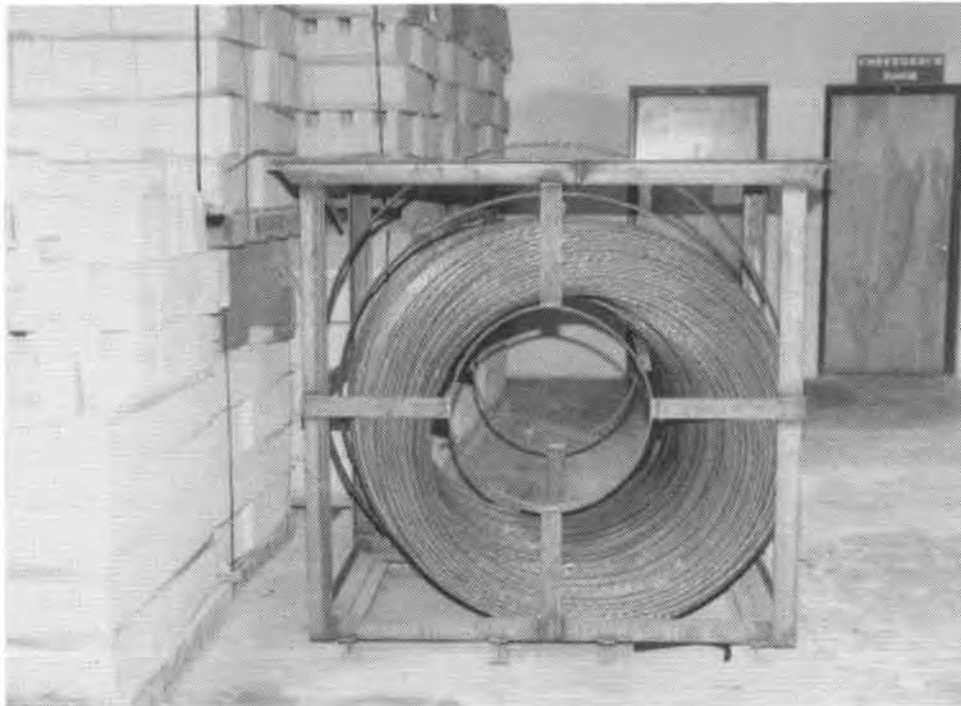


Figure 5.10 Strand supplied for testing, with steel cage

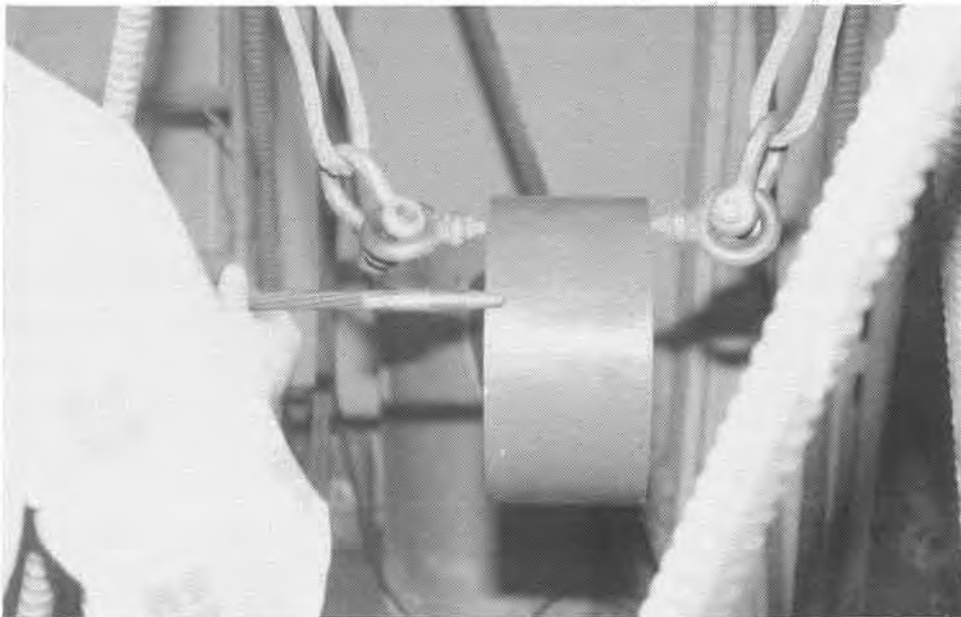


Figure 5.11 Hollow steel "bullet" to aid strand in passing through pipe assembly untangled

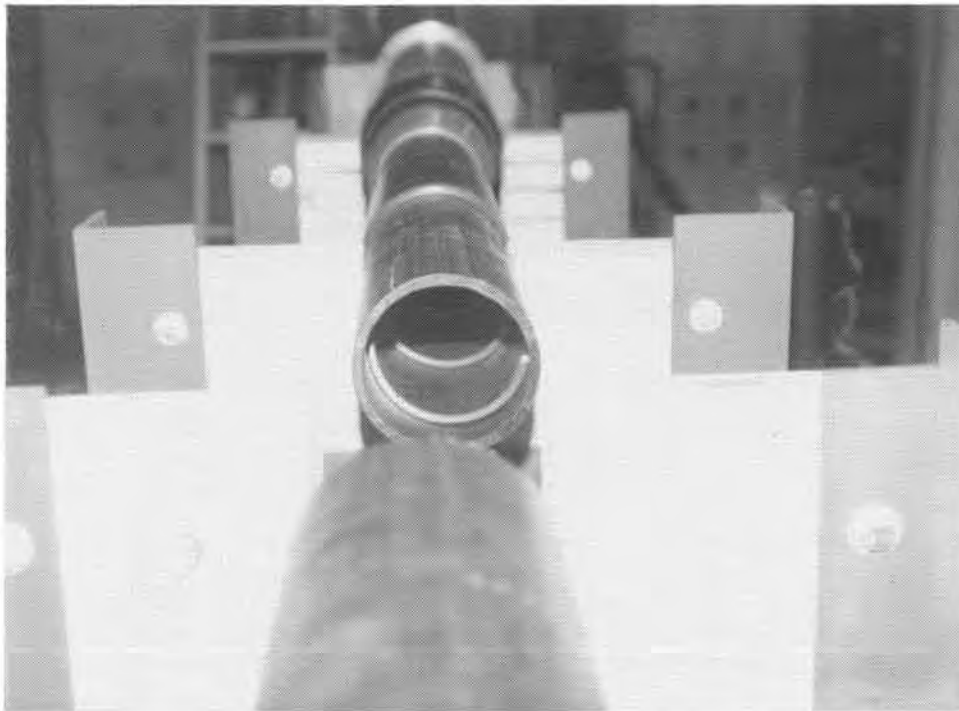


Figure 5.12 Steel helical spacer inserted in polyethylene stay length

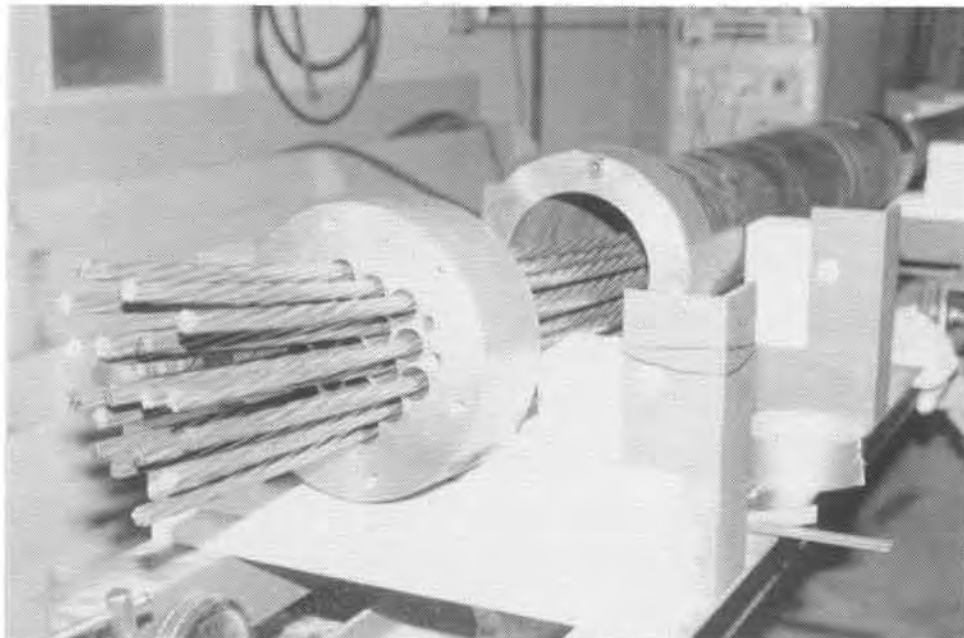


Figure 5.13 All 19 strands installed

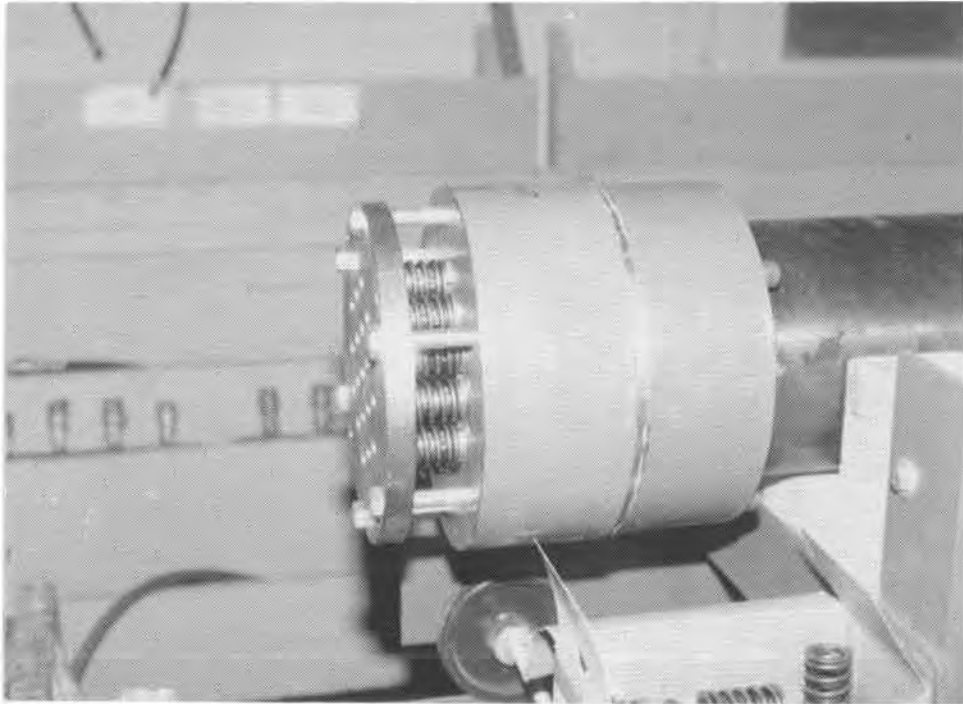


Figure 5.14 Spring plate mounted on lower anchorhead

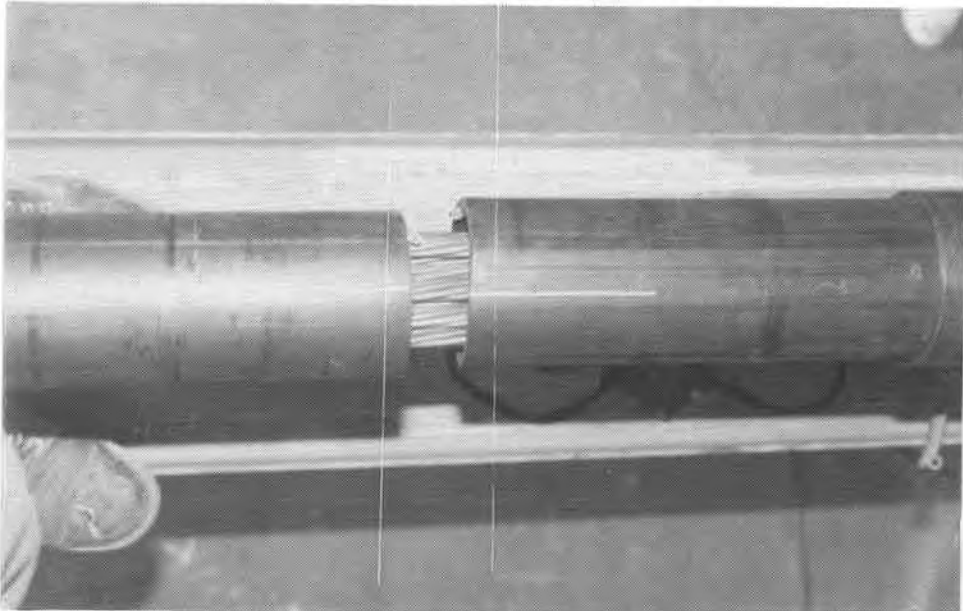


Figure 5.15 Gap in polyethylene stay pipes to allow bending during installation

crane the ungrouted specimen was then installed in the test machine by passing it through the centerhole ram at the top of the test machine. Figure 5.16 shows the bending that occurred at the gap during lifting of the specimen. Once installed, the ends of the two stay pipes were mated with a polyethylene pipe sleeve that was slid over the two ends. This sleeve was strapped in place.



Figure 5.16 Lifting of specimen

The wedges were then preloaded to a load of 3 kips using a monostrand jack as shown in Figure 5.17. They were visually inspected for equal engagement depth. The final tested specimen length, measured between bearing ends of the anchorheads, was 213 inches.

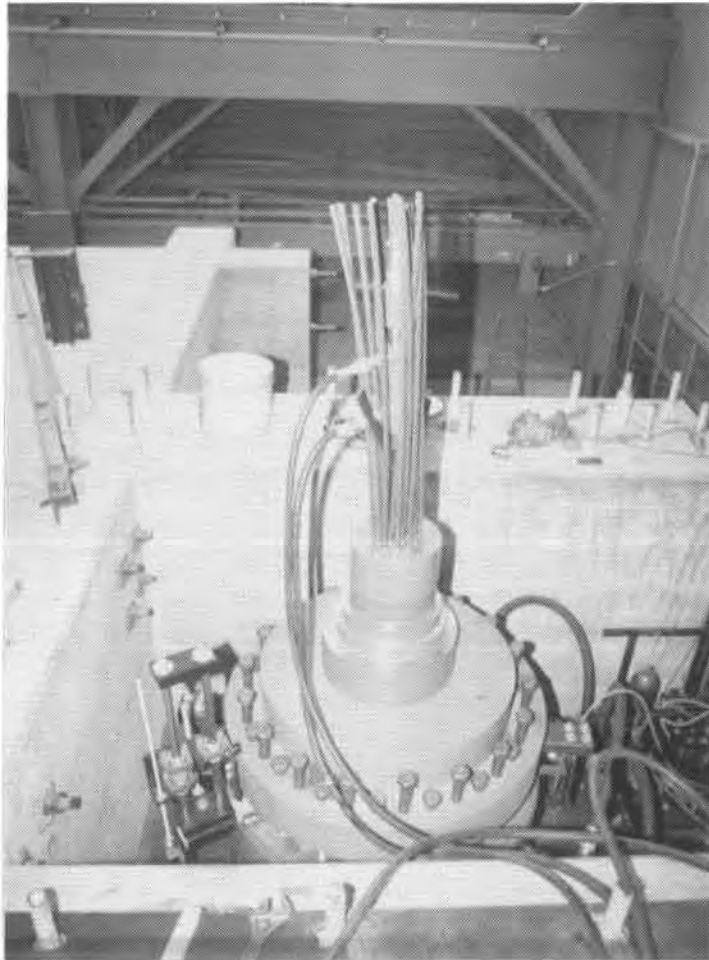


Figure 5.17 Preseating of wedges with monostrand jack

5.3 Test Procedure

Specimen testing was conducted by UT personnel in accordance with the sponsor's test provisions. All phases of the testing were witnessed by representatives of the sponsor and Texas Department of Highways and Public Transportation personnel.

Table 5.1 summarizes the loading sequence for the specimen over time, beginning with the initial preseating of the wedges, and includes cycling interruptions due to ram leaks and pump overheating problems. The ungrouted specimen was loaded from an initial load of 25.9 kips (the observed load on the specimen resulting from the final preseating of the wedges) to the lower fatigue load. Center wire and wedge seating for strands 1, 6, and 17 were measured at the top and bottom anchorheads. The anchorhead reference points were also measured. Total elongation of the specimen at each load level was recorded. This procedure was repeated three times. The strand/wedge seating data is shown in Table 5.2 and the specimen elongations are noted in Table 5.3. The actual load at which measurements were taken differed by $\pm 4\%$ from the desired lower fatigue load of 406.3 kips. These loads are noted as well in Tables 5.2 and 5.3.

The ungrouted specimen was then statically loaded to the prescribed upper and lower fatigue load levels of 500.9 kips and 406.3 kips, respectively. The test loads were calculated using a nominal strand area of 0.217 in^2 to produce a maximum stress of 121.50 ksi (45% of the strand guaranteed ultimate tensile strength, or GUTS) and a minimum stress of 98.55 ksi (36.5% of GUTS). Center wire and wedge seating for the measurement points were recorded. Specimen elongation at each load level was also recorded.

Loading to the upper and lower load levels was repeated three times with measurements being made at each load. The stiffness of the ungrouted specimen was calculated based on the actual load levels and the change in specimen elongation. The values for the stiffness of the ungrouted specimen are shown in Table 5.3. A displacement of 0.012 inches at the bottom load distribution plate was observed during the static cycling of the specimen between the upper and lower fatigue loads. The elongations recorded in Table 5.3 were adjusted for this displacement by subtracting

Table 5.1 Load Events Versus Time

Date	Time	Cycles	Comments
1/5/89	14:00	0	Seating of Wedges Completed
1/5/89	18:50	0	Static Loading of Ungrouted Specimen
1/6/89	11:10	0	Grouting of Specimen
1/10/89	8:55	0	Static Loading of Grouted Specimen
1/16/89	15:31	500,000	Seating/Stiffness Checks
1/18/89	11:09	724,457	Pump Overtemp Error
	11:26		Restarted
1/20/89	9:08	960,772	Pump Overtemp Error
	9:43		Restarted
	14:29	986,504	Pump Overtemp Error
	14:37		Restarted
	17:05	1,000,018	Seating/Stiffness Checks
1/23/89	11:20	1,470,639	Pump Overtemp Error
	11:24		Restarted
	14:40	1,475,646	Pump Overtemp Error
	14:43		Restarted
	19:37	1,483,479	Pump Overtemp Error
	19:40		Restarted
1/24/89	21:50	1,495,123	Pump Overtemp Error
	22:27		Restarted
	23:25	1,500,000	Seating/Stiffness Checks
1/25/89	8:39	1,505,949	Pump Overtemp Error
	8:46		Restarted
	11:50	1,514,800	Pump Overtemp Error
	11:53		Restarted
	19:44	1,544,229	Pump Overtemp Error
	19:47		Restarted
1/26/89	9:20	1,560,000	Pump Overtemp Error
	9:26		Restarted
	10:23	1,565,000	Ram Leaking, Cycling Interrupted

Table 5.1 - continued

Date	Time	Cycles	Comments
2/02/89	16:37		Restarted
	21:24	1,590,290	Stopped Cycling due to Excessive Leaks
2/03/89	16:04		Restarted
	16:51	1,594,520	Stopped Cycling Overnight
2/07/89	16:35		Restarted
	21:16	1,603,178	Pump Overtemp Error
	21:23		Restarted
2/08/89	8:30	1,621,111	Pump Overtemp Error
	8:35		Restarted
	10:59	1,633,329	Stopped Cycling due to Excessive Leaks
	13:48		Restarted
2/09/89	0:28	1,690,281	Stopped Cycling Overnight due to Low Oil Level in Pump
	9:20		Restarted
2/10/89	9:40	1,781,017	Pump Overtemp Error
	9:45		Restarted
	9:50	1,781,709	Stopped Cycling due to Excessive Leaks
	14:14		Restarted
2/12/89	7:05	2,000,003	Seating/Stiffness Checks
2/14/89	10:02		Begin Ultimate Strength Test
	10:28		End Ultimate Strength Test

Table 5.2 19-Strand Specimen Center Wire and Wedge Seating Data

Description	Load Cycle	Load Level, k	Seating in top anchorhead, inches			Wedge 17	Wedge 6	Wedge 1	Ref. pt. AT	Ref. pt. BT	Comments	
			Strand 17	Strand 6	Strand 1							
UngROUTED Specimen	1	25.2	2.673	2.395	2.430	3.595	3.591	3.596	3.667	3.665	REFERENCE VALUES PRIOR TO CYCLING CHANGE IN SEATING FROM PREVIOUS READING	
	2	403.2	.069	.067	.065	.058	.062	.060	.001	.003		
		25.2	-.002	-.004	-.005	-.003	-.003	-.005	-.001	-.002		
		421.0	.003	.008	.007	.005	.006	.006	.001	.001		
	3	25.2	-.001	-.004	-.006	-.002	-.004	-.004	.000	.000		
		406.0	.002	.002	.006	.003	.004	.005	.000	.000		
		501.0	.011	.013	.010	.008	.010	.009	.001	.001		
	4	406.7	-.002	-.001	-.001	.000	-.001	-.001	.000	-.001		
		501.0	-.002	-.002	-.004	.000	.000	.000	.000	.000		
		404.6	-.001	-.001	-.003	.000	.001	-.001	.000	.000		
		500.4	.002	.001	.000	.000	.000	.002	.000	.000		
	Grouted Specimen before cycling	1	402.3	-.003	-.002	-.001	-.001	-.002	-.002	-.002		-.001
			503.0	.001	.002	.001	.001	.001	.001	.000		.000
		2	402.0	-.001	-.001	.000	-.001	-.001	.000	.000		.000
			500.0	-.001	-.002	.000	.001	.001	.001	.000		.000
3		398.0	.001	-.002	-.002	-.001	.000	-.001	.000	.000		
		502.0	.000	.001	.003	.001	.000	.001	.000	.000		
500,000 cycles	1	404.0	.000	-.001	-.001	.000	.000	-.001	.001	.001		
		498.0	.001	.001	.001	.000	.001	.001	.000	.000		
1,000,018 cycles	1	403.0	.000	.000	-.001	.000	.000	.000	.000	.000		
1,500,000 cycles	1	303.0	-.001	-.001	.000	.000	.000	-.001	.000	.000		
2,000,003 cycles	1	310.0	.000	.000	.000	.003	.000	.000	.000	.000		
			2.753	2.477	2.507	3.667	3.666	3.666	3.668	3.667	REFERENCE VALUES AFTER CYCLING	
			.080	.082	.077	.072	.075	.070	.001	.002	CHANGE FROM INITIAL READINGS AFTER CYCLING	
After Ultimate Test		.0	2.819	2.540	2.555	3.730	3.727	3.712	3.667	3.666	REFERENCE VALUES AFTER ULTIMATE TEST	
			.146	.145	.125	.135	.136	.116	.000	.001	CHANGE FROM INITIAL READINGS AFTER ULTIMATE	

Table 5.2 - Continued

Description	Load Cycle	Load Level, k	Seating in bottom anchorhead, inches								Comments	
			Strand 17	Strand 6	Strand 1	Wedge 17	Wedge 6	Wedge 1	Ref. pt. AB	Ref. pt. BB		
UngROUTED Specimen	1	25.2	2.188	2.127	2.037	3.562	3.572	3.566	3.667	3.668	REFERENCE VALUES PRIOR TO CYCLING CHANGE IN SEATING FROM PREVIOUS READING	
	2	403.2	.052	.060	.061	.053	.054	.055	.001	.001		
		25.2	-.004	-.005	-.007	-.005	-.006	-.041	-.002	-.002		
		421.0	.010	.008	.006	.007	.009	.042	.001	.001		
	3	25.2	-.005	-.007	-.008	-.005	-.007	-.007	-.001	-.001		
		406.0	.003	.008	.008	.006	.008	.008	.003	.002		
		501.0	.010	.010	.013	.008	.008	.009	.000	.000		
	4	406.7	-.001	-.001	-.004	.000	-.001	-.001	-.001	-.002		
		501.0	.000	.000	.001	.001	.002	.001	.000	.000		
	5	404.6	-.001	-.001	-.004	-.001	-.002	-.002	.000	.000		
		500.4	.002	.002	.000	.001	.002	.002	.000	.000		
	Grouted Specimen before cycling	1	402.3	.001	-.002	.000	-.002	-.003	-.002	-.002		.001
			503.0	.000	.001	.002	.001	.001	.001	.001		.000
		2	402.0	.002	-.001	-.002	-.001	-.001	-.002	.001		.000
			500.0	.000	.001	.002	.000	.001	.002	.000		.000
500,000 cycles	1	404.0	-.001	-.001	-.002	-.001	-.002	-.002	.000	.000		
		498.0	.001	.001	.001	.001	.001	.002	.000	.000		
1,000,018 cycles	1	403.0	.000	.000	.000	.000	.000	.000	.000	.000		
1,500,000 cycles	1	303.0	-.001	-.001	-.002	-.001	-.001	-.002	-.003	.001		
2,000,003 cycles	1	310.0	.000	.000	.000	.000	.000	.000	.000	.000		
AFTER ULTIMATE TEST		.0	2.256	2.199	2.102	3.625	3.636	3.629	3.665	3.669	REFERENCE VALUES AFTER CYCLING	
		.0	.068	.072	.065	.063	.064	.063	-.002	.001	CHANGE FROM INITIAL READINGS AFTER CYCLING	
AFTER ULTIMATE TEST		.0	2.329	2.270	2.166	3.697	3.705	3.687	3.668	3.669	REFERENCE VALUES AFTER ULTIMATE TEST	
		.0	.141	.143	.129	.135	.133	.121	.001	.001	CHANGE FROM INITIAL READINGS AFTER ULTIMATE TEST	

Table 5.3 19-Strand Specimen Elongation Data

Description	Load Cycle	Load, kips	Displacement, inches	Change in Disp., inches	Adjust for bottom plate distortion	Stiffness, kips/inch	Average Stiffness, kips/inch	
Ungrouted Specimen	1	25.2	.000		*			
		403.2	1.004	1.004	*	376.5		
	2	25.2	.175	-.829	*	456.0		
		421.0	1.046	-.871	*	454.4		
	3	25.2	.192	-.854	*	463.5		
		406.0	1.019	-.827	*	460.5		
	4	501.0	1.240	-.221	-.209	454.5	554.4 ** note: average does not include first load cycle to upper fatigue load	
		406.7	1.061	-.179	-.167	564.7		
	5	501.0	1.244	-.183	-.171	551.5		
		404.6	1.057	-.187	-.175	550.9		
			500.4	1.243	-.186	550.6		
	Grouted Specimen	1	402.3	1.067	-.183	-.171	588.9	611.7
			503.0	1.250	-.175	-.163	619.6	
		2	402.0	1.075	-.172	-.160	612.5	
			500.0	1.247	-.177	-.165	618.3	
3		398.0	1.070	-.180	-.168	619.0		
		502.0	1.250					
500,000 cycles	1	501.0	1.266	-.163	-.151	624.5	629.9	
		406.7	1.103	-.161	-.149	634.0		
	2	501.3	1.264	-.162	-.150	630.7		
		406.7	1.102	-.162	-.150	628.7		
	3	501.0	1.264	-.162	-.150	630.7		
		406.4	1.102					
1,000,018 cycles	1	501.0	1.269	-.174	-.162	582.1	592.4	
		406.7	1.095	-.170	-.158	596.8		
	2	501.0	1.265	-.171	-.159	596.0		
		406.1	1.094	-.171	-.159	593.1		
	3	500.4	1.265	-.171	-.159	593.1		
		406.1	1.094					
1,500,000 cycles	1	500.7	1.285	-.175	-.163	580.4	586.5	
		406.1	1.110	-.174	-.162	580.2		
	2	500.1	1.284	-.171	-.159	591.3		
		406.1	1.113	-.172	-.160	589.4		
	3	500.7	1.285	-.172	-.160	589.4		
		406.4	1.113					
2,000,003 cycles	1	501.0	1.293	-.176	-.164	576.8	578.2	
		406.4	1.117	-.174	-.162	580.2		
	2	500.4	1.291	-.174	-.162	580.2		
		406.4	1.117	-.176	-.164	576.8		
	3	501.0	1.293	-.175	-.163	576.7		
		407.0	1.118					

*. Adjustments for bottom plate distortion not made
 **. Average stiffness calculations based on data from cycling between upper and lower fatigue loads

0.012 inches from the change in displacement given by the potentiometer for the upper and lower fatigue loads.

The specimen was then loaded to 428.0 kips, or 99.6% of the prescribed intermediate grout load level of 429.8 kips (38.6% of GUTS, or 104.22 ksi). The load maintainer bolts were set and the corresponding displacement was held constant during the grouting and curing phase. A large variance in the loads recorded during the curing of the grout (from a minimum of 388.0 kips-6 hours and 50 minutes after beginning the primary grout, to a maximum load of 431.6 kips prior to static cycling-93 hours and 45 minutes after beginning the primary grout) is believed to be due to temperature changes experienced by the specimen during the curing and shrinkage of the grout.

Prior to grouting, the strand/wedge measurement points on both the top and bottom anchorheads were generously greased to prevent bonding of the grout at those points. Primary grouting was accomplished by pumping the grout through the grout cap attached to the bottom anchorage and through grout holes in the bottom anchorhead, as shown in Figure 5.18. This procedure continued until the grout in the specimen reached a level of approximately 1 foot below the top anchorhead. During the primary grouting procedure, water was observed emanating from interstices between the wires in each strand at the top anchorhead. The grout was then cured for four hours. Bleed water was then siphoned off from the specimen at the top anchorhead, as is shown in Figure 5.19. A secondary grout which filled the remaining ungrouted specimen length was then performed by pouring the grout mixture through a funnel and hose which was extended through a vent hole in the top anchorhead. Secondary grouting continued until the strand protruding from the top anchorhead was completely submerged in grout. This secondary grout procedure is shown in Figure 5.20.

The grout was allowed to cure for 3-1/2 days. The top and bottom grout caps were then removed from the anchorheads. The grout fractured during removal of the caps at the level of the strands as shown in Figure 5.21. Grout was removed from the strand and wedge measurement points to allow center wire and wedge seating checks during the remainder of the test.



Figure 5.18. Primary grouting from lower anchorage



Figure 5.19. Siphoning of bleed water from top anchorage



Figure 5.20. Secondary grouting procedure



Figure 5.21. Grout cap removed; break occurred at top of strand extensions

The grouted specimen was then loaded statically to the prescribed upper and lower fatigue load levels prior to the fatigue tests, 94 hours after the end of the secondary grout. Center wire and wedge seating and the specimen elongation at each load level were recorded. This procedure was repeated three times. During the first loading of the grouted specimen to the upper load level, a number of cracking sounds were heard. These sounds are presumed to be due to the cracking of the grout as the tensile load was increased above the grout load.

The strand/wedge measurement data for the grouted specimen are given in Table 5.2. The stiffness of the grouted specimen was calculated based on the change in load levels and change in specimen elongation for the load levels. Calculations for the measured stiffness of the composite section are shown in Table 5.3.

The bolt extension in the mechanical load maintainer was adjusted prior to the start of the fatigue test. This adjustment was necessary to keep the bolts from contacting the bearing ring during cycling.

Cyclic loading between the upper and lower fatigue load levels was begun. The loading was applied sinusoidally with the function generator at a constant amplitude corresponding to the prescribed stress range. The error between the desired loads and the actual loads achieved during cycling was $\pm 0.3\%$. The frequencies at which cycling took place ranged between 0.80 and 1.5 Hz. The load levels were monitored throughout the entire test with the peak detector and adjusted, along with the cycling frequency. Cycling of the specimen was interrupted at 5×10^5 cycle intervals to monitor centerwire and wedge seating and to measure the specimen stiffness. This data may also be found in Tables 5.2 and 5.3. Specimen elongation was held by the load maintainer plate during cycling interruptions due to oil leakage from the centerhole ram or automatic pump temperature error limits. The average load corresponding to this elongation was 308.6 kips, with a variance of $\pm 2\%$.

Upon completion of the fatigue load test, an ultimate tensile test of the specimen was performed. The loads obtained and the specimen elongation during the static loading were plotted with an X-Y recorder. The specimen was loaded statically from a load of 314.4 kips held by the load maintainer plate. During the static loading of the specimen, at 1014.3 kips, a single popping sound was heard from the specimen. The specimen continued to be loaded until the load reached

1139.5 kips, at which time a number of large popping sounds in short succession were heard and the load dropped off. The test was concluded at this point. A plot of load versus specimen elongation for the ultimate tensile test is shown in Figure 5.22.

Upon completion of the static ultimate strength test, the specimen was removed from the test machine. It was then carefully disassembled by the sponsor and UT personnel to determine the nature of the failure that occurred.

5.4 Test Results

Table 5.1 gives a time history of the events that took place during the loading of the specimen. This includes cycling interruptions for strand/wedge seating and stiffness checks, as well as interruptions due to centerhole ram leaks and pump overheating problems.

Table 5.2 summarizes the center wire and wedge seatings for the gage points on the top and bottom anchorheads during the test. It also demonstrates the measurement repeatability of the anchorhead reference points AT, BT, AB, and BB to within ± 0.002 inches. Table 5.2 also shows that the change in seating reduces as the specimen was cycled. By the end of the fifth load cycle of the ungrouted specimen, all wedge seating changes were essentially within the repeatability of the reference values.

Table 5.3 lists the specimen elongations recorded for each load level at every 5×10^5 cycle increment. The correction of -0.012 inches to the specimen elongation was not made for cycling ranges outside of that between the given upper and lower fatigue load because the given displacement of the bottom fatigue plate was not actually witnessed or measured until after cycling had already begun.

The stiffness of the specimen was calculated by dividing the change in load by the change in elongation (corrected for bottom plate distortion) between the upper and lower fatigue loads. Expressed in equation form,

$$K = \frac{dP}{(dE - 0.012)}$$

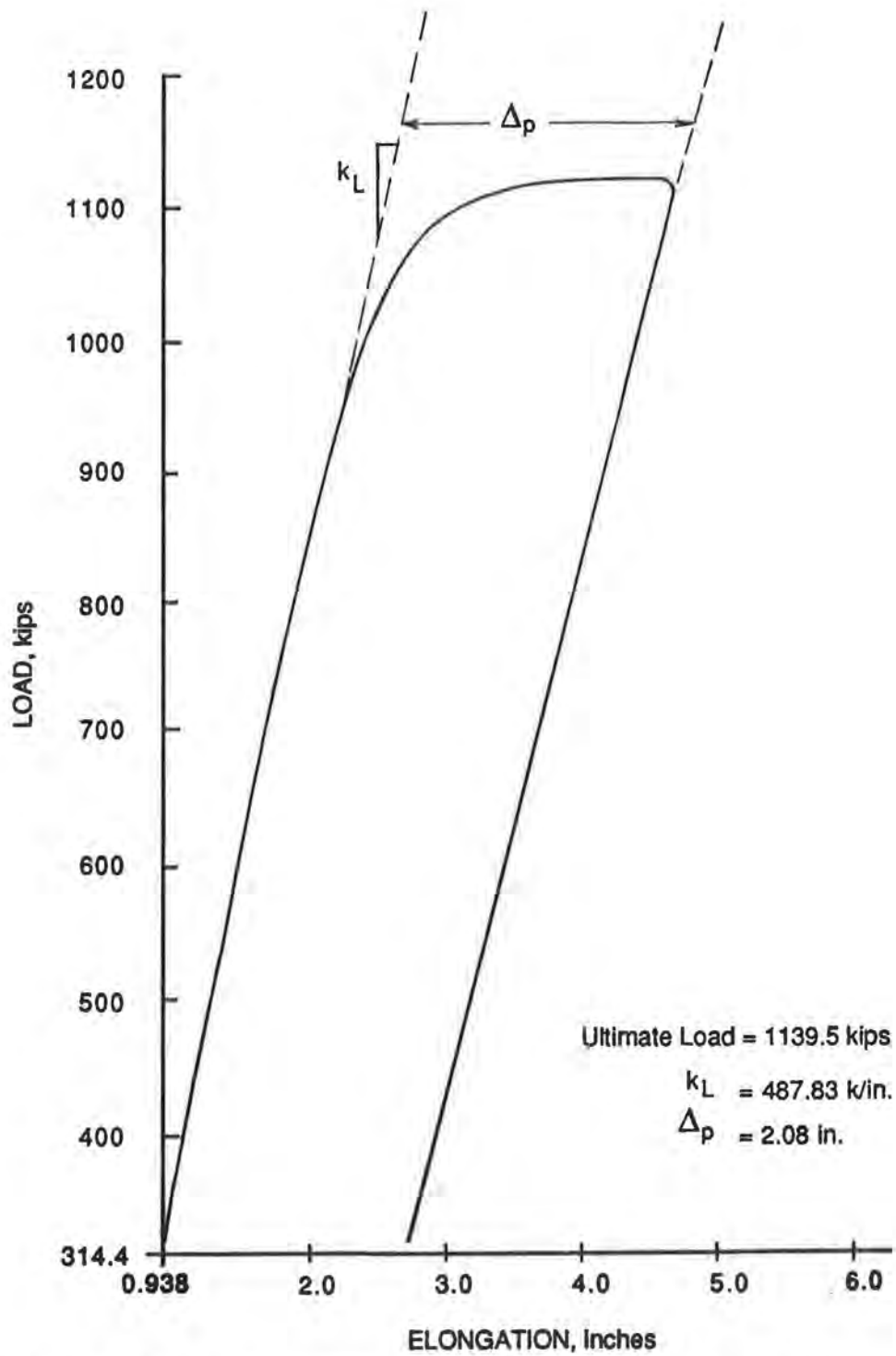


Figure 5.22 Load-elongation curve for 19 strand cable stay specimen

where dP is the change in load (kips) and dE is the change in displacement (inches). Note in Table 5.3 that the average stiffness of the ungrouted specimen does not include values from the first cycle to the upper fatigue load, cycle 3. These values were not used as significant wedge seating was still occurring at this time, as is evident from Table 5.2.

Examination of the stiffness calculations made every 5×10^5 cycles reveals a number of points of interest. First, and most importantly, it is noted that the measured stiffness of the grouted specimen during cycling never fell below that of the ungrouted specimen, at 554.4 k/in. However, the measured stiffness of the grouted specimen after 2×10^6 cycles was only 4.3% greater than the measured stiffness of the ungrouted specimen. Secondly, the stiffness of the grouted specimen actually increased by 3% (from 611.7 k/in to 629.9 k/in) during the time that elapsed between 0 and 5×10^5 cycles. Lastly, from the load-elongation curve shown in Figure 5.22, the estimated stiffness in the elastic range is 487.83 k/in. This value is significantly lower than those calculated between the upper and lower fatigue loads. In fact, the estimated value is 15.6% lower than the value calculated at 2,000,003 cycles. The low stiffness value can be attributed to significant wedge seating that occurred during the ultimate strength test, as shown in Table 5.2.

The results of the ultimate tensile test show that the specimen reached an ultimate load of 1139.5 kips. This figure represents 95.1% of the tested ultimate tensile strength of the specimen, as determined by the results of individual strand tests performed by the TDHPT for the sponsor.

It appears from Figure 5.22 that the specimen began to exhibit inelastic behavior at an elongation of approximately 2.63 inches. The total amount of plastic deformation that took place during the ultimate tensile test was 2.08 inches.

Inspection of the top anchorhead upon removal of the specimen from the test machine revealed that the tops of all wedges had seated below the face of the anchorhead, with the exceptions of strands 4 and 10. Wedges in strands 4 and 10 moved away from the anchorhead. Additionally, the center wire in strand 4 slipped as shown in Figure 5.23. Inspection of the bottom anchorhead revealed that the wedges had seated below the face of the anchorhead, with the exceptions of strands 1, 2, 4, 7, and 10. The wedges for these strands pulled out from the anchorhead.

The seating of the wedges for strands 1, 6, and 17 were measured prior to cycling and are given in Table 5.2. No measurements were made for the other wedges.

Disassembly of the specimen revealed circumferential cracking of the grout. These cracks were spaced at about 1/2 to 1 inch along the entire length of the specimen. These circumferential cracks are believed to be the result of tensile loads reached during cyclic and static portions of the test that exceeded the grouting load. Figure 5.24 shows the typical crack spacing and orientation. Longitudinal cracks in the grout that ran the entire length of the specimen were also found. The locations of these cracks corresponded to the grout cover directly above strands 4 and 10. The orientation of these cracks is shown in Figure 5.25.

Only minor distress of the polyethylene pipe was observed. This occurred in the tension ring region, where it was evident that the strands had been rubbing against the inner wall of the polyethylene pipe. The contact points on the pipe are shown in Figure 5.26.

Grout was chipped away from the specimen and the individual strands were examined. Wire failures were found in strands 4, 10, and 18 at locations shown in Figure 5.27. The nature of these failures is described below.

Strand 4: Six wire failures were found in the grip within the top anchorhead. One outer wire contained a fatigue crack. The fracture surface of this wire is shown in Figure 5.28. The other five outer wires failed in a ductile manner. The center wire slipped and did not break. For purposes of comparison, a ductile wire break from a strand is shown in Figure 5.29.

Strand 10: Six wire failures were discovered approximately 3 to 6 inches below the bearing face of the top anchorhead as shown in Figure 5.30. One of the fractured outer wires had a fatigue crack. The fracture is shown in Fig. 5.31. The other five wires showed no evidence of fatigue cracking. The remaining outer wire failed within the grip region of the top anchorhead and contained a fatigue crack. The fractured surface of this wire is shown in Fig. 5.32.

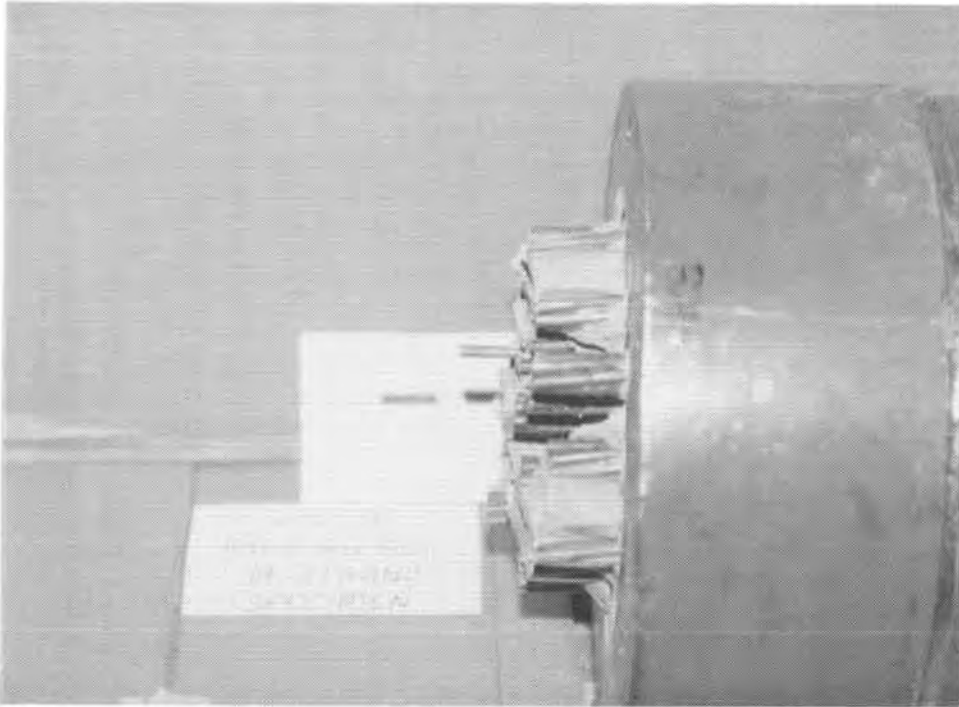


Figure 5.23 Center wire slip in strand 4 at bottom anchorhead

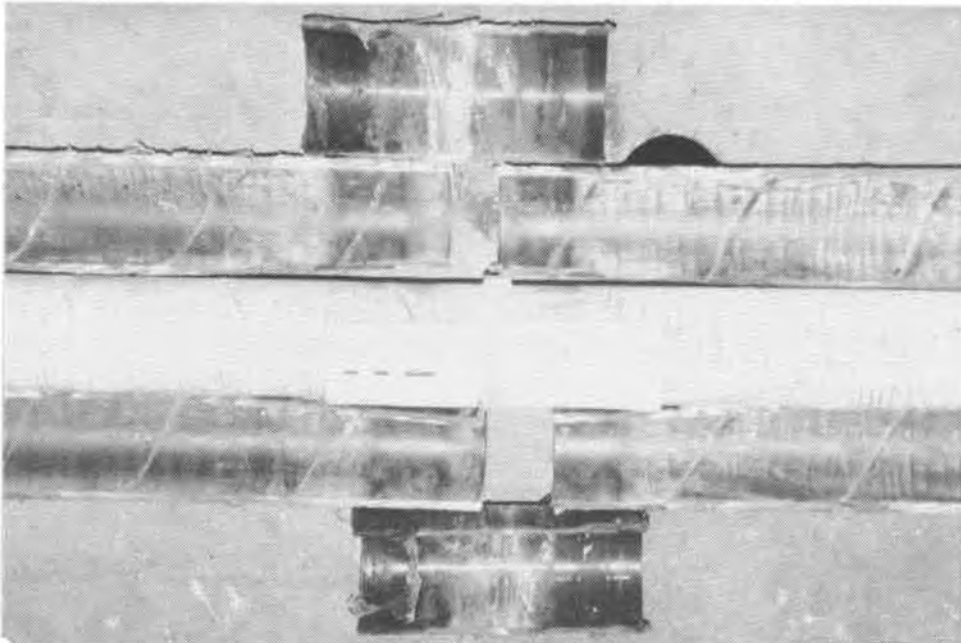


Figure 5.24 Circumferential crack distribution in grout

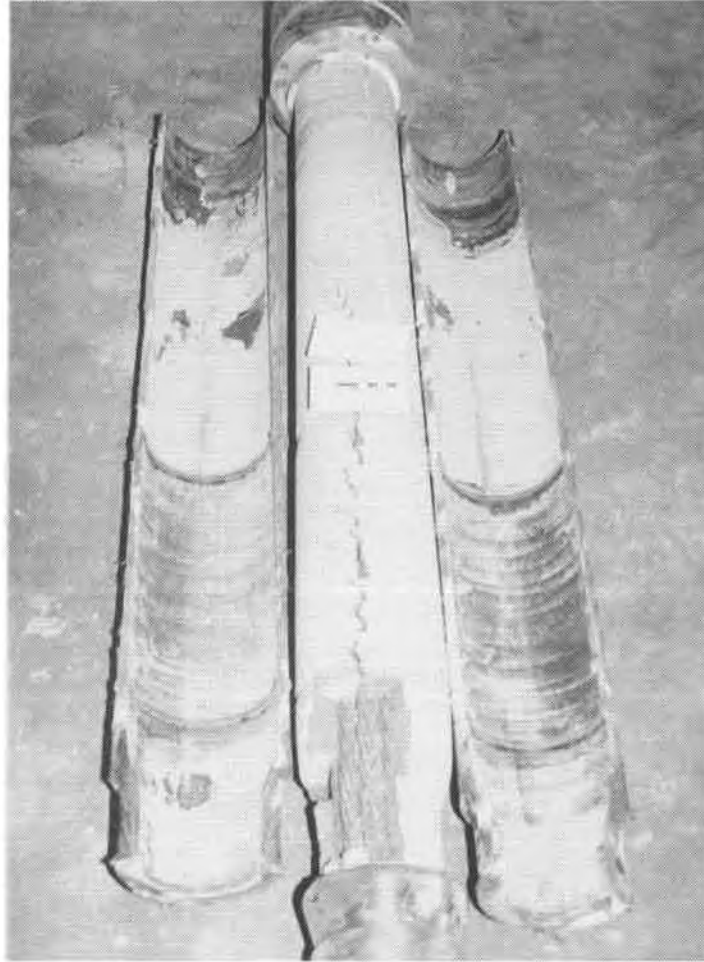


Figure 5.25 Longitudinal cracking of grout



Figure 5.26 Strand contact points on polyethylene pipe

Strand 18: A total of two wire breaks were found, both with fatigue cracks. One fracture, shown in Figure 5.33, occurred in an outer wire in the stay below the upper tension ring assembly, 6'-03" below the bearing face of the top anchorhead. The other outer wire fractured in the grip region of the top anchorhead. Figures 5.34 and 5.35 show the fracture surface of these wires.

The velocity transducer system used to monitor the specimen during cyclic testing did not provide a reliable means of detecting wire breaks. The constant shut-off of the loading system due to oil leaks and high oil temperature caused false indications. The change in stiffness between 1,500,000 and 2,000,000 cycles, where the majority of fatigue breaks would be expected to occur, is only 1.4%. Based on strand area alone, two wire breaks would cause a change of stiffness of 1.5%. Therefore, it is unlikely that the five wires which contained fatigue cracks failed in this last increment of cycling.

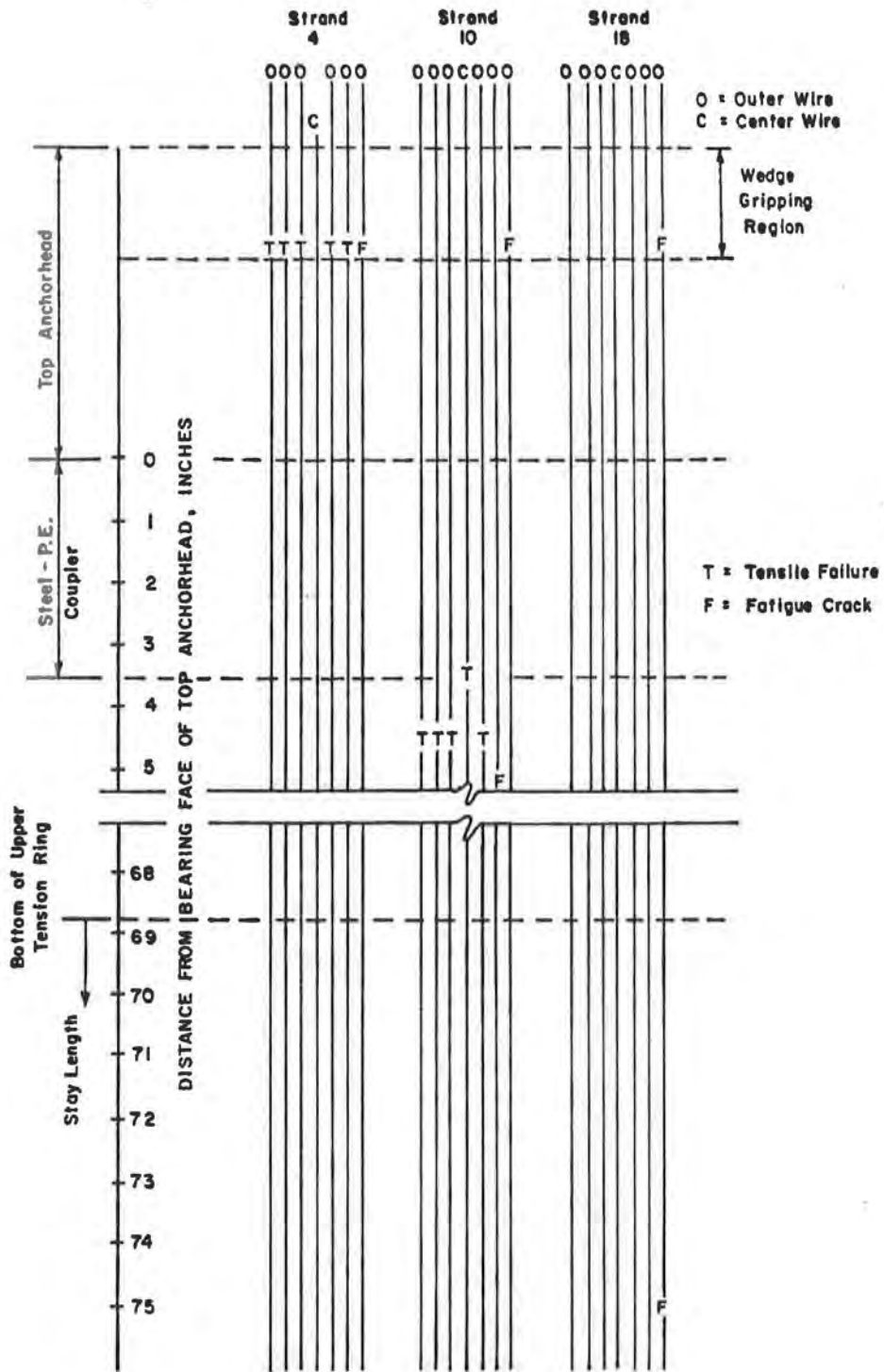


Figure 5.27. Wire break locations

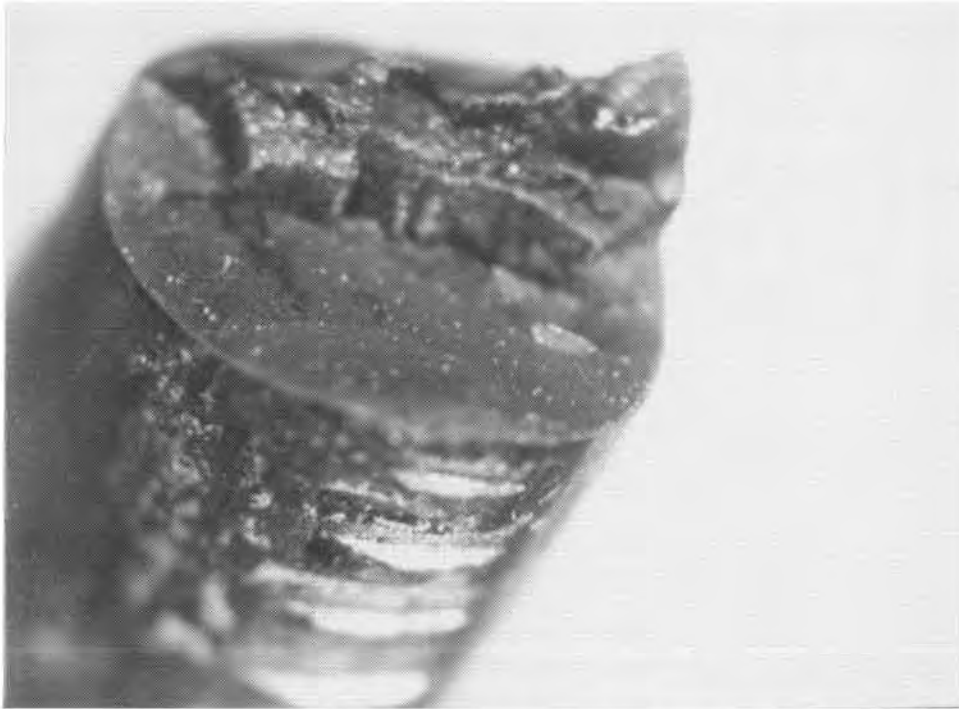


Figure 5.28. Outer wire failure in wedges of top anchorhead, strand 4

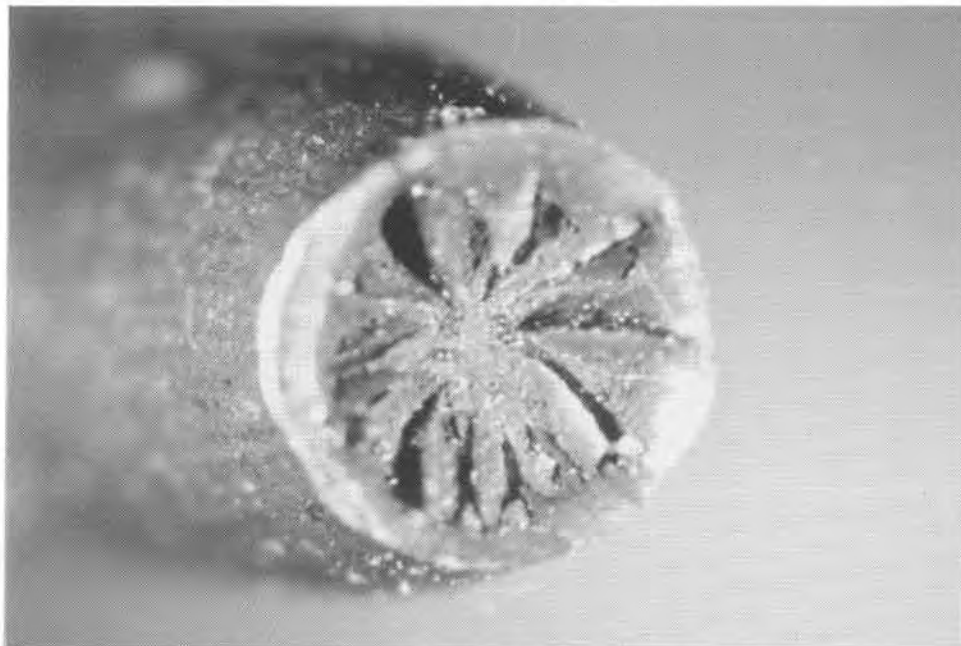


Figure 5.29. Ductile wire break in strand 4

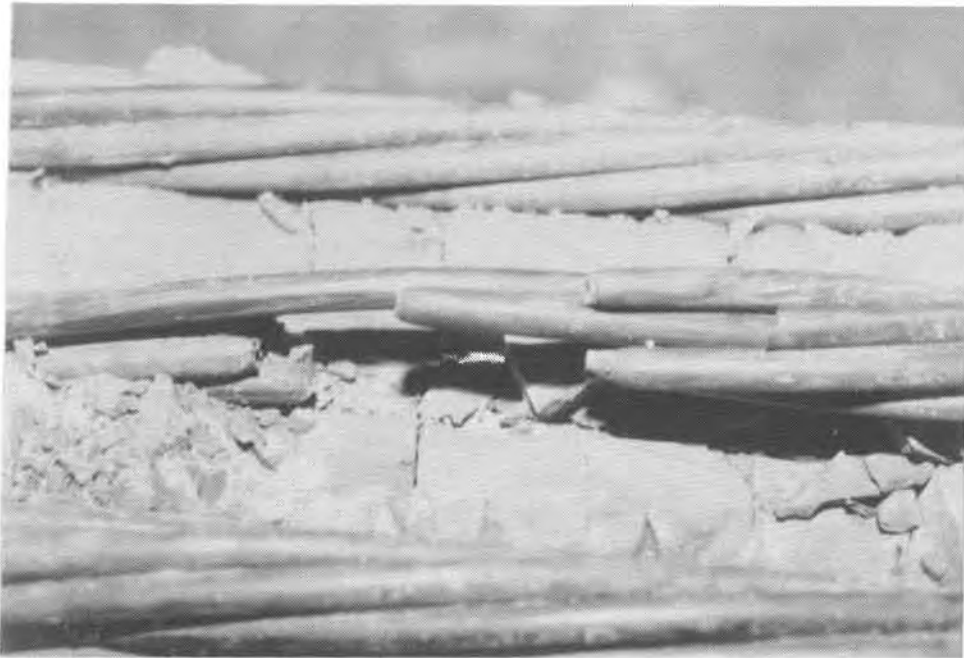


Figure 5.30 Wire breaks near top anchorhead in strand 10



Figure 5.31. Outer wire failure 3 to 6 inches from bearing face of top anchorhead, strand 10



Figure 5.32 Outer wire failure in wedges of top anchorhead, strand 10

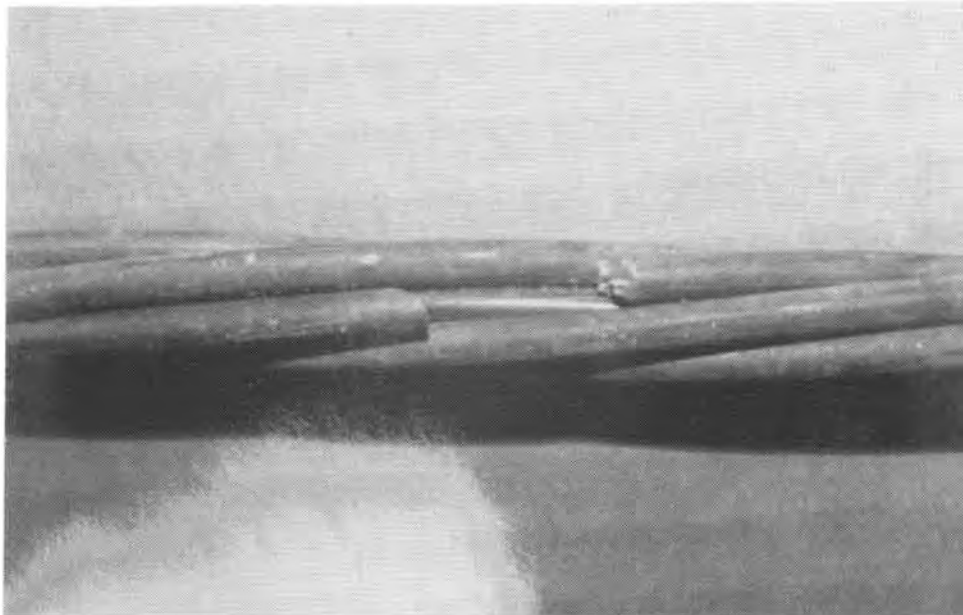


Figure 5.33 Wire break in strand 18 in stay length



Figure 5.34 Outer wire failure in stay lengths, strand 18



Figure 5.35 Outer wire failure in wedges of top anchorhead, strand 18

Appendix B contains axial strain information collected during the testing.

5.5 Summary of Test Results

5.5.1 Load Behavior The specimen sustained 2×10^6 cycles of loading at a maximum nominal fatigue load of 500.9 kips and a minimum fatigue load of 406.3 kips. At completion of the fatigue test the specimen was loaded to 95.1% of the actual strength of the strand (1139.5 kips) when failure occurred. This value represents 102.3% of GUTS.

5.5.2 Wire Breakages Upon dismantling, 15 wire breaks were found. Eight wire breaks occurred in the upper anchorhead; six approximately 3 to 6 inches below the anchorhead; and one below the upper tension ring. Five of the breaks were initiated by fatigue while the remaining ten wire breaks were ductile "cup cone fractures." During the test, wire breaks were only heard at loads of 1014.3 kips (a single popping sound) and at ultimate load 1139.5 (a number of popping sounds). Inspection of the breaks revealed five were initiated during the fatigue test but likely fractured during the static test.

5.5.3 Longitudinal Cracking The two longitudinal cracks in the grout cover were located directly above strand 4 and 10. Strand 10 contained a total of 6 wire failures. Strand 4 also contained a total of 6 wire failures. A simple explanation exists for the correlation of these facts; when the wires failed in the ultimate strength test, a compression wave travelled back down the strand, forcing the strand to buckle out and crack its grout cover.

5.5.4 Stiffness and Wedge Seating The specimen stiffness measured at the fatigue test loads increased after grouting and continued to increase during the first 500,000 cycles. The stiffness gradually reduced with continued cycling. The reason for the increase in stiffness to 500,000 cycles is fairly straightforward. Figure 5.36 shows that significant increases in the grout strength (stiffness) took place in the specimen during cycling. According to Figure 5.36, this increase appears to be on the order of 33% of the strength from the time of initial cycling to completion of the fatigue test. Grouting took place at an intermediate level at 38.4% of GUTS. Therefore the grout was in compression at the lower load level, at 36.5% of GUTS. The increase in grout strength, and therefore stiffness, contributed to the increase in the total specimen stiffness.

The increase in grout strength, and therefore stiffness, contributed to the increase in the total specimen stiffness.

No significant seating during the fatigue test of the wedges or strand was measured after the first five cycles of the fatigue loading.

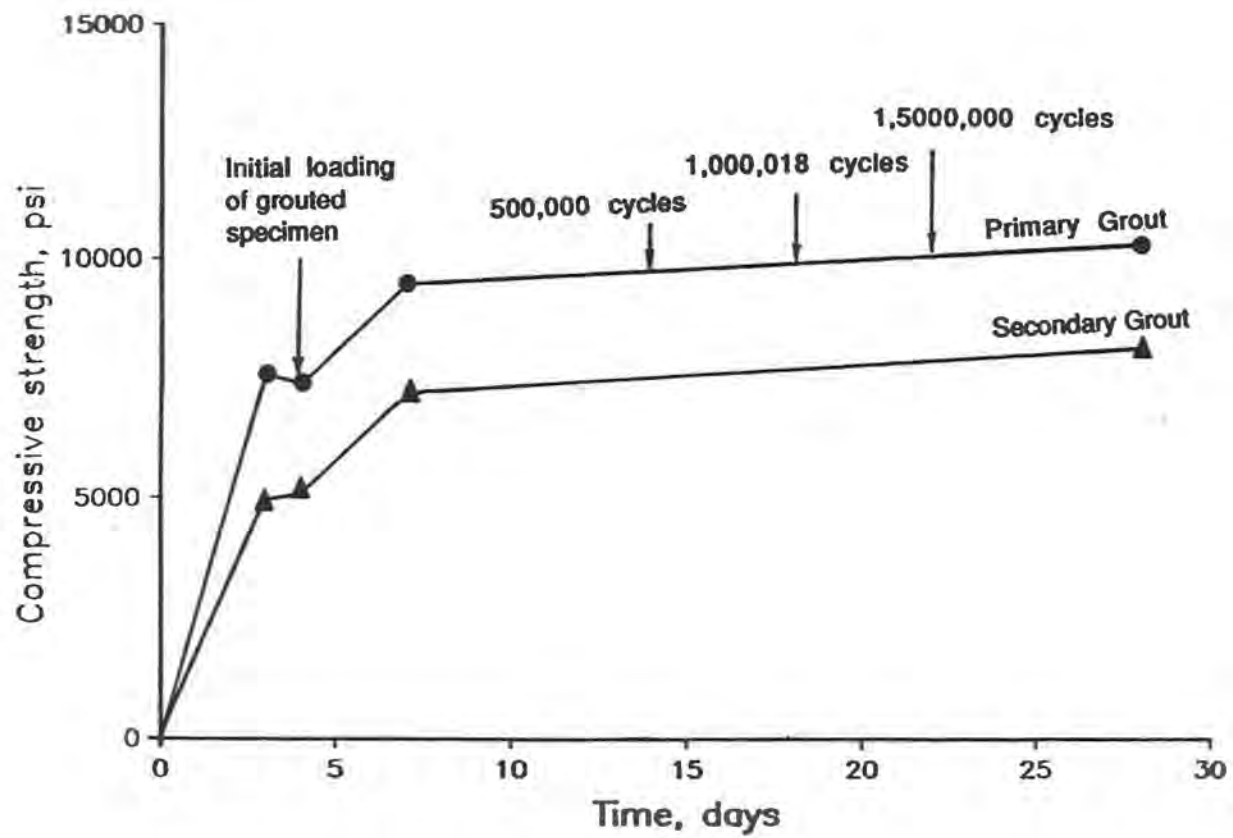


Figure 5.36 Grout cube strength over time

CHAPTER 6

SUMMARY AND RECOMMENDATIONS FOR FURTHER STUDY

In conclusion, research conducted at The University of Texas Phil M. Ferguson Structural Engineering Laboratory has made contributions to a better understanding of the behavior of stay cable anchorage systems. In particular strand failure modes, such as fretting fatigue in grip regions, have been identified and practical measures, such as the use of softer wedges in a double-chuck anchorage, have been established to eliminate these failures. Additionally, the relative insignificance of locking end plates and buttonheads with respect to load-carrying capacity has been established for parallel wire stays with Hi-Am anchorages.

Certain observations and recommendations can be drawn from the parallel strand stay test conducted by the author. First, the significance of the number of fatigue cracks found to occur within the wedge gripping region of the anchorhead cannot be understated. Second, disassembly of the specimen revealed the presence of circumferential cracking in the protective cement grout along the entire specimen length. The presence of these cracks leads to questions regarding the actual protection afforded the stay by the grout. Also, with respect to the grout, it is recommended by the author that bridge designers do not account for the presence of the grout in calculating the total stay stiffness. This is because the measured stiffness of the grouted specimen after 2×10^6 cycles, when compared to the measured ungrouted stiffness, was not significantly higher. If grouting is performed much closer to the upper fatigue load, then under normal service conditions the added stiffness may be taken into account.

During the writing of this thesis, several points of interest have occurred to the author which could provide topics for further research at The University of Texas and elsewhere.

First, research in the area of cable corrosion protection is of vital importance. The lack of existence of an adequate means of corrosion protection, and cable inspection due to the protective measures employed, will hamper the continued advancement and use of the cable-stayed bridge.

Related to the topic of cable corrosion, fatigue problems continue to plague strand systems utilizing friction-type wedge anchors. Research in the field of an improved anchorage for strand-type systems should be investigated further. In particular, continued development of a simple anchorage system using softer wedges in a double chuck system should be considered.

Further research in the use of polyethylene pipe in cable stay systems is needed. The problems encountered thus far in the use of this material, such as the unfavorable thermal characteristics and history of splitting, need careful laboratory investigations. Tests involving the thermal cycling of polyethylene pipe while under tensile load would help to establish the fatigue characteristics of the pipe due to temperature fluctuation.

Investigations are also needed to establish the applicability of high-pressure cement grouting with stays using either epoxy coated or uncoated parallel strand. Evidence was presented in Chapter 2 which pointed to high-pressure cement grouting techniques as a cause of corrosion fatigue in epoxy coated strand. While the problem of water intrusion in uncoated strand was also noticed in the test described in Chapter 5, no evidence of corrosion fatigue was found. Perhaps this is because the epoxy coating of strands prevents the water from leaving the strand once it has entered, whereas the uncoated strand allows water to be drawn back out during the curing process. Research in the performance of a stay using an epoxy or petroleum wax corrosion protection should also be sought. The temperature properties of these materials and their bonding properties to steel and polyethylene pipe need to be established.

It is also suggested that studies are conducted on the two-piece wedge system described earlier in Chapter 2. Finite element studies and laboratory tests should be conducted to determine the uniformity of gripping around the strand. In addition, the strength and fatigue behavior of the wedges should be investigated, as each piece in the wedge is split; this should result in the presence of a stress concentration.

Finally, research in the applications of cable stays for use as tendons on deepwater tension leg drilling platforms (TLP's) should be studied. The loads seen by the tendons are similar in nature to those seen by cable stays; they are primarily

tension members, however they are subjected to lateral load due to current forces. Currently TLP's use either large diameter welded tubes with threaded connectors or small bore tubulars with mechanical or threaded connectors. In either case, the strength of these tendons is not nearly as high as that of wires or strands used in cable stays. A corrosion protection system would have to be devised which would allow the stay to operate in a corrosive marine environment.

APPENDIX A: LOAD CELL CALIBRATION INFORMATION

Removal of the load cells for calibration was made possible by removing the centerhole ram, work platform, and upper steel spacer from the test frame shown in Figure 1 of the test report. Each load cell was then calibrated individually with the NBS-calibrated load cell and using a 600 kip capacity machine. The individual load cell calibrations are shown in Figures A1 through A4. Calibration of the load cell group was made possible by placing a 4 inch thick steel plate over the 4 load cells, centering the calibration load cell on top of the steel plate, and applying load through the 600 kip test machine. This arrangement is shown in Figure A5. The steel plate was chosen for its stiffness and ability to distribute the load evenly among the load cell group. The load cell group calibration with a strain indicator is shown in Figure A6. A final calibration with the control unit used for the cable test is shown in Figure A7. It is evident from Figure A7 that for the loads encountered in the test of the 19 strand specimen, the system error was $\pm 0.15\%$.

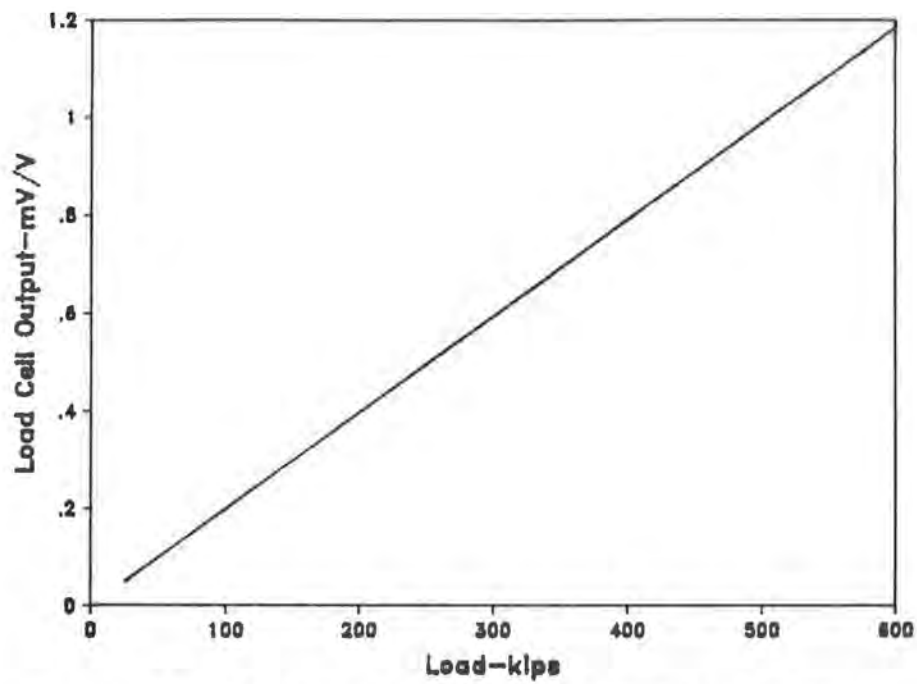


Figure A.1 Calibration of load cell SN 850326C UT 397640

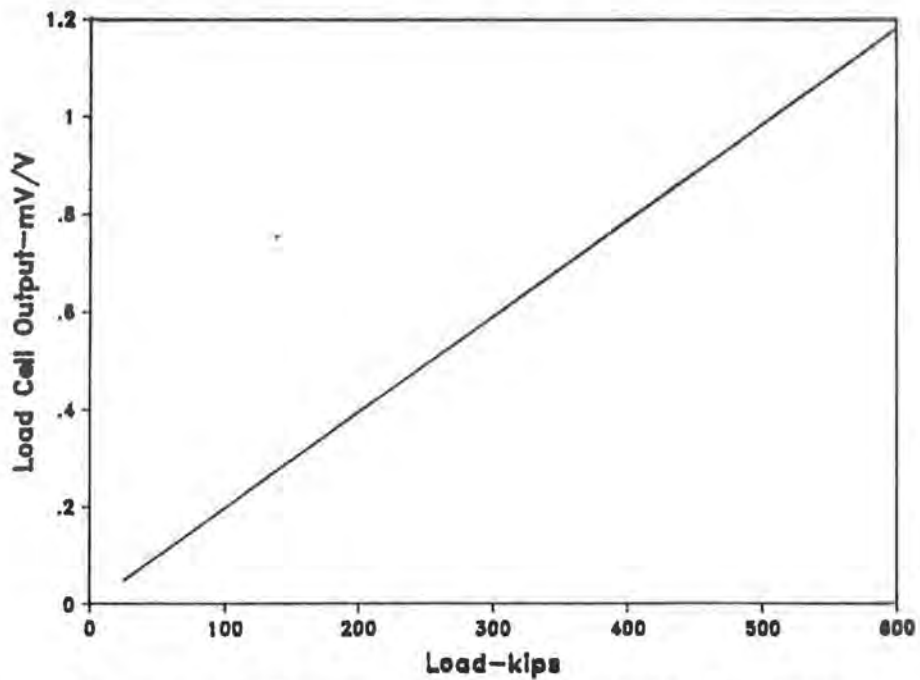


Figure A.2 Calibration of load cell SN 850326A UT 397642

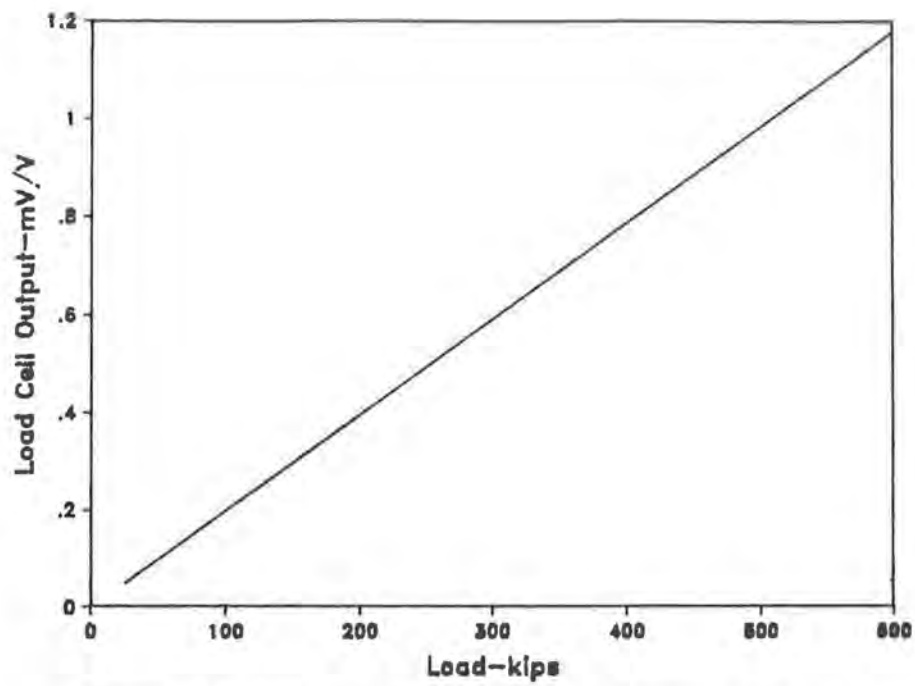


Figure A.3 Calibration of load cell SN 850326D UT 397641

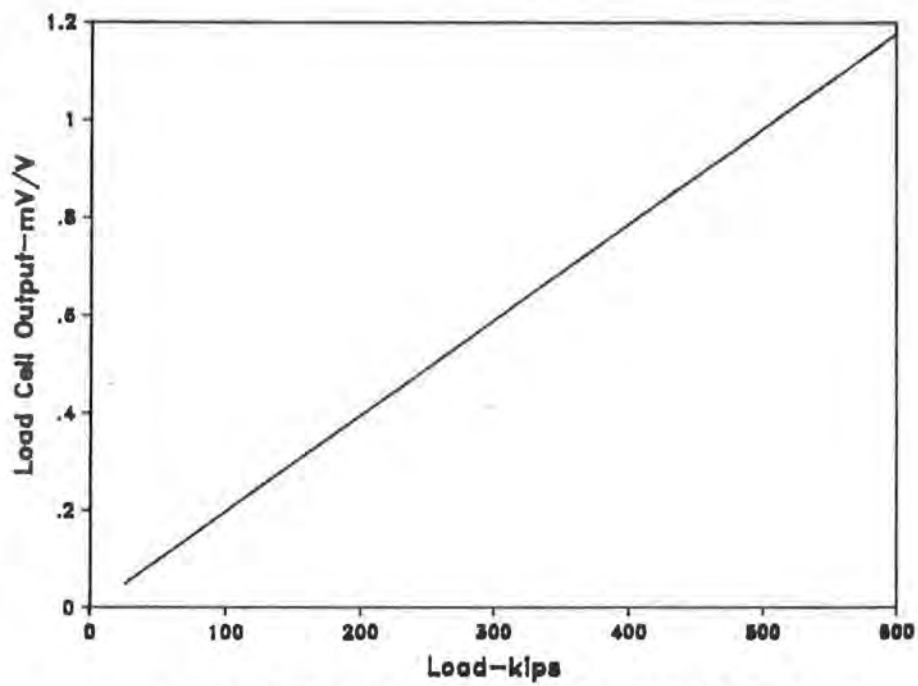


Figure A.4 Calibration of load cell SN 850326B UT 397639

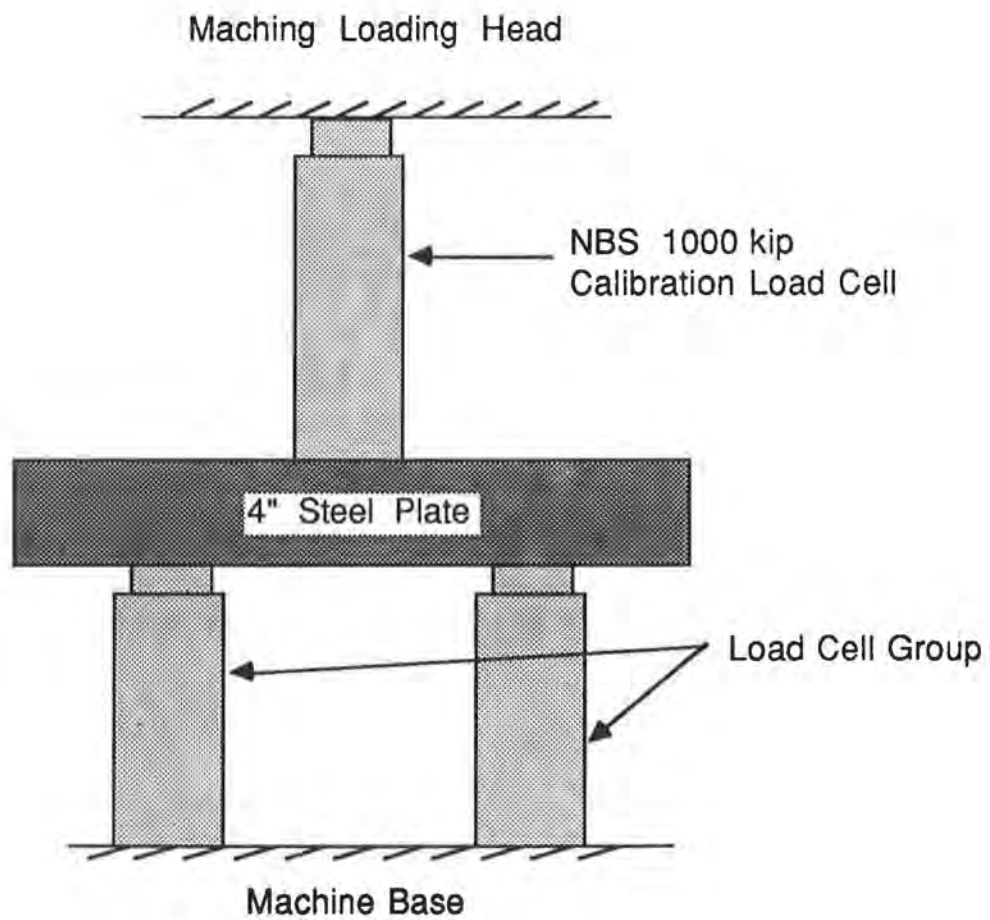


Figure A.5 Load cell group calibration

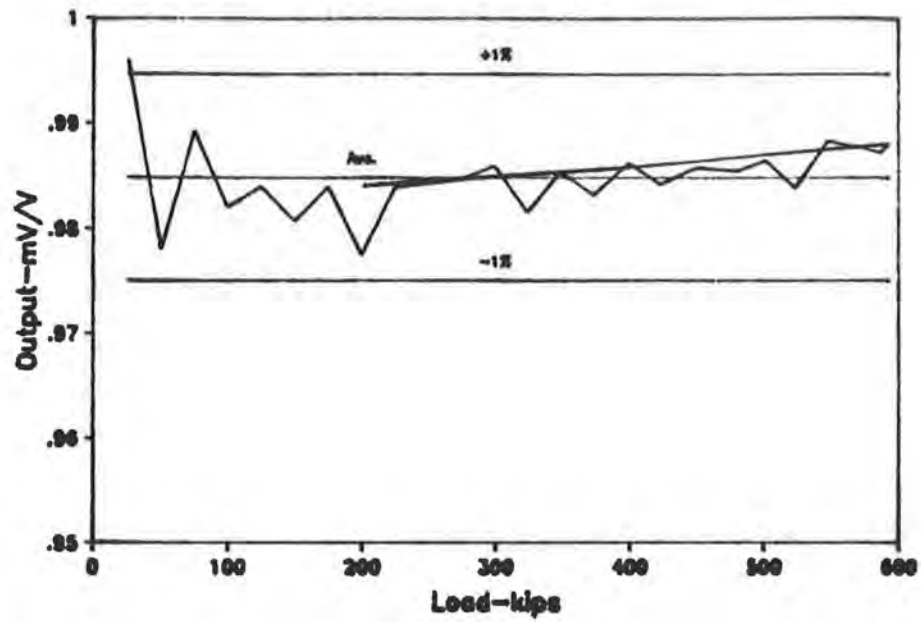


Figure A.6 Group calibration with strain indicator

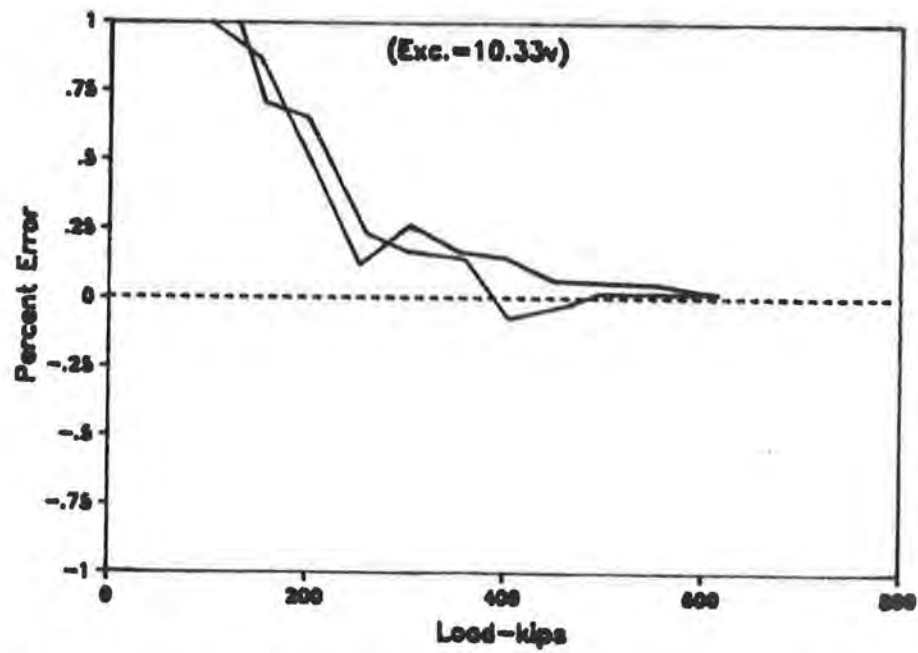


Figure A.7 Group calibration with closed loop test control unit

APPENDIX B: STRAIN GAGE DATA

Figure B.1 Strain gage data for 19 strand specimen

(microstrains)

Time from initial loading (hours)	COMMENTS	Load (kips)	Disp. (in.)	Gage 10	Gage 11	Mean	Gage 12	Gage 13	Mean	Gage 20	Gage 21	Mean	Gage 23	Gage 24	Mean	Gage 31	Gage 34	Mean
.00	pulling up bottom anchorage	2.5	.741	2	0	1	1	1	1	-1	0	-1	0	2	1	0	*	
26.21	final preseating of wedges	24.9	.001	420	-241	89	-24	23	-1	251	-668	-209	-674	-18	-346	-293	*	
26.45	1st cycle lower-ungROUTed specimen	405.8	1.003	556	271	413	221	354	288	655	299	477	26	19	23	-127	*	
27.30	2nd cycle lower load	421.1	1.046	573	321	447	289	416	353	834	658	746	130	32	81	-90	*	
27.52	3rd cycle unloaded	24.9	.192	456	-43	207	85	199	142	634	-152	241	-257	473	108	-164	*	
27.84	3rd cycle lower load	406.6	1.019	563	308	435	301	448	374	836	967	901	105	-14	45	-106	*	
42.71	begin primary grout	428.5	1.124	-95	-264	-179	42	143	92	540	624	582	-387	-332	-359	788	*	
43.16	end primary grout	420.3	1.124	-235	-413	-324	147	389	268	724	786	755	-69	20	-25	1226	*	
47.68	begin secondary grout	416.0	1.122	-348	-532	-440	351	457	404	578	512	545	-93	-32	-63	1900	*	
49.56	end secondary grout	387.6	1.122	-704	-835	-770	1212	1202	1207	502	300	401	-233	-281	-257	2652	*	
67.87	holding at grout load	429.7	1.122	710	-47	332	1950	1736	1843	882	947	914	-40	249	104	1524	*	
94.29	holding at grout load	434.3	1.122	612	-94	259	2059	1803	1931	925	1020	972	-18	298	140	954	*	
113.90	initial cycling of grouted specimen (rezero)	434.1	1.123	-1	0	-1	-1	0	0	0	0	0	0	0	0	-1	2	1
136.43	lower load, 1st cycle seating/stiffness check	403.0	1.068	-184	-109	-146	-122	-132	-127	-184	-252	-218	-179	-262	-221	-184	-288	-236
136.75	upper load, 1st cycle seating/stiffness check	503.6	1.250	471	315	393	522	496	509	643	562	603	574	417	495	-103	-224	-163
136.96	lower load, 2nd cycle seating/stiffness check	402.1	1.075	-67	-108	-87	-5	-87	-46	-103	-241	-172	-159	-316	-237	-322	-407	-364
137.14	upper load, 2nd cycle seating/stiffness check	500.2	1.247	354	319	336	557	521	539	672	530	601	542	380	461	-117	-230	-174
137.42	lower load, 3rd cycle seating/stiffness check	398.6	1.069	-154	-129	-141	27	-58	-16	-123	-275	-199	-190	-355	-272	-333	-391	-362
137.65	upper load, 3rd cycle seating/stiffness check	502.7	1.250	315	324	320	574	540	557	703	543	623	550	386	468	-87	-166	-127
285.26	500,000 cycle checks, 1st cycle upper load	501.1	1.263	-157	0	-78	438	564	501	282	-19	131	515	292	403	613	702	658
285.30	lower load, 1st cycle seating/stiffness check	406.4	1.103	-632	-553	-592	-212	-76	-144	-425	-711	-568	-126	-353	-239	360	544	452
285.32	upper load, 2nd cycle seating/stiffness check	501.2	1.264	-154	2	-76	439	564	502	284	-17	133	516	295	406	612	700	656
285.34	lower load, 2nd cycle seating/stiffness check	406.5	1.101	-633	-554	-593	-213	-78	-146	-424	-714	-569	-127	-353	-240	368	549	459
285.36	upper load, 3rd cycle seating/stiffness check	501.3	1.264	-154	3	-75	439	564	502	284	-17	134	516	294	405	613	702	658
285.38	lower load, 3rd cycle seating/stiffness check	406.3	1.102	-630	-551	-590	-211	-76	-144	-423	-710	-567	-125	-353	-239	369	552	461
384.82	1,000,018 cycle check; scan at mean load	453.9	1.183	-403	-318	-360	133	251	192	-140	-446	-293	170	-62	54	645	799	722
384.89	upper load, 1st cycle seating/stiffness check	500.9	1.272	-119	-22	-70	484	591	538	216	-106	55	504	272	388	775	869	822
384.91	lower load, 1st cycle seating/stiffness check	406.5	1.098	-629	-617	-623	-153	-38	-96	-450	-784	-617	-138	-371	-255	514	725	620
384.96	upper load, 2nd cycle seating/stiffness check	501.0	1.269	-123	-22	-73	484	592	538	220	-105	58	505	273	389	774	871	822
384.99	lower load, 2nd cycle seating/stiffness check	406.2	1.097	-630	-618	-624	-155	-41	-98	-452	-786	-619	-139	-372	-256	516	724	620
385.04	upper load, 3rd cycle seating/stiffness check	500.4	1.269	-121	-24	-72	482	590	536	215	-107	54	504	272	388	773	866	819
385.06	lower load, 3rd cycle seating/stiffness check	406.0	1.096	-629	-617	-623	-155	-41	-98	-452	-787	-620	-141	-374	-257	514	721	617
487.39	1,500,000 cycle check; 1st cycle lower load	406.0	1.103	-632	-627	-630	-44	62	9	-384	-702	-543	-98	-326	-212	583	864	724
487.41	upper load, 1st cycle seating/stiffness check	500.9	1.289	-104	128	12	622	709	665	335	-10	163	547	312	429	688	870	779
487.43	lower load, 2nd cycle seating/stiffness check	405.9	1.115	-623	-547	-585	-55	52	-1	-408	-734	-571	-122	-348	-235	418	720	569
487.45	upper load, 2nd cycle seating/stiffness check	500.2	1.288	-116	122	3	604	691	647	313	-30	142	532	297	415	671	858	764
487.45	lower load, 3rd cycle seating/stiffness check	406.2	1.116	-629	-551	-590	-61	46	-7	-414	-743	-578	-128	-352	-240	414	713	563
487.47	upper load, 3rd cycle seating/stiffness check	500.6	1.289	-115	124	4	603	691	647	312	-32	140	532	299	416	671	858	764
926.72	2,000,000 cycle checks, 1st cycle upper load	500.9	1.297	-118	33	-43	748	777	762	310	-53	128	523	275	399	623	876	750
926.76	lower load, 1st cycle seating/stiffness check	406.5	1.119	-669	-675	-672	113	178	146	-351	-702	-527	-154	-394	-274	315	677	496
926.79	upper load, 2nd cycle seating/stiffness check	500.4	1.295	-120	28	-46	746	773	760	309	-55	127	521	272	397	611	863	737
926.82	lower load, 2nd cycle seating/stiffness check	406.6	1.120	-666	-674	-670	110	176	143	-354	-705	-529	-154	-395	-275	298	664	481
926.84	upper load, 3rd cycle seating/stiffness check	501.4	1.297	-115	36	-40	757	784	770	317	-44	137	533	284	408	590	848	719
926.86	lower load, 3rd cycle seating/stiffness check	406.9	1.121	-666	-672	-669	114	179	146	-353	-700	-526	-148	-390	-269	279	649	464
977.13	scan before ultimate strength test (rezero)	314.4	.939	0	0	0	-1	0	-1	0	0	0	-1	0	0	-1	-1	-1
977.59	minimum fatigue load	406.0	1.081	327	648	487	443	449	446	738	750	744	569	622	596	77	25	51
977.61	maximum fatigue load	500.9	1.271	912	1405	1158	1109	1043	1076	1491	1501	1496	1255	1297	1276	125	3	64
977.66	680 kips	599.1	1.471	1570	2116	1843	1828	1750	1789	2251	2264	2258	1977	1963	1970	175	51	113
977.71	700 kips	699.0	1.683	2266	2935	2600	2591	2470	2531	3038	3019	3029	2715	2645	2680	246	51	148
977.76	800 kips	799.8	1.903	3053	3746	3399	3360	3187	3273	3824	3792	3808	3525	3312	3419	289	23	156
977.84	900 kips	899.2	2.135	3902	4683	4293	4089	3889	3989	4612	4611	4611	4221	3910	4065	270	2	136
977.90	1000 kips	999.5	2.404	5094	6132	5613	4982	4700	4841	5600	5642	5621	5016	4628	4822	217	-23	97
978.01	scan near ultimate load	1,138.2	4.060	18301	20101	19201	9613	8763	9188	18108	17131	17620	7845	6865	7355	-56	-282	-169
978.77	specimen hanging	-.1	1.831	11550	11894	11722	3968	3319	3643	15439	12216	13827	-433	-1818	-1125	-3907	1039	-1434

Figure B.1 Continued

Time from initial loading (hours)	COMMENTS	Load (kips)	Disp. (in.)	Gage 40	Gage 41	Mean	Gage 42	Gage 43	Mean	Gage 30	Gage 44	Mean	Gage 32	Gage 33	Mean
.00	pulling up bottom anchorage	2.5	.741	1	1	1	0	1	0	1	0	0	-1	-1	-1
26.21	final preseating of wedges	24.9	.001	-156	546	195	140	24	82	-1043	500	-271	326	-596	-135
26.45	1st cycle lower-ungROUTed specimen	405.8	1.003	-80	1172	546	616	153	385	-1676	1532	-72	840	-506	167
27.30	2nd cycle lower load	421.1	1.046	13	1209	611	621	176	398	-1592	1614	11	835	-410	213
27.52	2nd cycle unloaded	24.9	.192	96	618	357	271	54	162	-1062	836	-113	638	-423	108
27.84	3rd cycle lower load	406.6	1.019	29	1210	620	603	158	380	-1605	1623	9	834	-444	195
42.71	begin primary grout	428.5	1.124	-99	1109	505	110	-297	-93	-2236	1414	-411	490	-720	-115
43.16	end primary grout	420.3	1.124	-50	1164	557	847	568	707	-2028	1629	-199	932	-296	318
47.68	begin secondary grout	416.0	1.122	29	1261	645	1035	642	839	-2154	1360	-397	896	-333	282
49.56	end secondary grout	387.6	1.122	24	1265	644	2323	2085	2204	-1720	1138	-291	691	-589	51
67.87	holding at grout load	429.7	1.122	-120	853	366	2277	1791	2034	-820	1131	156	760	-598	81
94.29	holding at grout load	434.3	1.122	-107	854	373	2478	1886	2182	-792	1172	190	766	-565	101
113.90	initial cycling of grouted specimen (rezero)	434.1	1.123	0	-1	0	-1	-2	-1	-1	0	1	0	0	0
136.43	lower load, 1st cycle seating/stiffness check	403.0	1.068	-132	-133	-133	-121	-124	-122	-176	-198	-187	-161	-139	-150
136.75	upper load, 1st cycle seating/stiffness check	503.6	1.250	582	585	584	689	675	682	585	683	634	669	631	650
136.96	lower load, 2nd cycle seating/stiffness check	402.1	1.075	-24	-141	-83	6	-65	-30	-189	-139	-164	-126	-129	-128
137.14	upper load, 2nd cycle seating/stiffness check	500.2	1.247	612	549	580	678	636	657	575	683	629	648	622	635
137.42	lower load, 3rd cycle seating/stiffness check	398.6	1.069	-15	-174	-95	-30	-116	-73	-212	-148	-180	-148	-156	-152
137.65	upper load, 3rd cycle seating/stiffness check	502.7	1.250	644	560	602	693	637	665	598	725	662	664	642	653
225.26	500,000 cycle checks, 1st cycle upper load	501.1	1.263	867	493	680	819	596	708	340	779	560	695	663	679
225.30	lower load, 1st cycle seating/stiffness check	406.4	1.103	289	-153	68	102	-91	6	-369	45	-162	-14	-47	-30
225.32	upper load, 2nd cycle seating/stiffness check	501.2	1.264	869	494	681	819	596	708	344	780	562	698	665	681
225.34	lower load, 2nd cycle seating/stiffness check	406.5	1.101	288	-155	66	99	-94	2	-370	42	-164	-14	-48	-31
225.36	upper load, 3rd cycle seating/stiffness check	501.3	1.264	870	494	682	819	597	708	343	782	562	698	666	682
225.38	lower load, 3rd cycle seating/stiffness check	406.3	1.102	290	-153	69	102	-90	6	-367	45	-161	-13	-46	-29
334.82	1,000,018 cycle check; scan at mean load	453.9	1.183	588	160	374	438	231	334	-107	365	129	374	367	370
384.89	upper load, 1st cycle seating/stiffness check	500.9	1.272	862	475	669	787	574	681	260	746	503	733	721	727
384.91	lower load, 1st cycle seating/stiffness check	406.5	1.098	286	-169	59	44	-120	-38	-431	32	-200	27	40	33
384.96	upper load, 2nd cycle seating/stiffness check	501.0	1.269	864	474	669	788	576	682	262	747	505	734	721	728
384.99	lower load, 2nd cycle seating/stiffness check	406.2	1.097	286	-170	58	42	-122	-40	-433	29	-202	26	40	33
385.04	upper load, 3rd cycle seating/stiffness check	500.4	1.269	861	472	666	786	574	680	260	743	502	733	719	726
385.06	lower load, 3rd cycle seating/stiffness check	406.0	1.096	287	-171	58	41	-123	-41	-434	29	-203	24	38	31
487.36	1,500,000 cycle check; 1st cycle lower load	406.0	1.103	301	-152	75	75	-85	-5	-437	55	-191	93	105	99
487.39	upper load, 1st cycle seating/stiffness check	500.9	1.289	868	498	683	806	615	711	281	774	528	791	795	793
487.41	lower load, 2nd cycle seating/stiffness check	405.9	1.115	293	-153	70	66	-100	-17	-444	38	-203	68	93	80
487.43	upper load, 2nd cycle seating/stiffness check	500.2	1.288	861	490	676	798	604	701	265	757	511	775	781	778
487.45	lower load, 3rd cycle seating/stiffness check	406.2	1.116	289	-157	66	60	-105	-22	-450	33	-209	62	87	74
487.47	upper load, 3rd cycle seating/stiffness check	500.6	1.289	862	492	677	801	606	703	266	760	513	776	784	780
926.72	2,000,000 cycle checks, 1st cycle upper load	500.9	1.297	813	550	682	824	663	744	448	1004	726	753	802	778
926.76	lower load, 1st cycle seating/stiffness check	406.5	1.119	220	-98	61	97	1	49	-294	218	-38	35	84	59
926.79	upper load, 2nd cycle seating/stiffness check	500.4	1.295	812	549	680	824	661	743	445	1002	724	751	800	776
926.82	lower load, 2nd cycle seating/stiffness check	406.6	1.120	221	-98	61	97	2	49	-294	219	-38	34	83	59
926.84	upper load, 3rd cycle seating/stiffness check	501.4	1.297	819	555	687	831	671	751	456	1013	735	761	811	786
926.86	lower load, 3rd cycle seating/stiffness check	406.9	1.121	223	-95	64	102	5	53	-292	223	-35	38	87	62
977.13	scan before ultimate strength test (rezero)	314.4	.939	0	0	0	0	0	0	0	0	0	1	1	1
977.15	minimum fatigue load	406.0	1.081	443	463	453	568	488	528	567	638	602	610	605	607
977.61	maximum fatigue load	500.9	1.271	1048	1160	1104	1305	1169	1237	1347	1457	1402	1329	1344	1337
977.66	600 kips	599.1	1.471	1608	1752	1680	1975	1831	1903	2064	2306	2185	2049	2176	2113
977.71	700 kips	699.0	1.683	2198	2476	2337	2778	2630	2704	2790	3103	2946	2784	2882	2833
977.76	800 kips	799.8	1.903	2857	3275	3066	3525	3367	3446	3530	3966	3748	3483	3623	3553
977.84	900 kips	899.2	2.135	3554	4182	3868	4298	4136	4217	4286	4869	4577	4198	4376	4287
977.90	1000 kips	999.5	2.404	4446	5420	4933	5229	5071	5150	5230	5953	5591	5028	5289	5158
978.01	scan near ultimate load	1,138.2	4.060	8274	10658	9466	9585	9466	9426	12615	13712	13163	11202	11158	11180
978.77	specimen hanging	-1	1.831	1410	2926	2168	3583	3657	3620	9096	12291	10693	3451	6333	4892

REFERENCES

1. Podolny, W. and Scalzi, J. **Construction and Design of Cable-Stayed Bridges**. Second Edition, John Wiley and Sons, 1986
2. Aeberhard, H. U., Fischli, F., Luthi, K., and Schuler, W. "VSL Stay Cables for Cable-Stayed Bridges." VSL International Ltd., 1984.
3. Gimsing, N. J. **Cable Supported Bridges, Concept and Design**. John Wiley and Sons. 1983.
4. Troitsky, M. S. **Cable-Stayed Bridges—An Approach to Modern Bridge Design**. Second Edition, Van Nostrand Reinhold. 1988.
5. "Super Span Starts Soon." *Engineering News Record*. Vol. 222, No. 14. April 6, 1989. McGraw-Hill. p. 18.
6. Zellner, Wilhelm, and Saul, Reiner. Discussion of "Cable-Stayed Bridges: Degrees of Anchoring," by Gilsanz and Biggs (Paper 17621). *Journal of Structural Engineering*, American Society of Civil Engineers. Volume 110, No. 4. April 1984.
7. Dykers, S. R. **Cable Stayed Bridges: The Cable and Its Fatigue Resistance**. Masters Thesis, The University of Texas at Austin. May, 1984.
8. **Post-Tensioning Manual**. 4th Edition, the Post-Tensioning Institute. 1985.
9. "Stay Cable System Qualification Test Procedure: Houston Ship Channel Crossing." 4th Revision. VSL Corporation. November 1988.
10. "Plexco Yellowstripe PE 3408 Gas Pipe." Amsted Industries, Inc. 1988. p.4.
11. Waldner, Eugene H. and Kulicki, John M. "Quincy Bayview Bridge – Construction Control." Session proceedings, American Society of Civil Engineers Convention. Carl C. Ulstrup, Ed. May 9, 1988.
12. Tikalsky, P.J. "Cable Stayed Bridges: Building New and Rehabilitating the Old." Paper presented as partial fulfillment of the requirements for the Ph.D. Comprehensive Examination, The University of Texas. 1988.

13. Watson, S. C. and Stafford, D. "Cables in Trouble." *Civil Engineering*. Vol. 58, No. 4. April 1988. pp. 38-41.
14. Personal conversations with Mr. Jon Vought, Project Manager for VSL Corporation. April 13, 1989.
15. Lim, F. K. "Assessment of Alternative Materials and Designs for TLP Tethers." *Proceedings of 7th International Conference on Offshore Mechanics and Arctic Engineering*. Vol.1. 1988.
16. Schlaich, Jorg and Bergermann, Rudolf. "New Parallel Wire Bundle for Cable-stayed Bridges." Session proceedings, American Society of Civil Engineers Convention. Carl C. Ulstrup, Ed. May 9, 1988.
17. Dykers, S. R., and Frank, K. H. "Test of Luling Hybrid Socketed Cable Stays." Progress Report, Civil Engineering Structures Research Laboratory, The University of Texas at Austin. September, 1980.
18. Vasseghi, A., and Frank, K. H. "Test of Luling Hybrid Socketed Cable Stays 271 Wire Second Specimen." Progress Report, Civil Engineering Structures Research Laboratory, The University of Texas at Austin. November 21, 1980.
19. Vasseghi, A., and Frank, K. H. "Test of Luling Hybrid Socketed Cable Stays 271 Wire Third Specimen." Progress Report, Civil Engineering Structures Research Laboratory, The University of Texas at Austin. February 24, 1981.
20. Frank, K. H., Breen, J. E., and Campbell, M. A. "Creep, Ultimate Strength and Fatigue Tests of Two Stay Cables With Hybrid Epoxy- Steel Sockets." Civil Engineering Structures Research Laboratory, The University of Texas at Austin. June, 1976.
21. Paulson, C., Frank, K. H., and Breen, J. E. **A Fatigue Study of Prestressing Strand**. Research Report No. 300-1, Center for Transportation Research, The University of Texas at Austin. September, 1982.
22. Lamb, J. L., and Frank, K. H. **Development of a Simple Fatigue Resistant Stay Cable Anchorage**. Research Report No. 384-1F, Center for Transportation Research, The University of Texas at Austin. November, 1985.

23. Moore, Jeffrey A., and Frank, Karl H. "Fatigue and Static Tests of 19-Strand Stay Cable Specimen for the Baytown Bridge." Test report for the VSL Corporation. March 1989.
24. Yates, David Lee. "A Study of Fretting Fatigue in Post-Tensioned Concrete Beams." Masters Thesis, The University of Texas at Austin. December 1987.
25. Wollmann, Gregor Peter. "Fretting Fatigue of Multiple Strand Tendons in Post-Tensioned Concrete Beams." Masters Thesis, The University of Texas at Austin. December 1988.
26. "Recommendations for Stay Cable Design and Testing." Post-Tensioning Institute Ad Hoc Committee on Cable-Stayed Bridges. January, 1986.
27. **Standard Specifications for Highway Bridges.** 12th Edition, American Association of State Highway and Transportation Officials, 1977.
28. Canteli, A. F., Esslinger, V., and Thurlimann, B. "Ermudungsfestigkeit von Bewehrungs- und Spannstählen (Fatigue Strength of Reinforcing and Prestressing Steel)." Institut für Baustatik und Konstruktion. ETH Zurich (Swiss Federal Institute of Technology). Report 8002-1. February 1984.
29. Stallings, James Michael. **Probabilistic Evaluations of Stay Cable Fatigue Behavior.** Doctoral dissertation, The University of Texas. August 1988.
30. Bush, Lawrence H. and Kahlil, M. S. "Skytrain Crosses the River." Civil Engineering, Vol. 58, No. 3. March 1988. pp. 50-53.
31. "Stay Cables." Freysinnet stay cable brochure.
32. Weibull, W. **Fatigue Testing and Analysis of Results.** Pergamon Press. 1961.
33. Hsu, C. K., and Frank, K. H. "Fatigue and Static Tests of Three Samples of 0.60 Inch Diameter Seven Wire Prestressing Strand." Phase I Report, Phil M. Ferguson Structural Engineering Laboratory, The University of Texas at Austin. December, 1981.

VITA

Jeffrey Allen Moore was born in San Jose, California, on November 23, 1965, the son of Roger Dixon Moore and Judith Joan Moore. Upon completing his secondary education at Wheat Ridge Senior High School in Wheat Ridge, Colorado, in 1983, he entered the University of Colorado in Boulder, Colorado. He received the degree of Bachelor of Science in May, 1987, and then relocated to attend The University of Texas at Austin in the fall of that same year. Prior to completing his graduate studies he worked on a part-time basis for the Department of Interior as a geotechnical engineer.

Permanent Address: 10022 W. 31st Ave.
Lakewood, CO 80215
(303) 232-4922

This thesis was typed by Jeffrey A. Moore and typeset by Sharon Cunningham.

